THE VELOCITY OF SOUND IN LIQUID COPPER-TIN ALLOYS

by

ROBERT TURNER

B.A., Cornell University, 1968

A DISSERTATION SUBMITTED IN PARTIAL FULFILLMENT
OF THE REQUIREMENTS FOR THE DEGREE OF
DOCTOR OF PHILOSOPHY

in the Department

of

Physics

SIMON FRASER UNIVERSITY
March 1972

APPROVAL

Name: Robert Turner

Degree: Doctor of Philosophy

Title of Thesis: The Velocity of Sound in Liquid Copper-Tin Alloys

Examinining Committee: Date Approved: April 26, 1972

Chairman: K.E. Rieckhoff

J.F. Cochran
Senior Supervisor

E.D. Crozier
Examining Committee

D. Dunn
Examining Committee

R.R. Haering
Examining Committee

P.A. Egelstaff
External Examiner
Professor of Physics
Guelph University
Guelph, Ontario

ABSTRACT

A new technique for detecting acoustic waves in liquid metals has been developed, relying on the generation of electromagnetic waves by acoustic waves emerging from a metal surface in the presence of a static magnetic field parallel to the surface. This technique can easily be employed at temperatures well above 1000°C and has been used to measure the velocity of sound as a function of temperature in eleven different alloys of copper and tin, between 265°C and 1400°C. Agreement with previous measurements for the pure metals is good. Using earlier density data, and the present sound velocity measurements, the adiabatic and isothermal compressibilities of this system have been computed at 800°C and 1100°C, as a function of composition. The maximum percentage deviation of the isothermal compressibility from that expected for ideal mixing of the alloy components occurs at a composition Sn 78 At. % Cu, correlating well with other thermophysical data. The partial structure factors at zero wavevector have also been evaluated, as a function of composition. These show considerable variation with composition, in disagreement with the frequent assumption that the partial structure factors are independent of composition.

When Man first learnt to melt a Metal down,

He measured not th'Velocity of Sound;

Though Bronze it was, yea, Copper mixed with Tin,

With which our Forefathers did first begin,

And though Five Thousand Years have since flown by,

Th'Experiment was left for me to try.

So Science stumbles on, Unevenly:

Long lies the Seed, ere it becomes a Tree.

To Jean

TABLE OF CONTENTS

LIST OF TABLES

LIST OF FIGURES

ACKNOWLEDGMENTS

First and foremost I wish to acknowledge the enthusiastic and inspiring encouragement and guidance of Professor John Cochran, my supervisor for this thesis. I am also deeply indebted to Dr. Daryl Crozier, who suggested this experiment and gave me invaluable assistance in its design and development. I wish also to thank Mr. Jim Oxton for his careful preparation of the alloy specimens, Mr. Frank Wick and his machinists for their most skilful help in constructing the apparatus, Mr. Peter Hatch and the Glassblowers' Shop for forming the quartz delay line assemblies, and Dr. Sean McAlister for many stimulating discussions and a number of most helpful suggestions. Thanks also to Mrs. Jan Inouye for typing this thesis, and to the National Research Council of Canada for its financial support for this work.

CHAPTER 1

INTRODUCTION

1-1 General Introduction

The experiment described in this thesis is the measurement of the velocity of sound in liquid alloys of copper and tin. This quantity, together with the alloy density, can be used to evaluate the compressibility, a fundamental property of materials which one may attempt to calculate theoretically. Furthermore, the isothermal compressibility is proportional to the zero-wavevector limit of the structure factor of a pure liquid, and may be used to compute this otherwise experimentally inaccessible quantity. However, in liquid alloys more thermodynamic data are needed to calculate the partial structure factors in this limit. For the system studied these data are available.

Section 1-2 introduces the concept of the structure factor as it applies to liquid metals, and indicates the usefulness of this concept by demonstrating its role in calculations of the resistivity of pure liquid metals. Section 1-3 shows how the structure factor can be generalised to the case of liquid mixtures or alloys, and how it may be evaluated at zero wavevector using thermodynamic data. The thermodynamics of ideal alloy systems are outlined, with an indication of how real systems depart from the ideal.

Section 1-4 contains a brief survey of the more successful theoretical approaches to the compressibility of liquid metals. These theories are

clearly also theories for the velocity of sound, since the compressibility is very closely related to this quantity.

Since the technique by which we measure the velocity of sound has not been employed before, an outline of this and other methods is presented in Chapter 2, and the virtues of the present method are pointed out. A short discussion of some of the available refractory materials follows, since the delay line material is the primary limiting factor at high temperatures in the method used here.

Chapter 3 contains a description of the apparatus and electronics used, and an account of the actual measurement technique.

The experimental results are to be found in Chapter 4, and an analysis of them, in the light of what has been said in Chapter 1, is presented in Chapter 5. This Chapter also describes the behaviour, as a function of composition, of the zero-wavevector structure factors of Cu-Sn alloys, and contains some speculative remarks concerning the physical interpretation of these and other measurable properties of this alloy system.

Chapter 6 summarises our conclusions.

1-2 Liquid Metals in General

1-2-1 The Structure Factor in Pure Liquid Metals

Since there is no long-range order in liquids, the appropriate way to characterize their structure is by the use of correlation functions. These describe the correlation of the value of some physical quantity, such as velocity, density, concentration, and so forth, at one position

and time in the liquid to its value at other positions and times. The most important among these functions is the pair correlation function, or density-density correlation function; which is proportional to the probability of finding an atom at a point $\vec{r}$ and a time t, when there is an atom at $\vec{r} = 0$ and $t = 0$. In liquids, the time average of this function is of course isotropic. We write the probability per unit volume of finding an atom at a distance r from an atom at the origin as g(r), commonly known as the radial distribution function. A typical g(r) is shown in Fig. 1.1. Several thermodynamic quantities may be written in terms of g(r) and an appropriate effective interatomic potential (see Fisher 1964). Among these is the fluctuation in the number* of atoms $\bar{N}$ in a given volume V:

$$\overline{N^2} - (\bar{N})^2 = \bar{N}\left[1 + \frac{\bar{N}}{V}\int_0^\infty (g(r)-1)\,4\pi r^2 dr\right] \qquad (1.1)$$

We shall return to this equation later. Now let us consider how g(r) can be measured experimentally. It can easily be shown (Egelstaff 1967, Fisher 1964, to name but two textbooks from the many giving a full derivation) that the intensity of particles elastically scattered from a beam of particles striking the liquid is given by

$$I(q) = I_0(q)\left[1 + \frac{\bar{N}}{V}\int_0^\infty (g(r)-1)\,\frac{\sin qr}{qr}\cdot 4\pi r^2 dr\right] \qquad (1.2)$$

---

* Bars indicate time or ensemble averages throughout this thesis.

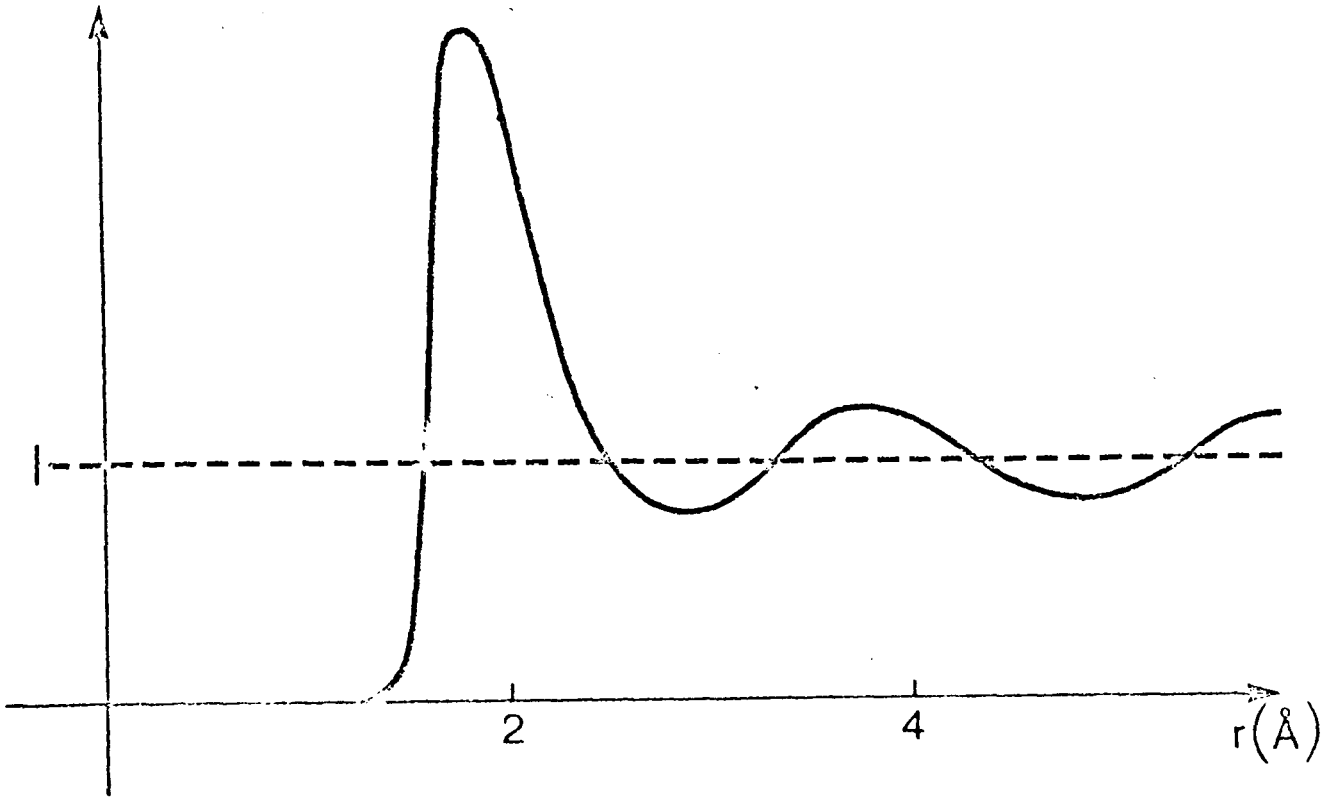

Fig. 1.1. Typical form of the radial distribution function g(r) for a liquid metal.

where $\vec{q}$ is the wavevector through which the particles are scattered and $I_o(q)$ is the scattered intensity from a system of N independent atoms. If the scattering angle is θ, then $q = 2k \sin \theta/2$, where k is the magnitude of the wavevector of the incident and outgoing particles. It is usual to employ X-rays or thermal neutrons as the particles to be scattered, since their wavelengths are close to typical atomic spacings in liquids; thus they interact strongly with the short-range order of the atoms. The ratio $I(q)/I_o(q)$ is usually written $a(q)$, and is referred to as the structure factor. The behaviour of $a(q)$ is shown in Fig. 1.2. It follows from (1.2) that

$$a(q) = 1 + \frac{\bar{N}}{V}\int_0^\infty (g(r)-1)4\pi r^2 \frac{\sin qr}{qr} dr \qquad (1.3)$$

1-2-2 The Relationship Between the Velocity of Sound and the Structure Factor

It is a familiar result of statistical mechanics (Huang 1967, p. 166, for example) that the isothermal compressibility K_T of a pure substance is related to the fluctuations in the number of particles in a given volume V:

$$K_T = \frac{V}{k_B T} \cdot \frac{\overline{N^2} - (\bar{N})^2}{(\bar{N})^2} \qquad (1.4)$$

Equation (1.1) enables us to express this immediately in another form:

$$K_T = \frac{V}{\bar{N} k_B T}\left[1 + \frac{\bar{N}}{V}\int_0^\infty (g(r)-1)4\pi r^2 dr\right] \qquad (1.5)$$

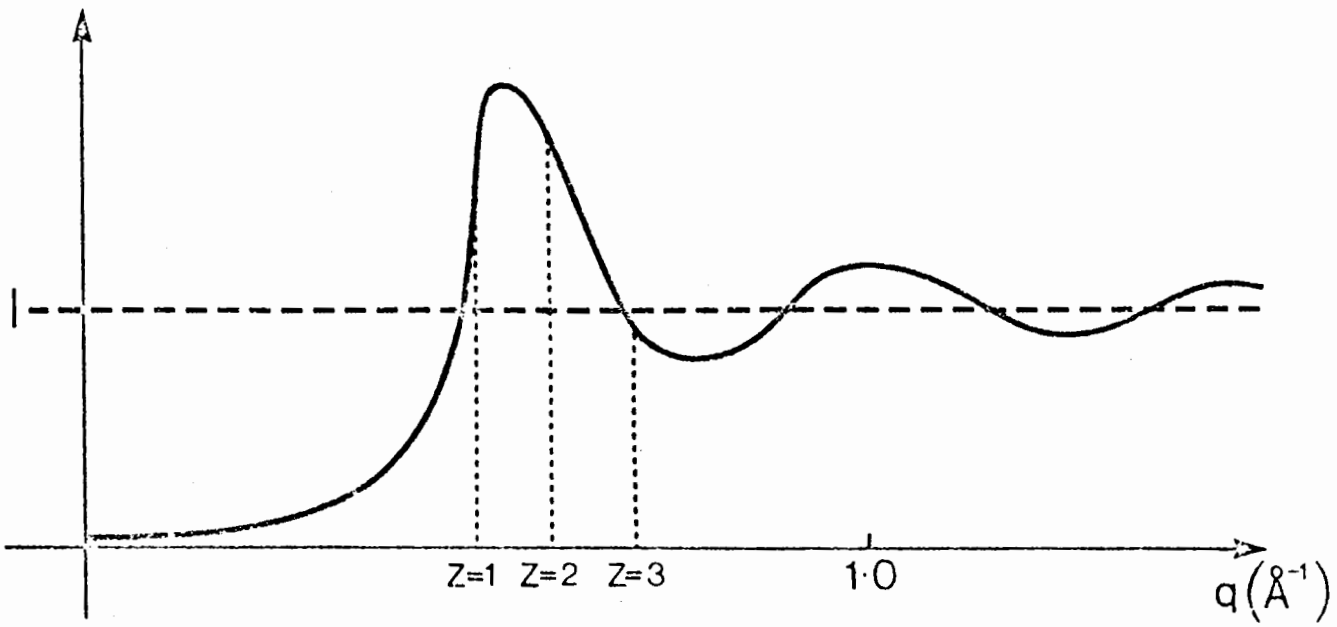

Fig. 1.2. Typical form of the structure factor a(q) for a pure liquid metal. The positions of $2k_f$ for Z = 1, 2 and 3 are shown.

This can be simplified with the aid of (1.3):

$$\frac{\bar{N}}{V} k_B T K_T = a(0) \tag{1.6}$$

Now we wish to relate K_T to the velocity of sound, s. To do this, we note that

$$K_T = -\frac{1}{V}\left(\frac{\partial V}{\partial p}\right)_T \tag{1.7}$$

and also that (Egelstaff 1967, for example)

$$s^2 = \frac{1}{\rho_M K_S} \tag{1.8}$$

where K_S is the adiabatic compressibility, given by

$$K_S = -\frac{1}{V}\left(\frac{\partial V}{\partial p}\right)_S \tag{1.9}$$

Furthermore,

$$\frac{K_T}{K_S} = \frac{-\left(\frac{\partial V}{\partial p}\right)_T}{-\left(\frac{\partial V}{\partial p}\right)_S} = \frac{\left(\frac{\partial T}{\partial p}\right)_V}{\left(\frac{\partial T}{\partial V}\right)_p} \cdot \frac{\left(\frac{\partial S}{\partial V}\right)_p}{\left(\frac{\partial S}{\partial p}\right)_V} \tag{1.10}$$

$$= \frac{\left(\frac{\partial S}{\partial T}\right)_p}{\left(\frac{\partial S}{\partial T}\right)_V} = \frac{C_p}{C_V} = \gamma$$

where γ is the ratio of the specific heats, which may be determined from the Equation

$$\gamma = 1 + \frac{s^2 \alpha_p^2 T}{C_p} \tag{1.11}$$

Hence, finally

$$a(0) = \frac{k_B T \gamma}{m s^2} \tag{1.12}$$

where m is the atomic mass of the liquid. We may thus evaluate the zero-wavevector limit of the structure factor for a pure liquid if we know the velocity of sound and the ratio of the specific heats. In fact, this is the only way in which this zero-wavevector limit may be determined since in scattering experiments the forward-scattered intensity drowns the contribution calculated here. Careful X-ray transmission experiments (Greenfield and Wiser 1972) can, however, follow a(q) down to quite small values of q ($\sim 0.2 \text{Å}^{-1}$).

1-2-3 Ziman Theory of Liquid Metal Resistivity

The simplest model one can reasonably adopt for a liquid metal is to think of it as two intermingled weakly interacting fluids, the ions and the electron gas. Such quantities as the electrical resistivity may then be calculated using the Born approximation for the electron-ion scattering. However, to do this one must replace the actual deep potential wells of the ions by the appropriate weak pseudopotentials which are chosen to reproduce the scattering phase shifts of the actual potential wells (see

Harrison 1966 for details). Furthermore, one must find some way of characterizing the arrangement of the ions themselves. The first approximation, that of uniform density, gives resistivities which are far too high. Ziman (1961) developed a formalism to deal with this problem. One reason that the resistance in liquid metals is low is the presence of short range order, as manifested in g(r) and a(q). We may illustrate the importance of the structure factor a(q) in the theory of liquid metals by showing how it is used in Ziman's theory to compute the resistivity. Let the appropriately screened pseudopotential (assumed local and spherically symmetric) of the ith ion, located at the position $\vec{R}_i$ in the liquid, be denoted $u_i(\vec{r}-\vec{R}_i)$. The resistivity* may then be written, according to Ziman, as

$$\rho = \frac{3\pi}{\hbar e^2 V v_f^2} \int_0^1 \overline{|U(q)|^2} \cdot 4\left(\frac{q}{2k_f}\right)^2 d\left(\frac{q}{2k_f}\right) \qquad (1.13)$$

where k_f is the radius of the Fermi surface, assumed sharp, and U(q) is given by

$$U(q) = \overline{U(q,t)} = \overline{\int_V \sum_i u_i(\vec{r}-\vec{R}_i(t)) e^{i\vec{q}\cdot(\vec{r}-\vec{R}_i)} d^3r} \qquad (1.14)$$

If we write

$$u_i(q) = \int_V u_i(\vec{r}) e^{i\vec{q}\cdot\vec{r}} d^3r \qquad (1.15)$$

---

* We use c.g.s. units throughout this thesis.

and assume we have a pure metal, so $u_i = u$ for all atoms, we get

$$\overline{|U(q)|^2} = (u(q))^2 \overline{\left|\sum_i e^{i\vec{q}\cdot\vec{R}_i(t)}\right|^2} \tag{1.16}$$

It may easily be shown (using the identity $g(r) = \overline{\sum_{i\neq j} \delta(\vec{r} - \vec{R}_i + \vec{R}_j)}$) that

$$\overline{\left|\sum_i e^{i\vec{q}\cdot\vec{R}_i(t)}\right|^2} = a(q) \tag{1.17}$$

(plus a delta function at q = 0 which does not contribute to the resistivity). Thus

$$\rho = \frac{3\pi}{\hbar e^2 V v_f^2} \int_0^1 (u(q))^2 a(q) \cdot 4\left(\frac{q}{2k_f}\right)^2 d\left(\frac{q}{2k_f}\right) \tag{1.18}$$

The Ziman theory of the resistivity works quite well for many liquid metals. One of its most striking features is its success in accounting for the behaviour of the resistivity as a function of the valency of the metal. The position of $2k_f$ with respect to the first peak in a(q) is crucial. This peak decreases in amplitude with an increase of temperature, because the liquid becomes more disordered. On the other hand, a(o) increases with temperature, as can be seen from (1.6). Thus (see Fig. 1.2) monovalent metals, where the integration (1.18) does not include the first peak should have a low resistivity and a positive temperature coefficient of resistivity; while the divalent metals, where the major contribution to the integral comes from the first peak, should have high resistivities and a negative temperature coefficient of resistivity. These predictions are

in accordance with experiment. The argument may be extended (see Lloyd 1968) to explain the behaviour at higher valencies. We shall return to this point in Chapter 5 in connection with the Cu-Sn alloy system.

Having introduced the concept of the structure factor we may now move on to the more complex problem of liquid metal alloys.

1-3 Liquid Alloys: Thermodynamics and Structure

As an abstract physical problem, liquid alloys are attractive, for several reasons. In comparison to solid alloys, they are very homogeneous and isotropic. In many systems the electron density may be varied considerably without extensive structural changes. Thus another parameter is available for those who calculate the electronic properties of disordered systems.

1-3-1 Generalisation of the Structure Factor

As with pure liquid metals, the most successful theoretical work has been done on the electrical resistivity. In the case of alloys we need a more sophisticated description of the structure of the liquid, and we shall consider two rival formalisms: the one due to Faber and Ziman (1965); and the other, which is mathematically equivalent, but a little more closely related to alloy thermodynamics, by Bhatia and Thornton (1970). We shall begin with the Faber and Ziman approach, and explore the thermodynamics of alloys later, as an adjunct to the Bhatia-Thornton theory.

Faber and Ziman's recipe for dealing with the problem of alloy structure is to define partial radial distribution functions, $g_{\alpha\beta}(r)$, in

such a way that $g_{\alpha\beta}(r) \to 1$ as $r \to \infty$. Here α and β stand for either of the two species comprising the alloy. The meaning of $g_{\alpha\beta}(r)$ is made clear by the fact that $\frac{N}{V} c_\beta g_{\alpha\beta}(r)$ is the number of atoms of species β per unit volume at a distance r from an atom of species α at the origin. The corresponding <u>partial structure factors</u> $a_{\alpha\beta}(q)$ are defined, as one would expect, by

$$a_{\alpha\beta}(q) = 1 + \frac{\bar{N}}{V} \int_0^\infty (g_{\alpha\beta}(r) - 1) \frac{\sin qr}{qr} 4\pi r^2 dr \qquad (1.19)$$

c_α and c_β are the concentrations of the two species α and β respectively. Clearly $c_\alpha + c_\beta = 1$. (Later we shall replace α and β by i and j respectively, where i and j can both refer either to species 1 or to species 2, to bring the notation into line with that of Bhatia and Thornton (1970) and other workers in this field.)

1-3-2 Methods of Determining the Partial Structure Factors

The partial structure factors $a_{\alpha\beta}(q)$ are rather less accessible to experiment than a(q) for a pure metal. Three different scattering experiments at each composition are necessary, each with different atomic scattering cross-sections, in order to disentangle these quantities. The difference in atomic cross-sections can be achieved by using different isotopes of one or the other component of the alloy to form the alloy and performing neutron diffraction experiments (Enderby et al. 1966), or by using the energy dependence of the neutron cross-section and performing three neutron diffraction experiments at different energies; but this has not been done to date. A combination of X-ray and neutron scattering

experiments is also feasible. The scattered intensity I(q) can be shown (analogously to Faber and Ziman 1965) to be given by

$$I(q) = N\{ f_1^2(q)[c_1 + c_1^2(a_{11}(q)-1)] + f_2^2(q)[c_2 + c_2^2(a_{22}(q)-1)] + 2c_1c_2 f_1(q) f_2(q)[a_{12}(q)-1]\} \quad (1.20)$$

where f_1 and f_2 are the coherent scattering amplitudes of each component of the alloy.

Isotopic enrichment experiments are difficult and expensive, and as a result workers in this field have sought simpler methods. The most obvious assumption is that the $a_{\alpha\beta}(q)$'s are independent of composition (Enderby et al. 1967, Halder and Wagner 1967, North and Wagner 1970). With this assumption, X-ray diffraction experiments at three different compositions are sufficient to determine all three partial structure factors. Indeed, North and Wagner (1970) using this assumption for Cu-Sn alloys obtain very good numerical agreement between values of the electrical resistivity derived with the help of the Faber-Ziman theory, from their X-ray scattering measurements and pseudopotentials from Animalu and Heine (1965), and resistivities measured by Roll and Motz (1957). They also obtain agreement with the values for the thermoelectric power measured by Enderby and Howe (1968) for this system.

However, it is our intent to show, later in this Section, that the assumption of composition-independence of the partial structure factors is unjustifiable, at least in the case of q = 0. How this affects the

results of North and Wagner, and others, will not be discussed here.

Efforts have been made to calculate the structure factor from first principles. A favourite first approximation to the ion-ion interaction potential in pure liquid metals is to treat the ions as hard spheres; the potential is zero outside a hard sphere radius, σ, and infinite inside this radius. Molecular dynamics and Monte Carlo calculations indicate a liquid-solid phase transition for this model, and the main features of the structure factor for pure metals are reproduced (Wood 1968). Using what is known as the Percus-Yevick approximation, which we will not attempt to describe here, an analytic form for a(q) can be deduced for the hard-sphere model (see, for example, Ashcroft and Lekner 1966). Enderby and North (1968) and Ashcroft and Langreth (1967a) independently extended the Percus-Yevick approximation to the case of binary mixtures of hard spheres; their conclusions as to the dependence of the partial structure factors on composition are compatible with the results which will be presented here. As for the pure metals, $a_{ij}(q)$ can be expressed analytically, but the expression is very complicated.

1-3-3 The Faber-Ziman Theory of the Resistivity of Liquid Alloys

To demonstrate the usefulness of the partial structure factors, and to connect with the Bhatia-Thornton treatment of alloy structure, we present briefly Faber and Ziman's theory of liquid alloy resistivities. Recalling Equation (1.13), which is quite general, we write for the case of an alloy

$$\overline{|U(q)|^2} = \sum_{\alpha,\beta} \sum_{R_\alpha, R_\beta} u_\alpha(q)\, u_\beta(q)\, e^{i\vec{q}\cdot(\vec{R}_\alpha - \vec{R}_\beta)}$$

$$= \sum_{\alpha} \bar{N} c_\alpha u_\alpha^2 + \sum_{\alpha \neq \beta} u_\alpha u_\beta \sum_{R_\alpha, R_\beta} e^{i\vec{q}\cdot(\vec{R}_\alpha - \vec{R}_\beta)} \tag{1.21}$$

where we assume $u_\alpha(q)$ is real and we have dropped the arguments for brevity. Now

$$\sum_{R_\alpha} \sum_{R_\alpha \neq R_\beta} e^{i\vec{q}\cdot(\vec{R}_\alpha - \vec{R}_\beta)} = \bar{N} c_\alpha c_\beta (a_{\alpha\beta}(q) - 1) \tag{1.22}$$

Thus (1.21) becomes

$$\begin{aligned}\overline{|U(q)|^2} = \bar{N} \{ & u_1^2 [c_1 + c_1^2 (a_{11} - 1)] \\ & + u_2^2 [c_2 + c_2^2 (a_{22} - 1)] \\ & + 2 c_1 c_2 u_1 u_2 [a_{12} - 1] \}\end{aligned} \tag{1.23}$$

where the arguments of $a_{\alpha\beta}(q)$ have been dropped, for brevity. The resistivity is found by substituting Equation (1.23) into (1.13). In the case of alloys where one can approximate $a_{11}(q) = a_{12}(q) = a_{22}(q) = a(q)$, that is, alloys whose constituent atoms have nearly the same size and cross-section (like Pb-Sn, for example) this theory can easily be compared with experiment. Qualitative, and indeed quantitative agreement is found. Where the $a_{\alpha\beta}$'s differ from each other, comparison with experiment is somewhat harder, owing to the difficulties in measuring these partial

structure factors. Ashcroft and Langreth (1967a) used partial structure factors calculated using the Percus-Yevick hard sphere model, and appropriate pseudopotentials, and were able to fit quite well the observed resistivities of a number of alloy systems. However, it is not hard to show that at least for $q \to 0$ the Percus-Yevick hard sphere model is unsatisfactory. See Section 1-3-5.

1-3-4 The Bhatia-Thornton Theory of the Resistivity of Liquid Alloys

The second formalism for the structure of liquid alloys that we shall discuss was developed by Bhatia and Thornton (1970). (We shall refer to this paper as BT.) Instead of looking at the particle-particle correlations, BT focus their attention on the density-density, concentration-concentration and density-concentration correlations. These can be shown (Appendix A) to be closely related to the compressibility, the heat of mixing and the change in molar volume on mixing. As in Faber and Ziman's treatment, the resistivity is written (see Equation (1.1)) as an integral of the function $|U(q)|^2$. It is in the analysis of this function that the difference arises. If the alloy consists of N_1 atoms of type 1 and N_2 atoms of type 2, in a volume, V, we write $\bar{n}_i = \frac{N_i}{V}$, the mean number density of atoms of type i, and $c = N_1/(N_1 + N_2)$, the average concentration (which we called c_1 earlier; naturally $c_1 + c_2 = 1$). If $n_i(\vec{r},t)$ is the number density at time t for the species i, then we define

$$\delta n_i(\vec{r},t) \equiv n_i(\vec{r},t) - \bar{n}_i = \sum_j \delta\left(\vec{r} - \vec{R}_j^i(t)\right) - \bar{n}_i \qquad (1.24)$$

Making the Fourier expansion

$$\delta n_i(\vec{r},t) = \frac{1}{V}\sum_{\vec{q}} N_i(\vec{q},t)\, e^{i\vec{q}\cdot\vec{r}} \tag{1.25}$$

we have

$$N_i(\vec{q},t) = \sum_j e^{i\vec{q}\cdot\vec{R}_j^i(t)} - N_i\,\delta_{\vec{q},0} \tag{1.26}$$

Similarly, if $N(\vec{q},t)$ denotes the Fourier transform of the local deviation $\delta n(\vec{r},t)$ in the total number density, $N(\vec{q},t) = \int_V e^{i\vec{q}\cdot\vec{r}}\,\delta n(\vec{r},t)\,d^3r$,

$$N(\vec{q},t) = N_1(\vec{q},t) + N_2(\vec{q},t) \tag{1.27}$$

Defining

$$\delta c(\vec{r},t) = \frac{V}{N}\left[(1-c)\,\delta n_1(\vec{r},t) - c\,\delta n_2(\vec{r},t)\right] \tag{1.28}$$

where $N = N_1 + N_2$

and Fourier-transforming

$$\delta c(\vec{r},t) = \sum_{\vec{q}} C(\vec{q},t)\, e^{-i\vec{q}\cdot\vec{r}} \tag{1.29}$$

we have

$$C(\vec{q},t) = \frac{1}{N}\left[(1-c)\,N_1(\vec{q},t) - c\,N_2(\vec{q},t)\right] \tag{1.30}$$

If we include the time dependence of $U(\vec{q},t)$ we obtain

$$U(\vec{q},t) = \sum_i u_i(\vec{q}) \sum_j e^{i\vec{q}\cdot\vec{R}_i^j(t)} \tag{1.31}$$

(where $u_i(\vec{q}) = \int_V u_i(\vec{r})\, e^{i\vec{q}\cdot\vec{r}}\, d^3r$);

which can be rewritten with the help of (1.26),

$$U(\vec{q},t) = u_1(\vec{q})\, N_1(\vec{q},t) + u_2(\vec{q})\, N_2(\vec{q},t) + (N_1 u_1 + N_2 u_2)\, \delta_{\vec{q},0}, \tag{1.32}$$

where $\delta_{\vec{q},0} = 1$ for $q = 0$
$= 0$ for $q \neq 0$,

or using (1.30)

$$U(\vec{q},t) = (cu_1 + (1-c)u_2)\, N(\vec{q},t) + (u_1 - u_2)\, N\, C(\vec{q},t) \tag{1.33}$$

where we have now dropped the delta function since in the integration for the resistivity it will disappear anyway. We may now evaluate $|U(q)|^2$:

$$\overline{|U(\vec{q})|^2} = N\left\{[cu_1 + (1-c)u_2]^2 S_{NN}(\vec{q}) + [u_1 - u_2]^2 S_{cc}(\vec{q}) + 2(cu_1 + (1-c)u_2)(u_1 - u_2) S_{Nc}(\vec{q})\right\} \tag{1.34}$$

where now

$$S_{NN}(\vec{q}) \equiv \frac{1}{N} \overline{|N(\vec{q},t)|^2}$$
$$S_{cc}(\vec{q}) \equiv N \overline{|C(\vec{q},t)|^2} \qquad (1.35)$$
$$S_{Nc}(\vec{q}) \equiv Re\ \overline{N(\vec{q},t)\, C(\vec{q},t)}$$

These expressions are as accurate as our initial assumption that the total potential which the electrons experience is decomposable into a sum of isotropic ionic potentials.

In the form (1.34) BT's expression is directly comparable to that of Faber and Ziman (Equation (1.23)). By comparing coefficients of u_1 and u_2, and remembering that $c_2 = 1 - c = 1 - c_1$, we obtain immediately

$$S_{NN}(\vec{q}) = c_1^2 a_{11} + c_2^2 a_{22} + 2c_1 c_2 a_{12}$$
$$S_{Nc}(\vec{q}) = c_1 c_2 \left[c_1 (a_{11} - a_{12}) - c_2 (a_{22} - a_{12})\right] \qquad (1.36)$$
$$S_{cc}(\vec{q}) = c_1 c_2 \left[1 + c_1 c_2 (a_{11} + a_{22} - 2a_{12})\right]$$

and conversely,

$$c_1^2 a_{11} = c_1^2 S_{NN} + 2c_1 S_{Nc} + S_{cc} - c_1 c_2$$

$$c_2^2 a_{22} = c_2^2 S_{NN} - 2c_2 S_{Nc} + S_{cc} - c_1 c_2 \qquad (1.37)$$

$$c_1 c_2 a_{12} = c_1 c_2 S_{NN} + (c_2 - c_1) S_{Nc} - S_{cc} + c_1 c_2$$

This is the most straightforward way of making the connection between the treatments of Faber and Ziman, and Bhatia and Thornton. There is also, it would appear, a direct link via statistical mechanics, independent of the potentials in the liquid. The derivation is certainly lengthy and tedious. The foregoing would seem to be a pointless exercise in rearrangement of terms, were it not for the fact that at q = 0 BT's structure factors can be evaluated from thermodynamic data. For a complete derivation, see Appendix A. The final results are

$$S_{cc}(0) = \frac{(1-c)}{\frac{1}{a_1}\left(\frac{\partial a_1}{\partial c}\right)_{T,P,N}}$$

$$S_{Nc}(0) = -\frac{1}{V}\left(\frac{\partial V}{\partial c}\right)_N \cdot \frac{(1-c)}{\frac{1}{a_1}\left(\frac{\partial a_1}{\partial c}\right)_{T,P,N}} \qquad (1.38)$$

$$S_{NN}(0) = \frac{N k_B T}{V} K_T + \left(\frac{1}{V}\left(\frac{\partial V}{\partial c}\right)_N\right)^2 \frac{(1-c)}{\frac{1}{a_1}\left(\frac{\partial a_1}{\partial c}\right)_{T,P,N}}$$

where a_1 is the activity of species 1, which is equal to the ratio of the partial vapour pressure of species 1 at a concentration c to the vapour pressure of pure species 1 at the same temperature, provided that these vapours are rarefied enough that they can be treated as ideal gases. For

the full definition of the activity, see Appendix A.

Evaluating (1.37) at q = 0, we obtain for the structure factors $a_{ij}(o)$

$$a_{11}(o) = \frac{N}{V} k_B T K_T - \frac{(1-c)}{c} + \frac{(1-c)}{\frac{1}{q_1}\left(\frac{\partial q_1}{\partial c}\right)_{T,P,N}} \left(\delta - \frac{1}{c}\right)^2$$

$$a_{22}(o) = \frac{N}{V} k_B T K_T - \frac{c}{(1-c)} + \frac{(1-c)}{\frac{1}{q_1}\left(\frac{\partial q_1}{\partial c}\right)_{T,P,N}} \left(\delta + \frac{1}{(1-c)}\right)^2 \qquad (1.39)$$

$$a_{12}(o) = \frac{N}{V} k_B T K_T + 1 + \frac{(1-c)}{\frac{1}{q_1}\left(\frac{\partial q_1}{\partial c}\right)_{T,P,N}} \left(\delta - \frac{1}{c}\right)\left(\delta + \frac{1}{1-c}\right)$$

where $$\delta \equiv \frac{1}{V}\left(\frac{\partial V}{\partial c}\right)_N = \frac{N(v_1 - v_2)}{V}$$

At this point it is worth mentioning that the expressions (1.39) for $a_{ij}(o)$ are consistent with the Kirkwood-Buff formula for the isothermal compressibility (Kirkwood and Buff 1951), derived in a similar way from an analysis of fluctuations of particle number

$$\frac{N}{V} k_B T K_T = \frac{((1-c)a_{11} + c)(c a_{22} + (1-c)) - c(1-c)(a_{12}-1)^2}{1 + c(1-c)(a_{11} + a_{22} - 2a_{12})}$$

It can also be easily seen from Equations (1.39) that as $c \to 1$ and $(1 - c) \to 0$, $a_{11}(o) \to \frac{N}{V} k_B T K_T$, as one would expect for pure species 1, $a_{22}(o) \to \frac{N}{V} k_B T K_T + 2\delta$, and $a_{12}(o) \to \frac{N}{V} k_B T K_T + \delta$. The two latter results follow from the fact that for c close enough to unity $a_1(c) = c$ for all alloys. Similar results hold for $c \to 0$. Furthermore, $a_{11}(o) > -\frac{1-c}{c}$, and $a_{22}(o) > -\frac{c}{1-c}$ for all c, in accordance with the inequalities derived

from Equation (1.23) by demanding that $|U(q)|^2$ be positive definite (Enderby et al. 1966). To evaluate these formulae we need the molar volume V of the mixture, its variation with concentration, $\left(\frac{\partial V}{\partial c}\right)_N$, the isothermal compressibility K_T, and the activity a_1 of component 1 as a function of concentration. It may easily be shown that

$$\frac{1}{1-c}\,\frac{1}{a_1}\left(\frac{\partial a_1}{\partial c}\right)_{T,P,N} = \frac{1}{N k_B T}\left(\frac{\partial^2 G}{\partial c^2}\right)_{T,P,N} \qquad (1.40)$$

where G is the Gibbs free energy of the mixture. BT give the Equations (1.38) in this form. Thus in cases where the activity of an alloy system has not been measured, knowledge of the free energy of mixing is sufficient. However, since the second derivative is required, the a_{ij}'s are more sensitive to experimental errors in G than to errors in the activity. Furthermore, free energies of mixing are not usually measured directly in actual practice; it is the enthalpy of mixing that is usually determined in calorimetric experiments.

1-3-5 Alloy Thermodynamics

The behaviour of the thermodynamic properties of typical and ideal alloy systems as a function of composition deserves a few comments. The primary experimental data are the values of the activity as a function of composition and temperature, and of course the molar volume. The activity is conveniently determined for metals by measuring the partial vapour pressure of the components with the aid of a Knudsen cell and a mass spectrometer. The method is simply to determine the mass (and thus number of atoms) of each species evaporated in a given time from a given

surface area of the metal (see Kubaschewski et al. 1967, for details). Hultgren et al. (1963) in their compilation of thermodynamic data for metals and alloys, give activity data for dozens of liquid alloy systems. Accuracies range from 1% to 10%, with a corresponding uncertainty in the value of $a_{ij}(o)$ calculated from Equations (1.59). Densities have also been measured for a large number of alloy systems usually with accuracies of a few tenths of a percent, or better, giving a contribution to the error in $a_{ij}(o)$ of perhaps a few percent (see Equation (1.39)).

Knowing the activity and its dependence on temperature, the enthalpy of mixing, the entropy of mixing and the free energy of mixing, as well as the partial counterparts of these quantities, may easily be calculated, using the Duhem-Margules equations:

$$\Delta G = (1-c)\int_0^c \frac{N k_B T \ln a_1}{(1-c')^2}\, dc'$$
$$\Delta H = (1-c)\int_0^c \frac{\Delta H_1\, dc'}{(1-c')^2} \qquad (1.41)$$
$$\Delta S = (1-c)\int_0^c \frac{\Delta S_1\, dc'}{(1-c')^2}$$

where

$$\Delta H_1 = -N k_B T^2 \left(\frac{\partial}{\partial T}(\ln a_1)\right)_{p,N,c}$$
$$\Delta S_1 = -N k_B \left(T\left(\frac{\partial}{\partial T}(\ln a_1)\right)_{p,N,c} + \ln a_1\right) \qquad (1.42)$$

Also $$\Delta G_1 = N k_B T \ln a_1$$

and similarly for component 2.

1-3-5-1 Ideal Alloys

We define an ideal system as one in which

$$a_1 = c \tag{1.43}$$

that is, the vapour pressure of species 1 in the alloy is proportional to its concentration over the entire range of concentration. As a result, with the aid of the equation relating a_1 and a_2 (Hatsopoulos and Keenan 1965), which can be derived easily from (1.61),

$$\frac{c_1}{a_1}\frac{\partial a_1}{\partial c_1} = \frac{c_2}{a_2}\frac{\partial a_2}{\partial c_2} \tag{1.44}$$

(Here $c_1 = c$, $c_2 = 1 - c$), we have

$$a_2 = c_2 = 1 - c \tag{1.45}$$

$$\Delta G = N k_B T \left(c \ln c + (1-c) \ln (1-c)\right) \tag{1.46}$$

$$\Delta S = -N k_B \left(c \ln c + (1-c) \ln (1-c)\right) \tag{1.47}$$

$$\Delta H = 0 \tag{1.48}$$

Note that ΔS is the same as for a mixture of ideal gases. Furthermore, using (A.16) and (A.22) we have

$$\begin{aligned} v_1 &= v_{10} \\ v_2 &= v_{20} \end{aligned} \tag{1.49}$$

where v_{10} and v_{20} are the atomic volumes in pure species 1 and 2 respectively. Thus the molar volume of the alloy is given by

$$V = N(cv_{10} + (1-c)v_{20}) \tag{1.50}$$

giving a linear variation with composition. Hence the compressibility K_T is given by

$$\begin{aligned} K_T &= \frac{N}{V}\left(\frac{\partial}{\partial p}\left(v_{10}c + v_{20}(1-c)\right)\right)_T \\ &= \frac{N}{V}\left(c\left(\frac{\partial v_{10}}{\partial p}\right)_T + (1-c)\left(\frac{\partial v_{20}}{\partial p}\right)_T\right) \\ &= \frac{N}{V}\left(cv_{10}K_{1T} + (1-c)v_{20}K_{2T}\right) \end{aligned} \tag{1.51}$$

where K_{1_T} and K_{2_T} are the compressibilities of the pure species. We may also compute the adiabatic compressibility K_S:

$$K_S = \frac{N}{V}\left(cv_{10}K_{1S} + (1-c)v_{20}K_{2S}\right) \tag{1.52}$$

For an ideal mixture, the partial structure factors $a_{ij}(o)$ are given by

$$a_{11}(0) = \frac{N}{V} k_B T K_T + c(1-c)\delta^2 - 2(1-c)\delta$$
$$a_{22}(0) = \frac{N}{V} k_B T K_T + c(1-c)\delta^2 + 2c\delta \qquad (1.53)$$
$$a_{12}(0) = \frac{N}{V} k_B T K_T + c(1-c)\delta^2 + (2c-1)\delta$$

Thus
$$a_{11}(0) = a_{12}(0) - \delta$$
$$a_{22}(0) = a_{12}(0) + \delta$$

where as before $\delta = \frac{N}{V}(V_1 - V_2)$, and is now independent of composition. The a_{ij}'s have equal separations for an ideal system (see Fig. 1.3, which shows the behaviour of an ideal alloy corresponding to the system Na-K).

1-3-5-2 Real Alloys

In the case of a real system, we must distinguish between dilute and concentrated alloys. It is often found that the solvent in a dilute alloy has an almost ideal activity; for $c \sim 1$ Equation (1.43) holds true. Over what range of concentration this Equation holds depend on how far the alloy departs from the ideal at intermediate compositions, but it can extend down to c = .6. This behaviour is known as Raoult's Law. See Fig. 1.4. Equation (1.64) gives us the counterpart of Raoult's Law for component 2; we get for $c \sim 1$

$$a_2 = b(1-c) \qquad (1.43a)$$

where b is a constant, dependent on the alloy system (see Fig. 1.4). This is known as Henry's Law. Clearly the

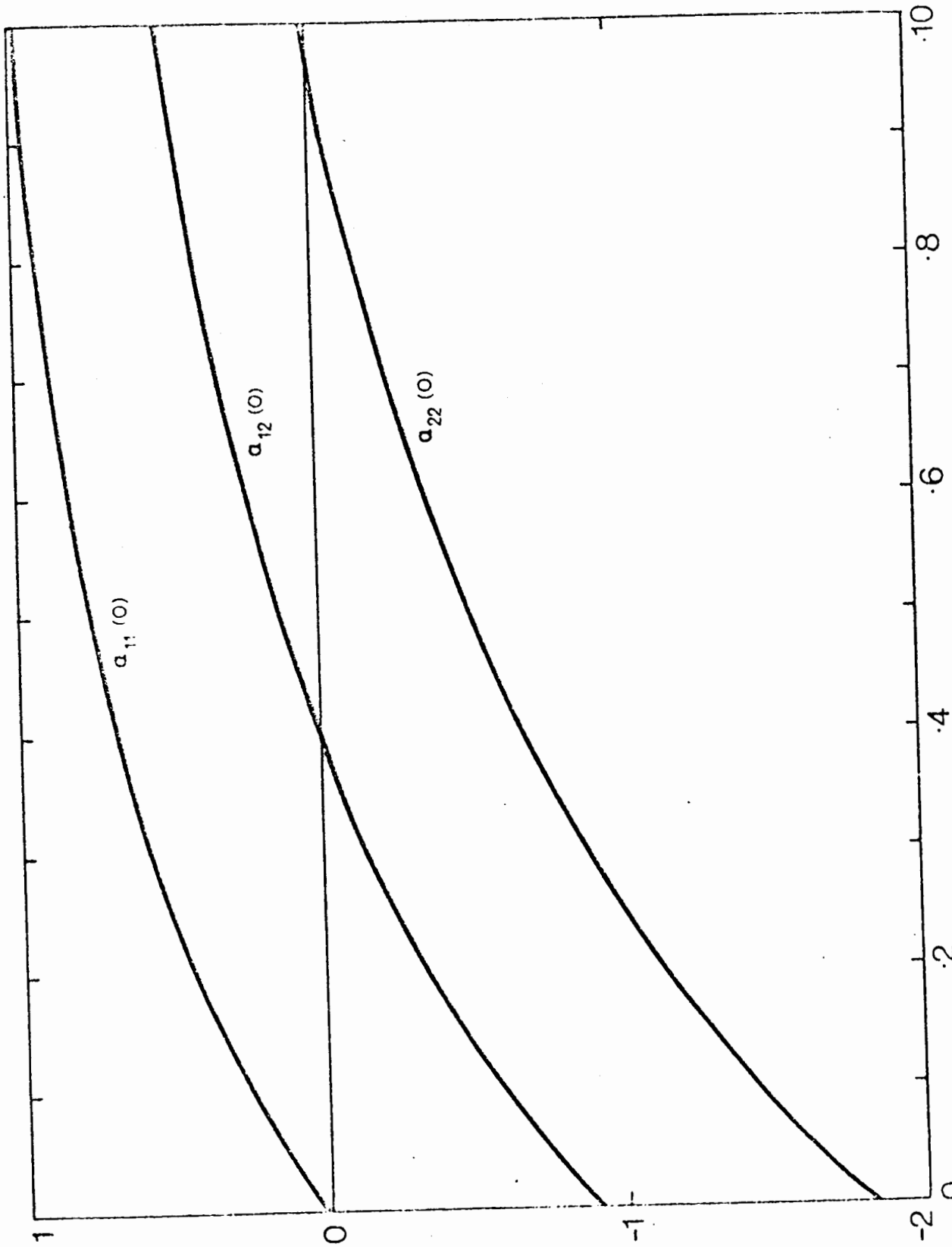

Fig. 1.3. Plot of $a_{ij}(o)$ for an ideal alloy system corresponding to Na-K.

roles of a_1 and a_2 can be reversed. In either case $\frac{1}{a_1}\frac{\partial a_1}{\partial c}$ is equal to unity for c = 1, a useful result in evaluating Equations (1.59).

Usually for concentrated alloys, a_1 lies (a) entirely above the ideal straight line, or (b) entirely below. Since for extremely high temperatures we intuitively expect the alloy behaviour to be closer to the ideal, we have for case (a) $\frac{\partial a_1}{\partial T} < 0$ and for case (b) $\frac{\partial a_1}{\partial T} > 0$. Using Equations (1.41) and (1.42) we see that this results, for case (a), in a positive enthalpy of mixing (an endothermic reaction), and for case (b) a negative heat of mixing (an exothermic reaction). The experimental results corroborate this general deduction.

Although in an ideal system the additivity of the molar volumes and the absence of an enthalpy of mixing ($\Delta H = 0$) arise from the same cause ($a_1 = c$), in a real system the molar volumes may vary linearly with composition while there is still a large enthalpy of mixing. ΔH depends on $\frac{\partial a_1}{\partial T}$, while V depends on $\frac{\partial a_1}{\partial p}$. In most alloys, for example K-Na, Pb-Sn, Cu-Sn, departures from the ideal case are much more pronounced in the enthalpy of mixing than in the molar volume. In Chapter 5 we shall discuss the case of Cu-Sn in detail.

It can be clearly seen from Equation (1.53) that $a_{ij}(o)$ varies substantially with composition, even in an ideal system. δ is typically about unity, while $\frac{N}{V} k_B T K_T$ is about .02 for most metals and alloys. The amplitude of the first peak in $a_{ij}(q)$ is typically about 3; so the variation of $a_{ij}(o)$ with composition is large on the scale of the rest of the curve. As mentioned earlier, the Percus-Yevick calculations (Enderby and

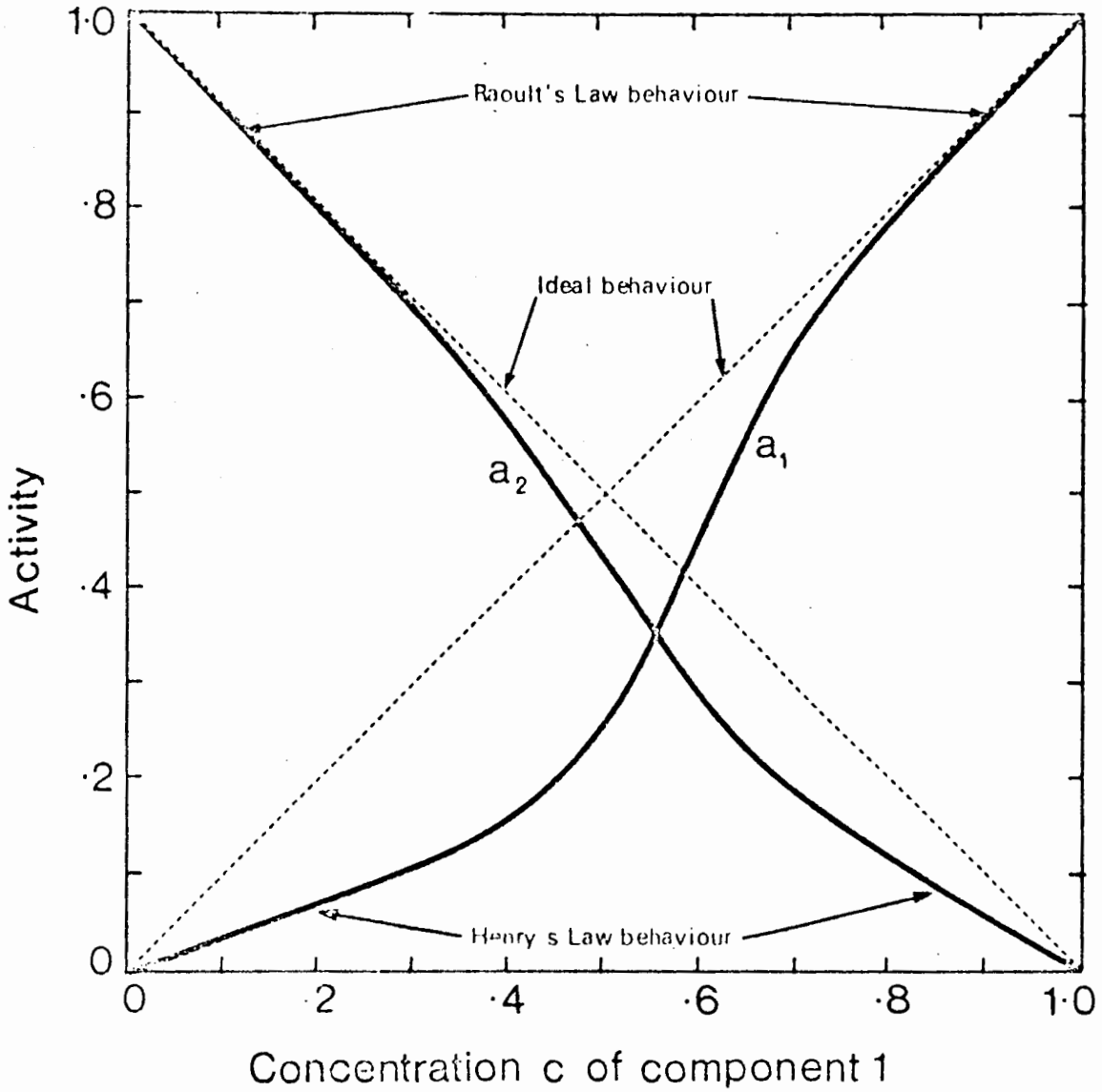

Fig. 1.4. Typical activity versus concentration curves for a liquid binary alloy.

North 1968, Ashcroft and Langreth 1967a) also show significant variations of $a_{ij}(q)$ at q = 0; for the case of Na 50 At. % K Enderby and North's calculation gives $a_{NaNa}(o) = 0.52$, $a_{NaK}(o) = 0.10$ and $a_{KK}(o) = -0.40$; in fair agreement with the case of an ideal mixture (Fig. 1.3), but quite different from the values calculated from actual thermodynamic data, which are still large compared with $\frac{N}{V} k_B T K_T$ (McAlister and Turner 1972). (This indicates that the P-Y hard-sphere model is inadequate for q = 0.) Thus the assumption that $a_{ij}(q)$ is constant is untenable, at least for low-q; however, since the formula (1.18) for the resistivity weights the high-q values of $a_{ij}(q)$ much more strongly than the low-q values, the agreement of the results of North and Wagner (1970) with the measured resistivity is perhaps not so surprising, if in fact their assumption is good for higher q, around the first peak of $a_{ij}(q)$, for example.

In order to evaluate the first terms in Equations (1.39) it is necessary to know the compressibility of the alloy as a function of composition. As before, in the case of the pure metal, it can be determined most easily by measuring the velocity of sound s, and applying Equations (1.8) and (1.10) to get

$$K_T = \frac{\gamma}{\rho_M s^2} \qquad (1.54)$$

The theoretical status of the compressibility will be discussed briefly in the next Section.

1-4 The Compressibility of Liquid Metals

1-4-1 The Compressibility of Pure Liquid Metals

A thorough review of the more rigorous theoretical approaches to the compressibility of liquid metals will be found in McAlister (1971). We shall outline the more salient features.

The compressibility that is usually calculated theoretically for liquid metals is the isothermal compressibility that the liquid metal would have if it were liquid at T = 0°K. The reason for this is that most compressibility calculations start off with an expression for the internal energy of the liquid, E, and the compressibility is taken to be given by

$$\frac{1}{K_T} \equiv \frac{1}{K_0} = V\left(\frac{\partial^2 E}{\partial V^2}\right)_{T=0} \tag{1.55}$$

However, for T ≠ 0 this becomes

$$\frac{1}{K_T}\left(1 + \frac{T}{K_T}\left(\frac{\partial K_T}{\partial T}\right)_V\right) = V\left(\frac{\partial^2 E}{\partial V^2}\right)_T \tag{1.56}$$

and it becomes a difficult task to extract K_T from this Equation. The correction factor can be estimated (McAlister 1971) to be ∿.9 to 1.1, for different metals.

We shall first discuss briefly the compressibility of pure metals, as an introduction. The simplest model of a metal that has any pretense to reality is the jellium model, in which the metal is taken to consist of a free electron gas moving through a uniform background of positive charge, which represents the ions. The compressibility may be easily evaluated (Bohm and Staver 1952, Pines 1963; there are many different but equivalent

derivations of this result)

$$K_{o_{B.S.}} = \frac{3}{2nE_f}, \tag{1.57}$$

where n is the electron density and E_f the Fermi energy. A glance at Table 1.1, giving a comparison of $K_{oB.S.}$ with the observed compressibilities of several metals at their melting points (Webber and Stephens 1968) shows that, although there is some agreement for alkali metals, for most metals agreement is order-of-magnitude only. Usually the compressibility is underestimated. The reason for this, it has been deduced subsequently, is that the B.S. result neglects entirely the short-range order of the liquid, and also the exchange and correlation terms in the electron energy itself. An improved version of the B.S. result has been suggested by Overhauser (1970). Using a simple and elegant approximation for the dispersion relation of a free electron gas, and including exchange and correlation, he obtains for K_o

$$K_{oo} = \frac{3}{2nE_f} \frac{1}{1 - \frac{m\alpha^2}{\pi\hbar^2 k_f}(1+\alpha)} \tag{1.58}$$

where k_f is the Fermi wavevector and α is a calculable term close to .10 for all metals. Table 1.1 also includes K_{oo}. It is clear that Overhauser's correction factor has a significant effect on the theoretical value of K_o, though agreement with experiment is not noticeably improved. Since the inclusion of the exchange and correlation energies of the electron gas clearly has a large effect, however, the agreement of the Bohm-Staver result with experiment for the liquid alkali metals must be regarded as

TABLE 1.1. The Compressibility of Some Pure Liquid Metals: Theory and Experiment

Metal	$K_{T_{exp}}$	$K_{o_{B.S.}}$	K_{oo}	$\frac{N}{V} k_B T_m K_{T_{exp}}$	$\frac{N}{V} k_B T_m K_{T_{Asc}}$
K	38.2	37.2	444	.0254	.0277
Cu	1.49	1.86	3.76	.0211	.0290
Zn	2.50	0.87	1.53	.0145	.0149
Hg	3.75	1.66	3.28	.0050	.0085
Al	2.42	0.55	0.91	.0147	.0115
Sn	2.71	0.67	1.14	.0067	.0068
Bi	4.21	0.64	1.08	.0092	.0058

K_T in units of $\times 10^{-12}$ cm^2/dyne

fortuitous. This conclusion is supported by the work of Shyu and Gaspari (1969) on the velocity of longitudinal sound waves in solid metals. Besides the direct exchange and correlation electron energy contributions, they include a band-structure contribution dependent on the form of the electron-ion interaction. Their results for solids are in quite good agreement with experiment. Now it is a well-known fact that the compressibility of metals changes by only 10-20% at the melting point, which is smaller, for polyvalent metals, than the band-structure contribution to the compressibility. We may therefore argue that the equivalent (in the liquid state) of the band-structure contribution to the internal energy must play an important role in determining the liquid compressibility. Shyu and Gaspari include a direct ion-ion interaction energy, which is also of importance. A similar calculation has been performed by Ashcroft and Langreth (1967b), in a simpler way, giving good agreement with experiment for solid metals. Price (1971) has extended Ashcroft and Langreth's approach to liquid sodium, but to obtain good agreement of the compressibility and energy with experiment the energy must be slightly modified, which has a large effect on the compressibility. Christman and Huntington (1965) performed an ab initio calculation of the energy and compressibility of liquid sodium and potassium, using the APW approach, but although their results were good for sodium, the predicted value for the compressibility of potassium was about 20% too low. Clearly such detailed calculations are very sensitive to errors in input data and details of the electron-ion potential.

In general, the energy of a metal can be written

$$E = E_K + E_X + E_C + E_{i-e} + E_{i-i} \qquad (1.59)$$

where E_k is the electron kinetic energy, E_x and E_c the electron exchange and correlation energies, respectively, E_{i-e} is the ion-electron interaction energy (including band-structure effects) and E_{i-i} is the direct ion-ion interaction energy.

We may separate out the last two terms by using the hard-sphere approximation. This approximation, as mentioned earlier, assumes that the ions are hard spheres, interacting only on contact with each other. Its justification in this context comes from calculating the ion-ion interaction potential $\phi(r)$ corresponding to the last two terms of (1.59), which rises very steeply within a certain radius. The compressibility of such a system can be evaluated in an analytic form using the Percus-Yevick approximation (Wertheim 1963, Thiele 1963). There are other statistical mechanical approximations which connect the inter-ionic potential with the liquid structure (e.g. the Born-Green approximation and the Hypernetted Chain approximation) but these do not lead to an analytic form for the compressibility, and they are, moreover, no more accurate than the P-Y approximation. See (for example) the Supplement by Rice and Gray to Fisher (1964) for full details.

The hard-sphere diameter is defined as σ, so

$$\phi(r) = \infty \qquad r < \sigma$$
$$\phi(r) = 0 \qquad r > \sigma$$

The packing fraction, or the fraction of the total volume occupied by the hard spheres is then

$$\eta \equiv \frac{N}{V} \frac{4\pi}{3} \left(\frac{\sigma}{2}\right)^3 = \frac{\pi}{6} \frac{N}{V} \sigma^3 \tag{1.60}$$

Its maximum value, for a close-packed solid array, is .74. The result from the Percus-Yevick theory for the isothermal compressibility, this time for $T \neq 0$, is

$$K_T = \frac{V}{N k_B T} \frac{(1-\eta)^4}{(1+2\eta)^2} \tag{1.61}$$

Comparison between the structure factors calculated from this P-Y approximation and the observed structure factors gives $\eta = .45$ at the melting point of most metals. a(o), which is equal to $\frac{Nk_B TK_T}{V}$, is thus seen to be a constant, .253.

That a(o) is a constant at T_m can be deduced more generally from Lindemann's Melting Law (Enderby and March 1966). This Law states that the Debye temperature $\theta_D \equiv \hbar\omega_D$, where ω_D is the Debye frequency, is related to the melting temperature T_m in this way

$$\theta_D \approx b \left(\frac{NT_m}{m}\right)^{1/2} \left(\frac{N}{V}\right)^{1/3} \tag{1.62}$$

where b is a constant which varies, in practice, by about 20% from metal to metal (Pines 1964). Now θ_D can also be expressed, in the Debye approximation $\omega = sk$, as

$$\theta_D = \frac{\hbar}{k_B} s \left(6\pi^2 \frac{N}{V}\right)^{1/3} \tag{1.63}$$

Hence $$\frac{N T_m}{V} = b' \rho_M s^2$$

where b' is a constant.

Thus, using (1.8) we have

$$\frac{N k_B T_m}{V} K_s = \text{constant} \tag{1.64}$$

Since $\gamma \approx$ const ≈ 1.15 for most metals,

$$\frac{N k_B T_m}{V} K_T = \text{constant} = C \tag{1.65}$$

Since the constant b in Lindemann's Law has been squared, the constant C in (1.65) has, in practice, at least twice the variation with the substance involved that b has, which amounts to ~40% for C. Further variation of C is caused by the fact that the velocity of sound has been taken to be that in the liquid, while one should really use the value in the solid state, usually about 10% higher, and this difference varies from substance to substance. Typical values of $\frac{N}{V} k_B T_m K_T$ are to be found in Table 1.1. They are almost always lower than the Percus-Yevick hard sphere result of .253, which indicates that this theory overestimates the compressibility.

Thus (a) the free-electron theory underestimates the compressibility and (b) the hard sphere theory overestimates it. Ascarelli (1968) proposed a combination of the two theories, whose parameters were chosen to

satisfy the "zero-pressure condition"; that is, $P = \left(\frac{\partial E}{\partial V}\right) = 0$ at the melting point. This condition corresponds to the experimental fact that most metals melt rather than sublime at normal (low) pressures. Ascarelli proposes the simple model for the free electron gas

$$E_e = E_K + \text{const.} \left(\frac{ZN}{V}\right)^{1/3} \tag{1.66}$$

where E_k is the electron kinetic energy and the second term includes the exchange and correlation energy. The Percus-Yevick result for the pressure of a hard sphere gas is added to the pressure of the electron gas calculated from (1.66), and the zero-pressure criterion is applied to evaluate the constant. The expression thus found for the pressure is again differentiated with respect to volume, with the result

$$a_{Asc}(0) = \frac{N k_B T_m}{V} K_{T Asc} = \frac{1}{27 + \frac{2}{15} \frac{Z E_f}{k_B T_m}} \tag{1.67}$$

where Z is the number of free electrons/atom of the metal in question. How these values agree with experiment is shown in Table 1.1. The worst deviations of the simple hard sphere model and the jellium model are corrected, but the results are very sensitive to the value of the packing fraction chosen. McAlister (1971) gives the example of Rb, where a change in packing fraction from .45 to .46 changes the predicted a(o) by 10%. Since there is no entirely rigorous way of estimating the packing fraction, depending as it does on the ions being treated as hard spheres, this theory is at best suggestive, and by no means the last word on the subject. Furthermore, there is disagreement with experiment for the noble metals,

which suggests that the presence of the d electrons should be taken care of somehow.

Faber (1972) has avoided the problem inherent in calculations of the compressibility via the cohesive energy; that is, the inaccuracy involved when the second derivative with respect to volume is taken of the cohesive energy, whose volume dependence is not very well known. Faber's calculation evaluates the change in energy of the metal when it is disturbed by a long-wavelength acoustic wave. The total volume is assumed to remain constant, and the effect of the sound wave on the structure factor is calculated. The result for the compressibility has the form

$$K_T = \frac{3}{2n E_f} f_1 f_2 f_3$$

where f_1, f_2 and f_3 are functions involving the undisturbed structure factor and the electron-ion pseudopotential. While these factors can be calculated, there is still enough uncertainty about the best pseudopotential to use that one cannot say the validity of this theory has yet been tested.

To summarize then, the Ascarelli model is the most successful so far for the calculation of liquid metal compressibilities. Other more exact theories are far more cumbersome at present, and the agreement with experiment is little better than Ascarelli's.

It is worth commenting at this point that there exists a strong

correlation between the velocity of sound in a liquid metal, and the combination of terms $b = \sqrt{\frac{a^2\gamma}{M}}$, where γ is the surface tension, M is the atomic mass and a is the cube root of the atomic volume. If b is plotted against s, for different metals, all the metals (with the exception of the alkali metals) appear to lie on a universal curve (Fig. 1.5) with little scatter. Thus if the sound velocity is known, the surface tension may be deduced, to ±10%, and vice-versa. What theoretical significance this correlation has is uncertain, but it is clear that both the surface tension and sound velocity are closely related to the binding forces at work in a liquid.

1-4-2 The Compressibility of Liquid Alloys

Now we turn to the even less tractable problem of the calculation of the compressibility of alloys. Since for most alloy systems the electrons continue to manifest nearly free-electron behaviour, we may evaluate the Bohm-Staver result (1.77), but since it is usually so wrong at the end points, it can hardly be expected to agree at intermediate compositions. However, it will reflect changes in electron density due to non-ideal alloying and thus perhaps echo corresponding departures from the ideal in the compressibility. The ideal compressibility is given by Equation (1.72); in fact this behaviour has been observed in several alloys (Khodov 1960), such as Pb-Sn, Pb-Cd and Bi-Cd, which have very simple phase diagrams without intermetallic compounds in the solid state, and nearly ideal molar volumes. Curiously enough, the system Na-K does not exhibit ideal mixing in the compressibility, a fact perhaps related to the non-ideal activity curves for this alloy (see McAlister and Turner 1972).

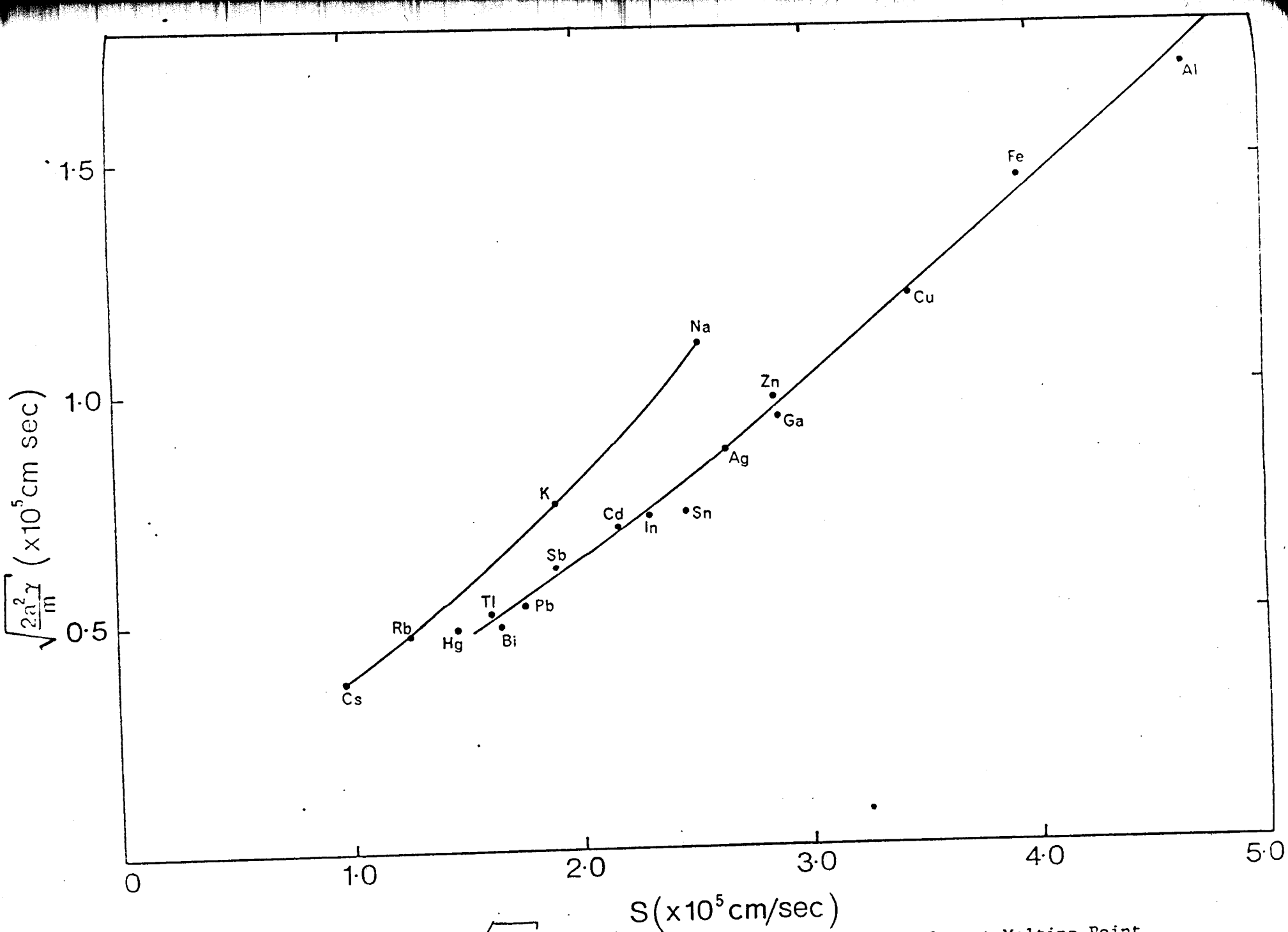

Fig. 1.5. Correlation between $\sqrt{\frac{2a^2\gamma}{M}}$ and Velocity of Sound in Liquid Metals, at Melting Point.

The Percus-Yevick theory may also be worked out for a binary mixture of hard spheres, with radii σ_1 and σ_2 (Lebowitz 1964). The packing fraction is now written

$$\eta = \frac{\pi}{6}\frac{N}{V}\left(c\sigma_1^3 + (1-c)\sigma_2^3\right) \tag{1.68}$$

and if σ_1 and σ_2 are defined so that their ratio, $\alpha = \frac{\sigma_1}{\sigma_2}$, is less than unity, then (Ashcroft and Langreth 1967a)

$$K_T = \frac{V}{Nk_BT}\,\frac{(1-\eta)^4}{(1+2\eta)^2 - \Delta} \tag{1.69}$$

where $$\Delta \equiv \frac{3c(1-c)\eta(1-\alpha)^2}{c+(1-c)\alpha^3}\left\{(2+\eta)(1+\alpha) + \frac{3\eta\alpha((1-c)\alpha^2+c)}{c+(1-c)\alpha^3}\right\}$$

Evaluation of (1.69) is not difficult provided one knows the concentration dependence of η and α. And therein lies the problem. One normally considers changes of composition at constant temperature, so for some alloy systems the temperature will be well above the melting point; thus η cannot be taken as .45 in general. The best way of finding η as a function of composition and temperature is to compare calculated Percus-Yevick hard sphere partial structure factors to the observed partial structure factors at each concentration, and to use the values of η and α that give the best fit. This would be a lengthy undertaking; and in any case the P-Y hard-sphere compressibility is known to be rather inaccurate for the pure metals.

The Ascarelli approach can also be extended to alloys, since it is a synthesis of the free-electron and Percus-Yevick approaches. However,

the same problem applies as in the last theory discussed; how does one determine η as a function of composition? Furthermore, in using the zero-pressure criterion at the melting point, which temperature does one take as the melting point? In general, an alloy has a temperature range between the homogeneous liquid and the solid state that may extend for 200°C. However, the change of η with temperature may be estimated (Ascarelli 1968, Jarzynski et al. 1969) and if one assumes a packing fraction of .45 at the liquidus temperature for each alloy (the only assumption one can reasonably make at this time), one could make a rough estimate of η if the temperature in question was not too far above the liquidus temperature. Furthermore, if the constant in (1.66) could be evaluated from first principles (e.g. by using Overhauser's work (1971)) the zero-pressure criterion need not be used. We shall discuss this approach further in Chapter 5.

1-4-3 The Copper-Tin System

Since many of the copper-tin alloys have a high liquidus temperature, the velocity of sound in this system has not previously been measured. However, fairly accurate density data exist (Bornemann and Sauerwald 1922, Watanabe and Saito 1972), the activity of both components has been accurately measured (Alcock et al. 1969), the resistivity has been accurately measured (Roll and Motz 1967), and, most important, it is on this system that the majority of work has been done in determining the partial structure factors using neutron and X-ray diffraction (Enderby et al. 1966, Halder et al. 1969, North and Wagner 1970, and others). Furthermore, the Hall coefficient has been measured (Busch and Güntherodt

1967, Enderby et al. 1967) with conflicting results for high-Sn alloys, and the optical constants have been measured by Comins (1972). An investigation of the velocity of sound as a function of composition could throw light on (a) the structure factor, and (b) the electronic behaviour of high-Sn alloys of the Cu-Sn system. In Chapter 5 we show, with the aid of other thermophysical data, that much can be said about the zero-wavevector limit of the partial structure-factors, and also that there is no evidence from the compressibility to support the conclusion of Enderby et al. (1967) that the number of free electrons per atom is depleted at low Cu concentrations by the formation of bound states.

As regards the theoretical calculation of the compressibility of Cu-Sn alloys, little can be said in this thesis. Attempts to go beyond the simple theories outlined in 1-4-1 would constitute a massive undertaking. See Chapter 5.

CHAPTER 2

REVIEW OF EXPERIMENTAL TECHNIQUES

2-1 Conventional Techniques

The usual methods of measuring the velocity of sound in liquids have been thoroughly reviewed by McSkimin (1964) and Gitis and Mikhailov (1966a). The most popular method at present is to connect a piezo-electric transducer, either directly or via a cooled delay line, to the liquid to be studied. Radio-frequency pulses a few microseconds long are then applied to the transducer, which may be of X-cut quartz or a lead zirconate titanate ferroelectric ceramic, at its mechanical resonance frequency. Acoustic r.f. pulses are thus transmitted into the liquid, where they are either reflected by a flat reflector plate and detected with the same transducer that was used to generate them, or transmitted into another detection transducer, via a delay line if necessary. The time of flight of the acoustic pulse through the liquid may be measured in a number of different ways, the crudest of which is to use a calibrated oscilloscope timebase. If the length of the liquid specimen is known, the velocity of sound may immediately be deduced. Other, more sophisticated, methods of measuring the time of flight include: (a) the sing-around technique, where the detected acoustic pulse is used to trigger the next pulse produced by the r.f. generator, and thus the time of flight is given simply by the inverse of the observed pulse repetition frequency; (b) the pulse superposition technique, whereby the pulse generator is designed to produce two pulses in rapid succession, in such a way that the echoes across the liquid metal from the first pulse are cancelled out by the echoes from the second pulse.

The time between the incident pulses, which are normally of large amplitude (up to 2KV) and are undistorted, can be measured accurately, and at cancellation this time is equal to twice the time of flight of the pulse in the liquid. Other methods, such as comparison with a standard liquid delay line (mercury is used as a standard) (Hill and Ruoff 1965) have been employed, and the accuracy claim is usually about 1 part in 10^4. Work by different experimenters on the same metal, however (see Gitis and Mikhailov 1966a) suggests that this figure does not include systematic errors (which will be discussed later), and the accuracy should be taken more usually as a few parts in 10^3.

Continuous wave methods have also been employed normally in the form of an acoustic interferometer (McAlister 1971, Pierce 1925; for an extensive bibliography see Del Grosso et al. 1954). The method consists in setting up acoustic standing waves in the liquid at the appropriate spacings between the transmitting surface and a reflector. The transducer is operated at resonance, and (for instance) the output of a marginal oscillator driving the transducer is measured as a function of reflector position. In this way a large number of standing wave resonances, spaced $\lambda/2$ apart, where λ is the wavelength of the sound in the liquid, may be observed. The virtue of this method is that the time-of-flight measurement is replaced by a measurement of frequency; $s = f\lambda$: and frequency is very easy to measure. McAlister (1971) claims an accuracy of 2 parts in 10^4, an estimate supported by other careful workers using the low-melting-point metals he studied (Na and Hg).

As one might expect, mercury has been measured most often and with greatest accuracy; but for metals with progressively higher melting points

one finds larger and larger discrepancies between the results of different workers, particularly above 500°C. There is a simple reason for this. No piezoelectric material has a Curie temperature higher than 550°C, this being the value for quartz. As a result, at these temperatures the transducer must be separated from the melt by a cooled delay line. This makes the straightforward continuous wave interferometric technique quite impracticable, and the effect on the pulse technique is also serious. There are four major problems.

(1) The delay line attenuates the acoustic wave before it enters the melt. For fused quartz delay lines this is not much of a problem, because the attenuation in quartz is not strongly temperature-dependent, but for metals like magnesium that react with quartz, one has a problem finding inert refractory delay line material with low acoustic attenuation. (See, however, Kurtz and Lux (1969) who use the metal to be studied as the delay line, melting only the top end, and cooling the rest of the delay line efficiently so that a transducer may be applied to it.)

(2) When the delay line becomes long, there are significant diffraction and wave-guide effects, which cause the shape of the acoustic pulse to become distorted. This diminishes the accuracy of a number of methods of measuring the time of flight.

(3) Mode conversion from longitudinal wave motion (the type used for ultrasonic studies in liquids) to transverse waves along the lateral surfaces of the delay lines gives rise to spurious echoes at the transducer. In poor observing conditions these echoes can obscure the signal of interest completely, as was observed repeatedly in the present experiment

when the transducer was used as a detector. This problem may be circumvented somewhat using a two-transducer technique, so that the liquid itself filters out some of the spurious echoes as the signal passes into another delay line, but it is hard to cure entirely. Roughening the lateral surfaces of the delay line can help considerably (McSkimin and Fisher (1950) ground a broken screw thread into the sides of the quartz delay line they used).

(4) For acoustic energy to be transmitted into the liquid metal, the liquid must wet the end of the delay line with which it is in contact. In all cases this puts severe demands on cleanliness in preparation of experimental specimens, and in some cases it is found that the chosen delay line material is almost incompatible with the metal used, so that a few molecular layers of oxide on the metal surface in contact with the delay line prevents wetting altogether.

2-2 Electromagnetic Detection Technique

The problem with piezoelectric transducers is that they do not work at high temperatures. However, there are methods of generating and detecting acoustic waves that do work, in particular the method of electromagnetic generation and detection (Randall et al. 1939, Houck et al. 1967). A phenomenological theory that explains this effect quantitatively has been published elsewhere (Turner et al. 1969); we shall now briefly outline that argument.

Consider a semi-infinite metallic slab, in the coordinate system of Fig. 2.1. Let an electromagnetic wave of angular frequency ω, polarized with the magnetic vector along y, fall upon the surface of the metal, at normal incidence. A current distribution $\vec{j}(z)$ is set up near the surface

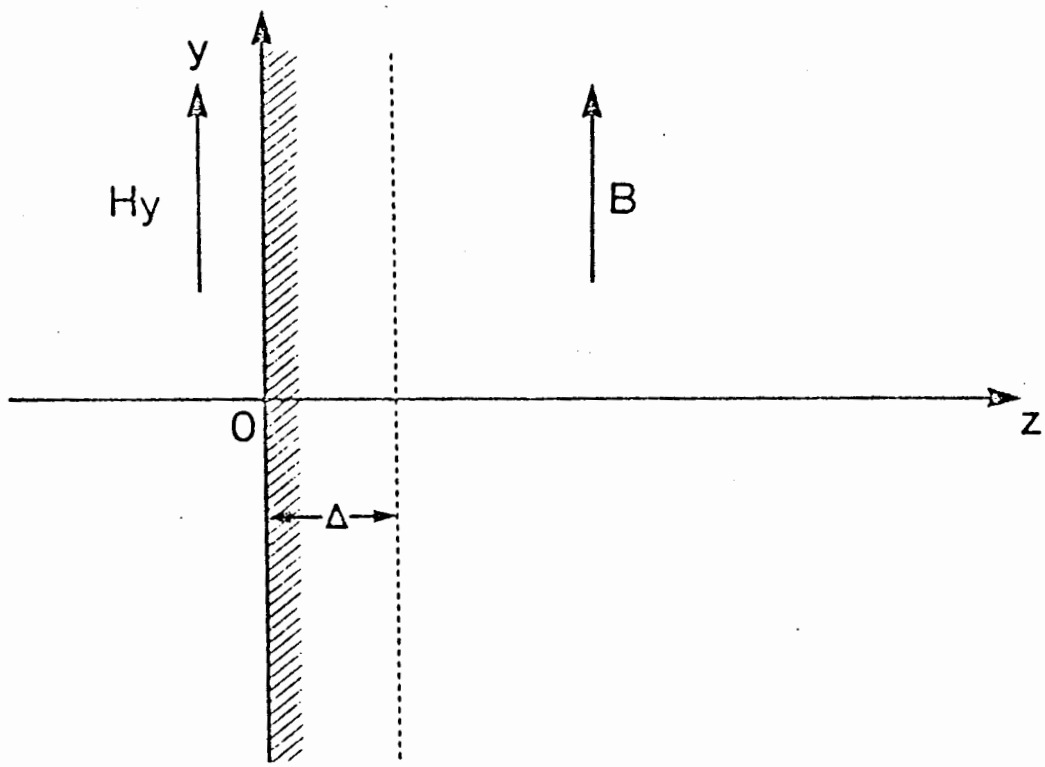

Fig. 2.1. Configuration of electromagnetic fields and metal surface used in calculating the electromagnetic generation of acoustic waves. Hy is the magnetic component of an r.f. electromagnetic wave incident from the left. B is the static magnetic field.

of the metal in such a way that the alternating fields are reduced effectively to zero within a distance Δ of the surface, where Δ is of the order of the skin depth. The total current contained in the surface is in the x direction and may be written

$$\vec{I}_o = \int_o^\infty \vec{j}(z)\,dz \tag{2.1}$$

The amplitude of $\vec{I}_o$ is related to the amplitude of the alternating magnetic field at the surface of the metal, $\vec{H}(o)$, by the expression

$$\vec{I}_o = \frac{c}{4\pi}\vec{H}_o(o) \tag{2.2}$$

The application of a steady magnetic field $\vec{B}_o$ in the direction parallel to the y axis, that is, to the surface, will induce a Lorentz force on the electrons moving in the surface. One can write for the total force per unit volume acting on the electron system

$$\vec{F}(z) = \frac{1}{c}(\vec{j}(z) \times \vec{B}_o) \tag{2.3}$$

If the current distribution is confined to the surface, we may write to a good approximation

$$\vec{F}(z) = \frac{1}{c}(\vec{I}_o \times \vec{B})\,\delta(z) \tag{2.4}$$

where $\delta(z)$ is the Dirac delta function.

Since the direction and magnitude of $\vec{I}_o$ is fixed (the interior of the

metal must be shielded from the applied alternating magnetic field), this force must also be communicated to the lattice, by whatever microscopic process is appropriate. Thus an acoustic wave may be set up in the metal. By Equation (2.4) the force is normal to the surface; thus a compressional wave is induced.

The reverse effect also takes place. The simplest explanation is to consider the movement of a conducting wire across a magnetic field; an electric field is induced between the ends of the wire. More rigorously, consider the situation of Fig. 2.2. We make the basic assumption that the electrons move with the lattice; that is, there is no net current in the surface. This assumption is justified in the paper by Turner et al. (1969) subject to the two conditions

$$\frac{\Delta}{\lambda} \ll 1 \tag{2.5}$$

$$\frac{\omega}{4\pi}\rho \ll 1 \tag{2.6}$$

where ρ is the resistivity of the metal. These conditions are easily met for f < 50MHz; the first is far more stringent than the second.

If the electrons move with the ions they must experience a Lorentz force, $\vec{F}_1$, where

$$\vec{F}_1 = -\frac{e}{c}(\vec{u} \times \vec{B}_0) \tag{2.7}$$

(here $\vec{u}$ is the electron velocity, equal to the ion velocity by our assumption above). But in a reference frame affixed to the lattice the

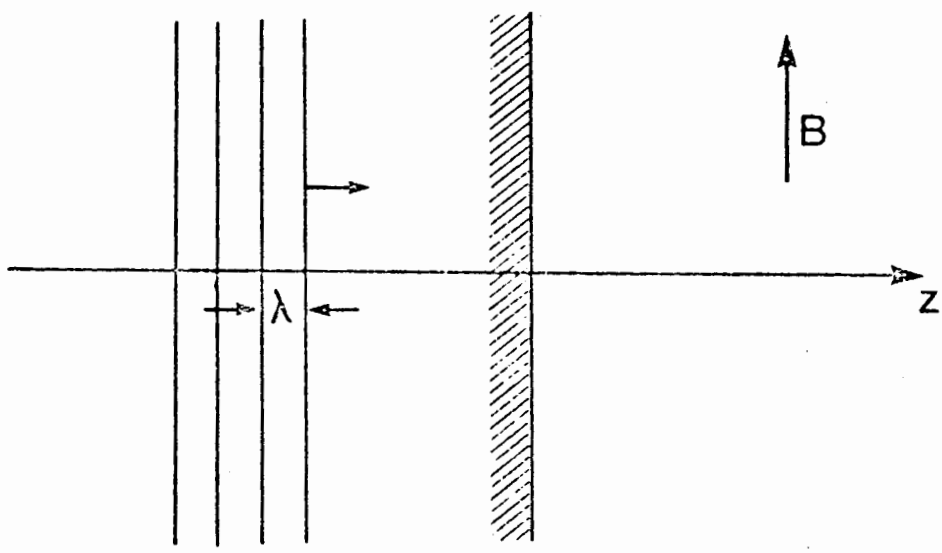

Fig. 2.2. Configuration of acoustic field and metal surface used in calculation of electromagnetic detection of acoustic waves. The acoustic wave, incident from the left, has wavelength λ and amplitude ξ.

electrons are at rest; thus an electric field must be set up in the metal in just such a way as to exactly cancel $\vec{F}_1$. On transforming back into the laboratory reference frame, and neglecting terms of order $(u/c)^2$, this electric field in the metal will be given by

$$\vec{\Delta E} = -\frac{\vec{u}}{c} \times \vec{B}_0 \qquad (2.8)$$

In particular, at the surface of the metal there will be an alternating electric field whose amplitude is proportional to the surface displacement velocity $\vec{u}(o)$. According to Maxwell's equations the tangential components of any electric vector must be continuous at the interface between two media; consequently an electromagnetic wave must be radiated from the slab whose electric vector is given by

$$\vec{\Delta E}(o) = -\frac{1}{c}\left(\vec{u}(o) \times \vec{B}_0\right) \qquad (2.9)$$

Thus a longitudinal acoustic wave reaching the surface of a liquid metal, with a static magnetic field parallel to the surface, will radiate an electromagnetic wave into space, which can be detected with a suitably designed antenna.

Under the conditions stated, the theory outlined here gives the same results as the more complex microscopic theories presented by Quinn (1967), Kravchenko (1969) and others (see the bibliography in Lyall (1970) for a complete list of references).

If we detect the electromagnetic wave with a coil of n turns, with a

cross-section of A cm^2, it is easy to see (assuming that the radiated field is constant) that the induced voltage V is given by

$$V = \left(\frac{\omega}{c}\right)^2 B_0 A z n \qquad (2.10)$$

where z is the ionic displacement associated with the acoustic wave. For a static magnetic field B of 10kG, a pickup coil of area 1 cm, and a frequency f = 10MHz, it is clear that to obtain a detected voltage of 10^{-6}V (which is large enough so that simple electronics may be employed), we need an ionic displacement of $\sim 10^{-7}$ cm. Using a ceramic piezoelectric transducer driven by a high-voltage r.f. generator ($\sim$1KV) this is not hard to obtain, if losses between the transducer and the metal are not too severe, but for a quartz transducer, with an efficiency of perhaps 1/10 of that of a ceramic transducer, the signal is near the borderline of detectability. In terms of the difficulties outlined in Section 2.1, such as wetting and delay line problems, it would be preferable to use the electromagnetic technique both for generation and detection, but the efficiency of the technique is unfortunately very low (a factor of $\sim 10^{-3}$ poorer than piezoelectric transducers) so electromagnetic generation and detection is not feasible except under very favourable conditions (see Gaerttner and Maxfield 1971).

In order to use the electromagnetic detection technique at high temperatures, then, we must introduce the acoustic waves into the liquid using a piezoelectric transducer, preferably ceramic. A delay line separating transducer and melt is necessary to enable the transducer to be cooled below its Curie point (about 300°C for lead zirconate titanate

transducers). This means that problems (1) and (4) of Section 2-1 still apply; the delay line will attenuate the sound wave and the wetting of the generating surface by the liquid metal may be poor. However, since the acoustic wave is detected directly at the surface of the liquid metal, problems (2) and (3) do not arise and we may expect to observe a very clean acoustic signal. The limitations of this technique are solely connected with the types of refractory material that can be employed as a delay line. A small coil sheathed in an electrically insulating refractory material is all that is needed to detect the acoustic wave, provided the furnace containing the liquid metal is placed between the poles of an electromagnet producing about 10kG.

2-3 Refractory Materials

If a vacuum furnace is used, there is no problem finding suitable materials for the majority of the heated parts. The second and third series of transition metals supply several high-melting point, low vapour pressure metals: Nb, Mo, Ta, W, Re, Ir, Pt, for example. Each of these has a melting point above 1800°C. Thus they are suitable for use as heat shields, pickup coils, resistive heating elements, and so on. Problems arise, however, with those components that are in contact with the liquid metal. Most liquid metals are highly reactive, particularly above 1000°C. In the course of developing the apparatus for this experiment we investigated alumina, silica, boron nitride and sapphire. All four were at some point employed as a delay line, and their acoustic properties were qualitatively observed. (Metals, in general, have a higher acoustic attenuation than ceramics; see, however, Kurtz and Lax (1970).)

(a) Boron Nitride. This material is usually obtained in a hot-pressed form, possessing strength comparable to graphite (which it resembles in many ways, though it is an insulator and not a conductor), density almost that of a single crystal, and easy machinability. It was tried for the latter reason. The nominal maximum temperature at which BN can be used is 3000°C. The porosity is very low (for a sintered ceramic), a few millimeters being sufficient to provide a vacuum seal. The velocity of longitudinal acoustic waves was measured to be $6.65 \pm .05 \times 10^5$ cm/sec; thus the acoustic impedance $Z = \rho_M s = 1.39 \times 10^6$ gm/sec cm is close to those of most liquid metals, about 2×10^6 gm/sec cm. The reflection coefficient, $\left|\frac{Z_1 - Z_2}{Z_1 + Z_2}\right|^2$, is fairly small for most liquid metals, suggesting that a large fraction of the acoustic power would be transmitted into the liquid metal from the delay line. BN is chemically very inert, and was not attacked by liquid Hg, Fe, Ni, Sn or Cu, we found.

The results for this material were rather disappointing. The disadvantages found were these:

(1) The acoustic attenuation was high (on the order of 1db/cm at 10MHz) and increased with temperature, owing to the porosity of the material. Furthermore, it increases rapidly with frequency.

(2) Difficulty was experienced even at room temperature in getting Hg to wet the BN surface. A coat of Nonaq grease was found to help; but the indication was that BN is not very wettable. It appears to be wetted by liquid Ni, however.

(3) BN absorbs water slowly when left in air. As a result, if it is heated rapidly, it spalls and cracks, becoming completely useless as an

acoustic delay line.

(4) At about 1200°C impurities (mostly B_2O_3) in the BN evaporate and cover the inside of the furnace with a sticky black coating. As one would expect, this makes the vacuum much poorer. However, BN that has been heat-treated at above 1400°C for some time becomes clean in this respect.

(b) Alumina. This polycrystalline form of Al_2O_3 is well-known for its excellent refractory properties. It is strong and very hard, and melts at 2050°C. The velocity of longitudinal acoustic waves in 99.8% pure alumina was measured to be $1.05\pm.01\times10^6$ cm/sec, at room temperature (20°C). Its acoustic impedance is then $3.98\times10^6 \frac{gm}{cm\ sec}$, also of the same magnitude as those of most liquid metals. In its polycrystalline form we found one major disadvantage to its use as a delay line at high temperatures, however. Though the acoustic attenuation is low below 1000°C, less than .1db/cm at 10MHz, at ∿1100°C the attenuation increases exponentially with temperature, so that by 1250°C no echo from the end of a 25 cm long delay line could be observed at all, at ∿10MHz. This can tentatively be explained by thermal activation of the grain boundaries of the microcrystallites forming the alumina so that their motion absorbs the acoustic wave. A maximum in the internal friction for low frequencies at these temperatures has been explained in this way.

(c) Sapphire. In an attempt to circumvent this problem a rod of sapphire 25 cm long was employed as a delay line. Leuco-sapphire, pure single-crystal Al_2O_3, was used, though the orientation of the crystal with respect to the axis of the rod was unknown. Unfortunately, though this material is highly chemically inert and does not appear to possess the exponential

rise in acoustic attenuation at 1100°C of polycrystalline alumina, it is not very resistant to thermal shock, and care must be taken in the design of a furnace to eliminate severe thermal gradients along the length of the sapphire. If this is not done, the sapphire cracks at the point of maximum thermal gradient.

(d) Silica. Fused quartz, or silica, is very widely used as an acoustic delay line. Its chief limitations are its reactivity (it is rapidly attacked by liquid Mg, for example) and its low softening point (1300°C) and melting point (1776°C). The acoustic attenuation is very low, however; although it increases somewhat with temperature, at 1000°C it is still $\sim$.05db/cm. Wetting is a problem for many liquid metals (Jarzynski and Litovitz 1964, for example) so that extreme cleanliness in sample preparation is necessary, but for the Cu-Sn system studied in this experiment silica was found to be ideal; a minimum of precautions was necessary in order to obtain wetting, and since Cu melts at 1083°C there was no danger of melting the silica. Neither Cu nor Sn attacks silica, although liquid Cu tends to embrittle it considerably. The velocity of longitudinal acoustic waves in silica at room temperature is 5.968×10^5 cm/sec, and the acoustic impedance Z is 1.31×10^6 gm/cm sec, close to that of boron nitride.

CHAPTER 3

DESCRIPTION OF EXPERIMENT

3-1 Introduction

As described in Section 1-3, it was decided to measure the velocity of sound in copper-tin alloys. From the considerations of Sections 2-1 and 2-2, the electromagnetic detection technique was employed. The acoustic waves in the form of r.f. pulses were generated by means of a Clevite PZT-4 lead zirconate titanate ceramic transducer, and transmitted along a fused silica delay line into the molten alloy. They were then detected using a platinum pickup coil, protected by a silica sheath. An electrical interferometric technique was used to measure the wavelength of the acoustic waves, and their frequency was monitored using an auxiliary cw oscillator and a frequency counter. The velocity was determined as the product of the wavelength and the frequency. The temperature of the alloy was measured with the aid of a tungsten 5% rhenium-tungsten 26% rhenium thermocouple. A cylindrical graphite resistive heating element provided a fairly uniform temperature in the melt (the temperature gradient was less than 2%), inside a water-cooled stainless steel furnace assembly. Since the vapour pressures of copper and tin are less than 10^{-1} torr below 1500°C, the furnace was maintained under vacuum to avoid contamination of the liquid metal.

3-2 Apparatus

3-2-1 Crucible and Delay Line

The crucible and delay line assemblies (Fig. 3.1a) were constructed from high grade fused quartz rod and tubing. No air bubbles could be seen in the quartz rods. Ten assemblies were made, so that the majority of the eleven alloys used could be formed, and their sound velocities measured, in the same crucibles. The delay lines were made 25 cm long so that a considerable length (~10 cm) could be cooled with a water jacket; however, radiant heat was a problem, since fused quartz transmits infrared radiation very well. The diameter and height of the crucible were determined by the need to be able to raise and lower a probe of about 1 cm diameter through a distance of about 2 cm while the end remained in the liquid metal.

3-2-2 Probe and Pickup Coil

Dipping into the crucible (see Fig. 3.1b) is a probe, consisting, at the top end, of a hollow brass cylinder; from which depend (a) a stainless steel tube, to provide a smooth bearing surface for an O-ring so that the probe can be raised and lowered without spoiling the vacuum, and also to support the silica probe sheath; (b) a molybdenum rod, to which is attached the coil former. The coil former is made from boron nitride, chosen for its easy machineability, which made it possible to put grooves in the sides of the former to separate the turns of wire. The coil itself consists of 10 turns of #28 gauge platinum wire, one end of which is wound tightly around the lower end of the molybdenum rod to provide a ground contact. The other end of the platinum wire goes

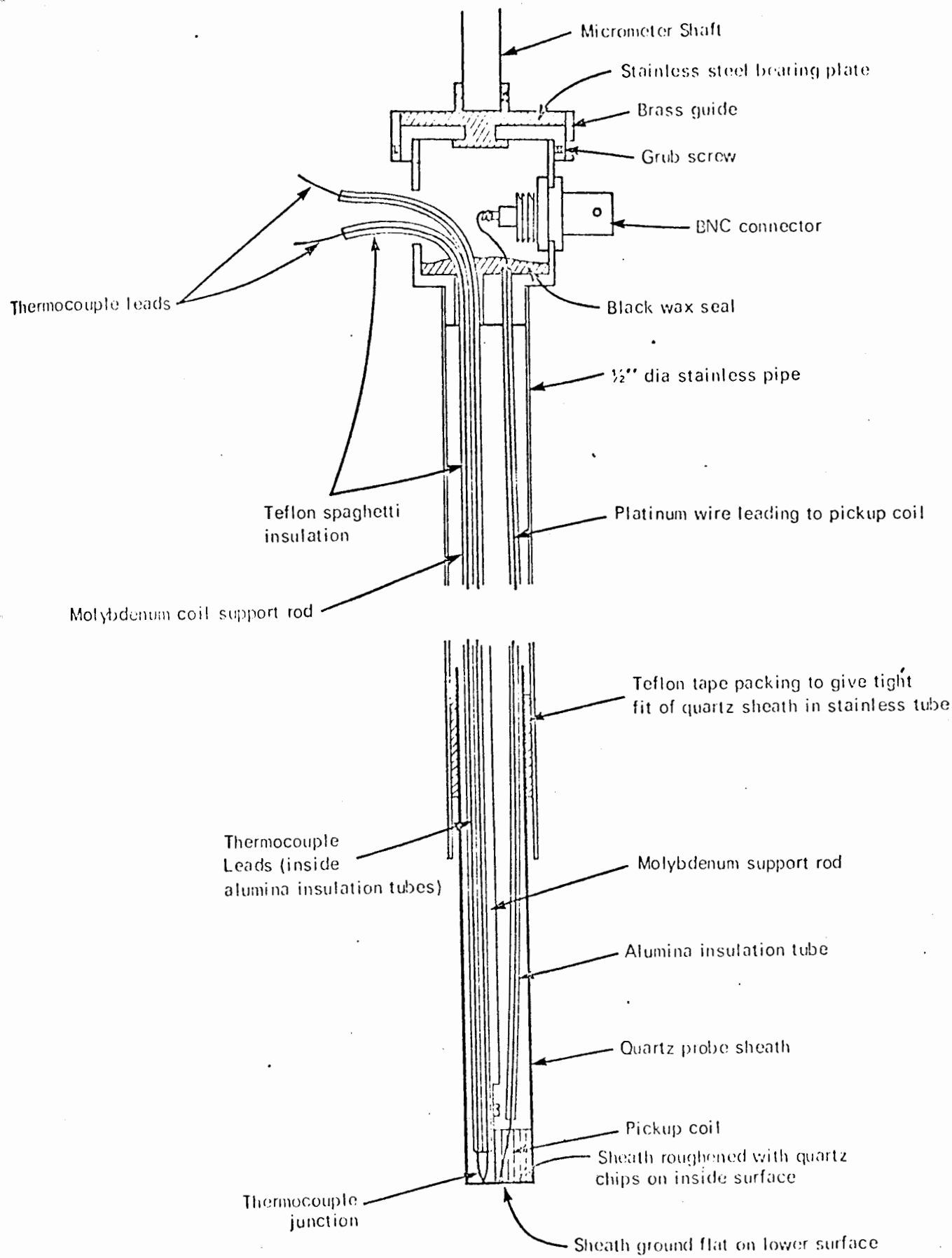
Micrometer Shaft
Stainless steel bearing plate
Brass guide
Grub screw
BNC connector
Thermocouple leads
Black wax seal
½" dia stainless pipe
Teflon spaghetti insulation
Platinum wire leading to pickup coil
Molybdenum coil support rod
Teflon tape packing to give tight fit of quartz sheath in stainless tube
Thermocouple Leads (inside alumina insulation tubes)
Molybdenum support rod
Alumina insulation tube
Quartz probe sheath
Pickup coil
Sheath roughened with quartz chips on inside surface
Thermocouple junction
Sheath ground flat on lower surface

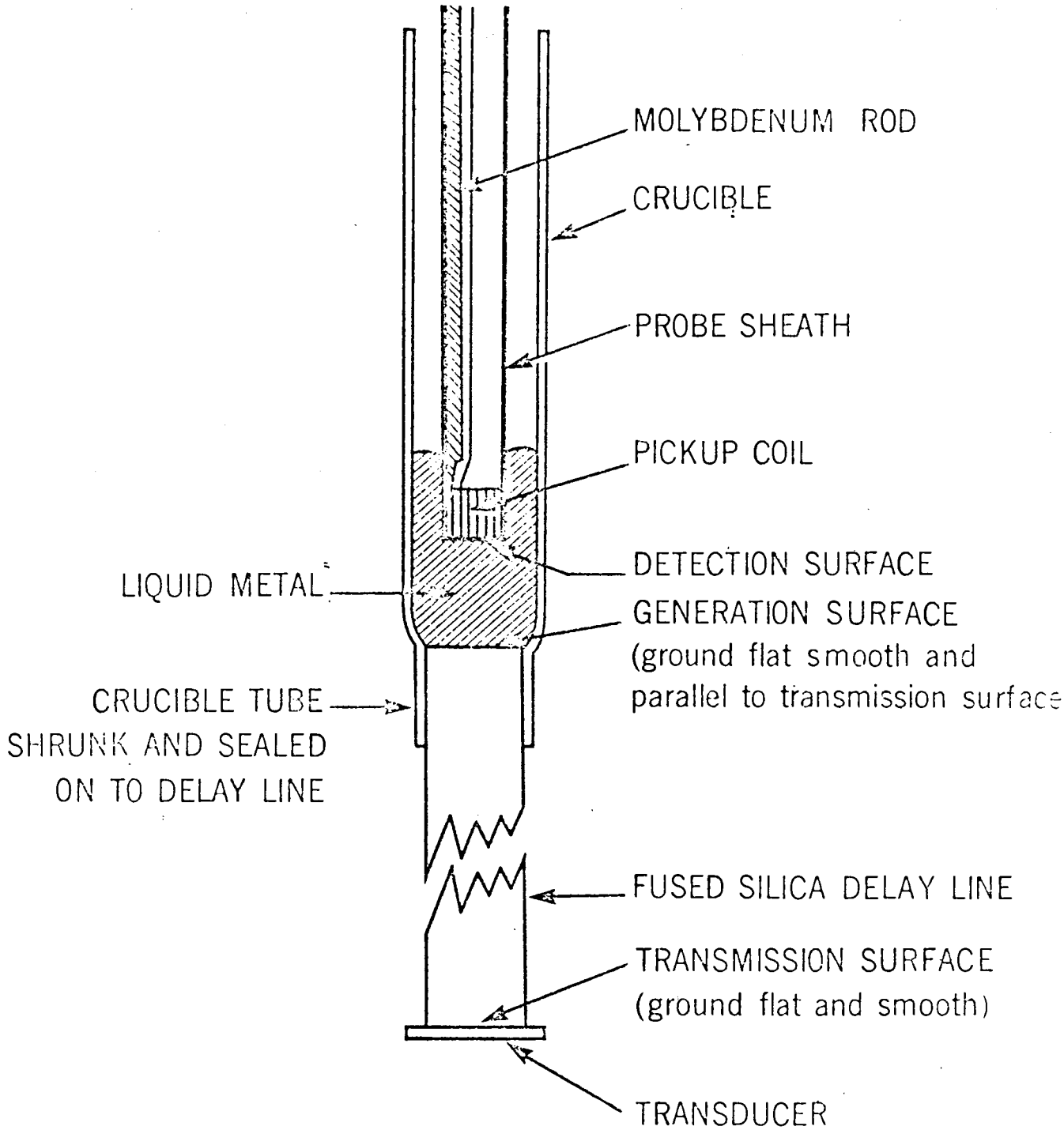

Fig. 3.1b. DELAY LINE

through a length of alumina tubing, for electrical insulation, and at the top (cooler) end a length of teflon tubing, for the same reason. It then emerges through a black wax seal into the brass cylinder, where it is soft-soldered to a BNC connector. The coaxial geometry of this connection to the coil enables much of the electromagnetic cross-talk from the transducer to be eliminated. The thermocouple is also contained inside the probe sheath, the individual wires being similarly insulated with alumina and teflon tubing. It was found that an a.c. ground, consisting of a .01 μf capacitor between one of the thermocouple leads and the body of the probe, prevented the thermocouple leads from acting as an antenna; thus the electromagnetic crosstalk was greatly decreased. The thermocouple junction was formed by a spot-weld. The fused quartz sheath was held in the stainless tube by wrapping teflon tape around it and jamming it into the stainless tube. This method gives a very secure and rigid joint, which had the virtues of withstanding fairly high temperatures, and of being demountable, to allow access to the pickup coil. The inside of the lower end of the quartz sheath was roughened to eliminate acoustic reflection from this surface by fusing a few ∿1/10 mm diameter grains of quartz into it, and the outside was ground smooth and flat using a diamond wheel. Since the wavelength of sound at these frequencies in liquid metals is ∿.3 mm, flatness to .01 mm is adequate to give an effectively plane detection surface.

3-2-3 Heating Element and Furnace (Fig. 3.2)

The heating element consists of a hollow cylinder of solid high purity, high density graphite, split at each side down to a thick connecting

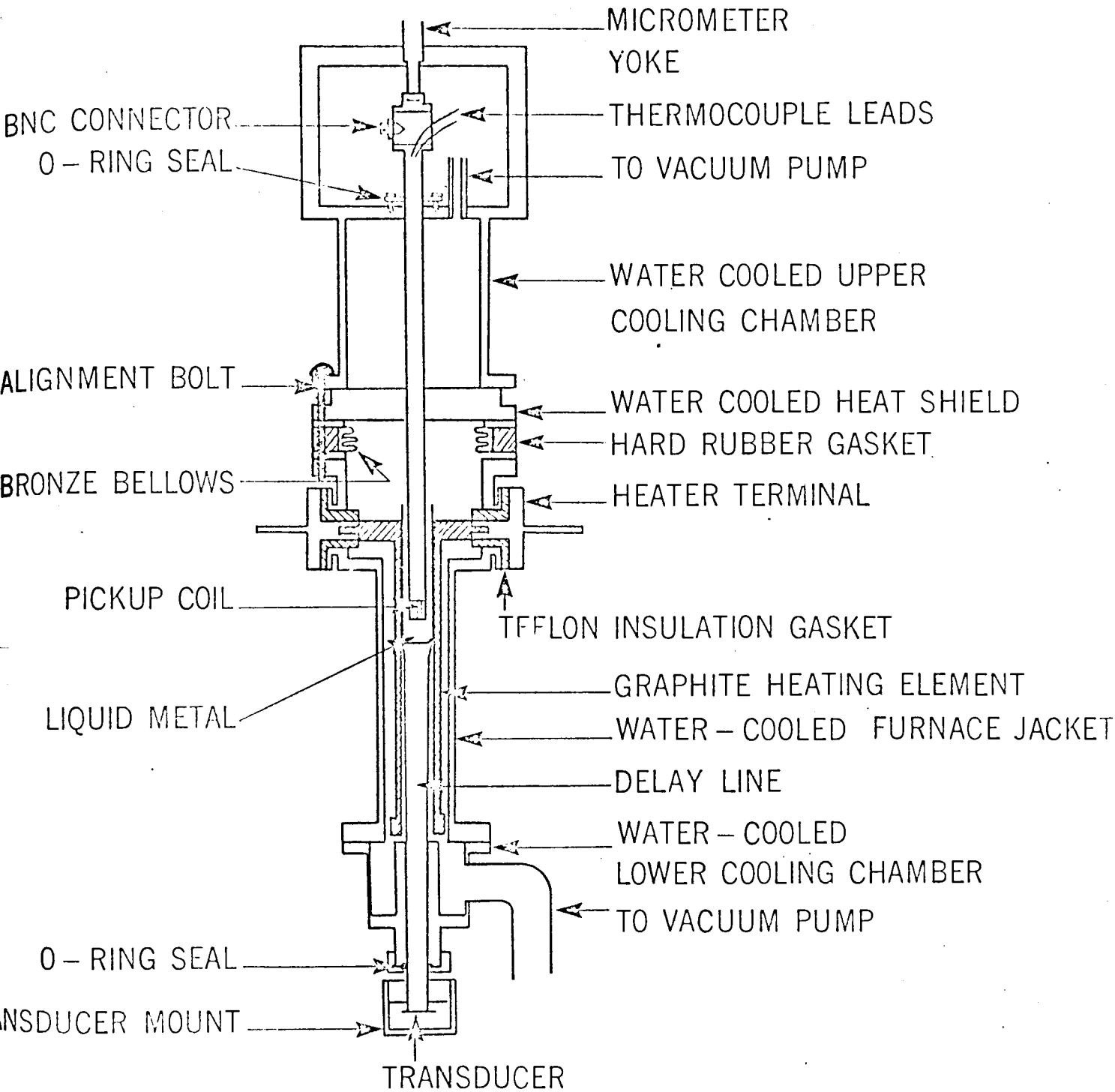

Fig. 3.2. SOUND VELOCITY FURNACE

ring at the bottom. Electrical contact is made at each side at the top end via thick graphite screws, the other ends of which screw into heavy copper water-cooled terminals. These terminals are electrically insulated by means of teflon spacers from the main body of the furnace, and are connected with heavy cables to a Hewlett-Packard* Harrison 6469A D.C. Power Supply, capable of delivering 300 amperes at 30 volts. This power supply is well regulated. With the help of the thermal lag time of the furnace (about 10 minutes for a change of 200°C usually, at temperatures ~600°C) the furnace temperature, once it had reached equilibrium, would drift by no more than one or two °C in 15 minutes. The heating element itself is surrounded by two concentric .005" thick polished molybdenum heat shields, spaced about 1/16" apart, the inner one of which contacts the heating element only at the thick ring forming its base; thus the molybdenum heat shields do not short out the heating element. Since the furnace was designed to fit inside the two-inch gap of a 12 kG electromagnet, there was considerable need to economise on space. The heat shield and heating element assembly fits into a water-cooled furnace jacket, the only pre-existing piece of apparatus, having provision for the attachment of terminals to the heating element. The furnace jacket also holds an ionization gauge. The crucible and delay line assembly fits snugly inside the heating element; since it is made from an insulating material, there is no danger of short-circuiting the heating element. The lower end of the delay line passes through a closely-fitting copper tube, water-cooled on the outside, which is part of the lower

*Hewlett-Packard Company, 1501 Page Mill Road, Palo Alto, California, U.S.A.

cooling chamber. This chamber also possesses a vacuum line which leads to a liquid nitrogen cold trap, an oil diffusion pump and a roughing pump, in that order. The lower end of the delay line passes through an O-ring seal, which holds it firmly and enables the vacuum to be maintained.

3-2-4 Upper Part of Apparatus, and Micrometer (Fig. 3.2)

Resting on the top flange of the furnace jacket is a short length of bronze bellows, with flanges at each end. The bellows is stiffened on the outside with three thick rubber rings, which fit between the flanges and are drilled to permit the passage of bolts. The purpose of the bellows is to allow alignment of the top part of the apparatus with respect to the lower part, so that the detecting surface of the probe sheath is exactly parallel to the generating surface of the delay line.

Above the bellows sits a stainless steel, water-cooled heat shield, with a hole in the middle only large enough to admit the probe. This is surmounted by an upper cooling chamber, which has its own evacuation line (since there is a severe constriction where the probe passes through the cooled heat shield) and also provision for electrical leads, probes, and so forth, to enter via O-ring and hermetic seals in its top surface. The probe itself is inserted through a central O-ring-sealed hole in the top surface, and passes down through the cooled heat shield to the interior of the crucible. The upper cooling chamber, cooled heat shield, bellows and furnace jacket are connected together by three long steel bolts at angular separations of 120°. Tightening these bolts against the pressure provided by the rubber rings around the bellows enables the apparatus to be aligned.

On top of the upper cooling chamber an aluminum yoke holds a Mitutoya micrometer having a travel of 1 inch, and readable to .0001 inches. The shaft of this micrometer is connected, via a coupling that takes out its rotary motion, to the hollow brass cylinder that forms the upper end of the probe. Typical backlash in the entire micrometer-probe assembly is less than .0005". Watch oil was used to lubricate the coupling. When the micrometer-probe assembly was aligned properly, the micrometer movement is smooth and easy.

3-2-5 Thermocouple

The thermocouple leads emerging from the probe can be clipped to the appropriate connection wires (made from the same material as the thermocouple leads themselves, but of a lower grade), and the connection wires were spot-welded to solid copper wires to make the cold junctions. These junctions were immersed in an icewater bath maintained at $0^{\circ}C$, and the voltage across the copper leads was measured using a Tinsley potentiometer, reading to 10^{-5} volts. The clips mentioned above were formed out of the connection wires themselves.

Calibration curves for the tungsten 5% rhenium-tungsten 26% rhenium thermocouple were given, with points at intervals of $10^{\circ}C$, by Hoskins Manufacturing Company, under the adoption date of November 23rd, 1962. This thermocouple calibration can be used up to $2800^{\circ}C$. The rhenium in the wires prevents the embrittlement normally found in tungsten after heating above $1000^{\circ}C$. However, the thermocouple used in this experiment had to be replaced twice due to breakage. A check of the calibration was performed on a thermocouple made in the same way as those used in the

experiment and fabricated from the same batch of wire. The melting points of pure copper and tin, which are very well-known (1083°C and 232°C respectively) were observed as arrests in the cooling curves of these metals, which were heated in quartz tubes using an oxyacetylene flame. Care was taken to ensure that the thermocouple was completely surrounded by the liquid metal, and the thermocouple calibration curves supplied with the wire were shown to be correct to ±1°C at these two temperatures.

3-2-6 Other Apparatus

As stated before, the furnace sits between the poles of a 12 kilogauss electromagnet. This magnet has a regulated power supply, but the field itself is not very uniform, varying by perhaps 20% across the relevant length although the contents of the furnace were designed in such a way that the molten metal would be centred between the poles of the magnet. However, this field inhomogeneity is not of any importance, since the magnetic field serves only to make the signal observable. Its effect on the velocity of sound at 10 kilogauss has been estimated (using the theory of Alpher and Rubin (1954)) to be less than one part in 10^5. This is a negligible correction within the limits of accuracy of the present experiment.

Though a diffusion pump is connected to the furnace, it was found that its use was unnecessary and only the rotary roughing pump was used, in practice, giving a vacuum of $\sim$30 μ. The purpose of the vacuum is to provide thermal insulation for the furnace and to prevent massive oxidation of the liquid metal; using our usual methods of sample preparation it was found that surface contamination was not a problem; see Section 3-4.

3-2-7 Transducer Mounting

As mentioned in 3-2-1, radiant heat transmitted down the delay line was a problem at high temperatures. The original transducer mounting (Fig. 3.3a) almost completely enclosed the transducer to give good electrical shielding; but this also meant that the transducer became quite hot (~100°C) and the coupling, using Nonaq stopcock grease, to the delay line was greatly impaired, because the grease became very fluid. However, for the high-tin alloys, where most of the measurements were made below 1000°C, this was not a problem. For the low-tin alloys a new transducer mount was constructed (Fig. 3.3b), which enabled a strong current of air to be played over the transducer, to cool it. This was most effective; when the molten alloy was at 1400°C the transducer appeared to function almost as well as at room temperature. For both mounts, the upper part of the mount was first attached to the lower end of the delay line; then the transducer was attached with Nonaq grease, pressing and sliding it around until only a thin film of grease was between it and the delay line, and lastly the lower section of the transducer mount was attached. An important feature of both mounts is that the transducer is touched as little as possibly by anything other than the electrical contacts and the end of the delay line; it was found that the pulse was broadened and split if substantial acoustic power went into the transducer mounting.

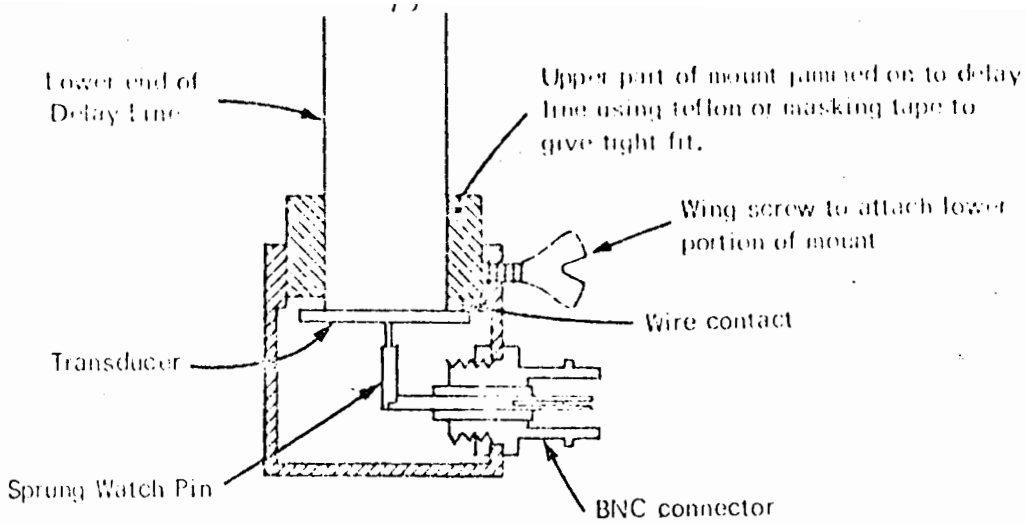

Fig. 3.3a. Transducer Mount #1 in cross-section. Lower part of mount is 1/16" thick copper. Top part is brass.

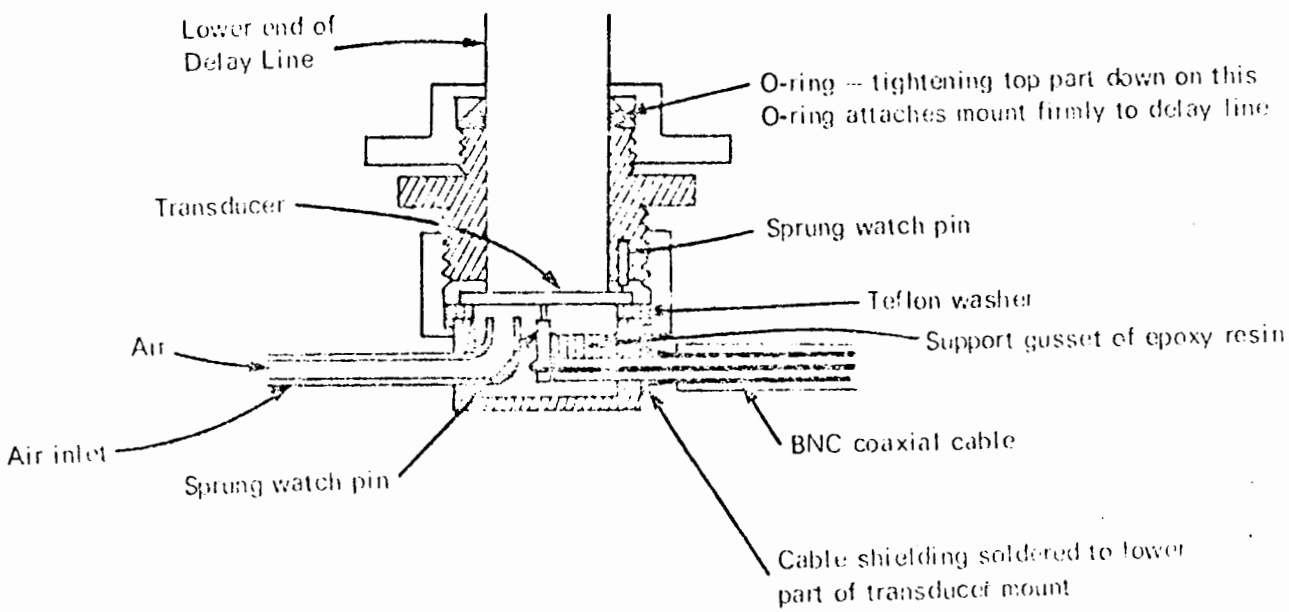

Fig. 3.3b. Transducer Mount #2 in cross-section. Air outlet omitted for clarity.

3-3 Electronics

For a block diagram of the electronics see Fig. 3.4. The Arenberg* P620-A two-stage pre-amplifier has a Q of about 10 per stage; however, when connected to the pickup coil, the Q of the first stage was no greater than 3 when the coil was at high temperatures, owing to the increase in resistance of the platinum wire. The signal to noise ratio for the entire amplification system is unity for an input signal of ∿1 μV as provided by a standard signal generator; an absolute calibration is extremely difficult and was not attempted owing to the non-linearity and continuously variable gain of both Arenberg components. An estimate of the size of the pickup signal was arrived at by observing the signal to noise ratio knowing that the noise level is ∿1 μV. Provided this ratio was greater than about two for the electromagnetically detected acoustic signal, measurements of sound velocity could be made with ease.

The High Power r.f. Pulse Generator* was operated usually at near-maximum output, giving pulses ∿2 KV peak to peak. This was necessary to obtain a usable signal to noise ratio. The maximum acoustic output at ∿10 MHz was obtained by operating a .050" thick PZT-4 ceramic transducer† at its fifth harmonic, about 12.6 MHz. Higher acoustic amplitudes could be obtained at lower harmonics, but the wavelength was increased so that lower accuracy was obtainable for the sound velocity measurements; fewer fringes could be counted, and acoustic interference from the free surface

*Arenberg Ultrasonic Lab., Inc., 94 Green St., Jamaica Plain, Mass., U.S.A.

†Vernitron (Clevite), Piezoelectric Division, 232 Forbes Rd., Bedford, Ohio, U.S.A.

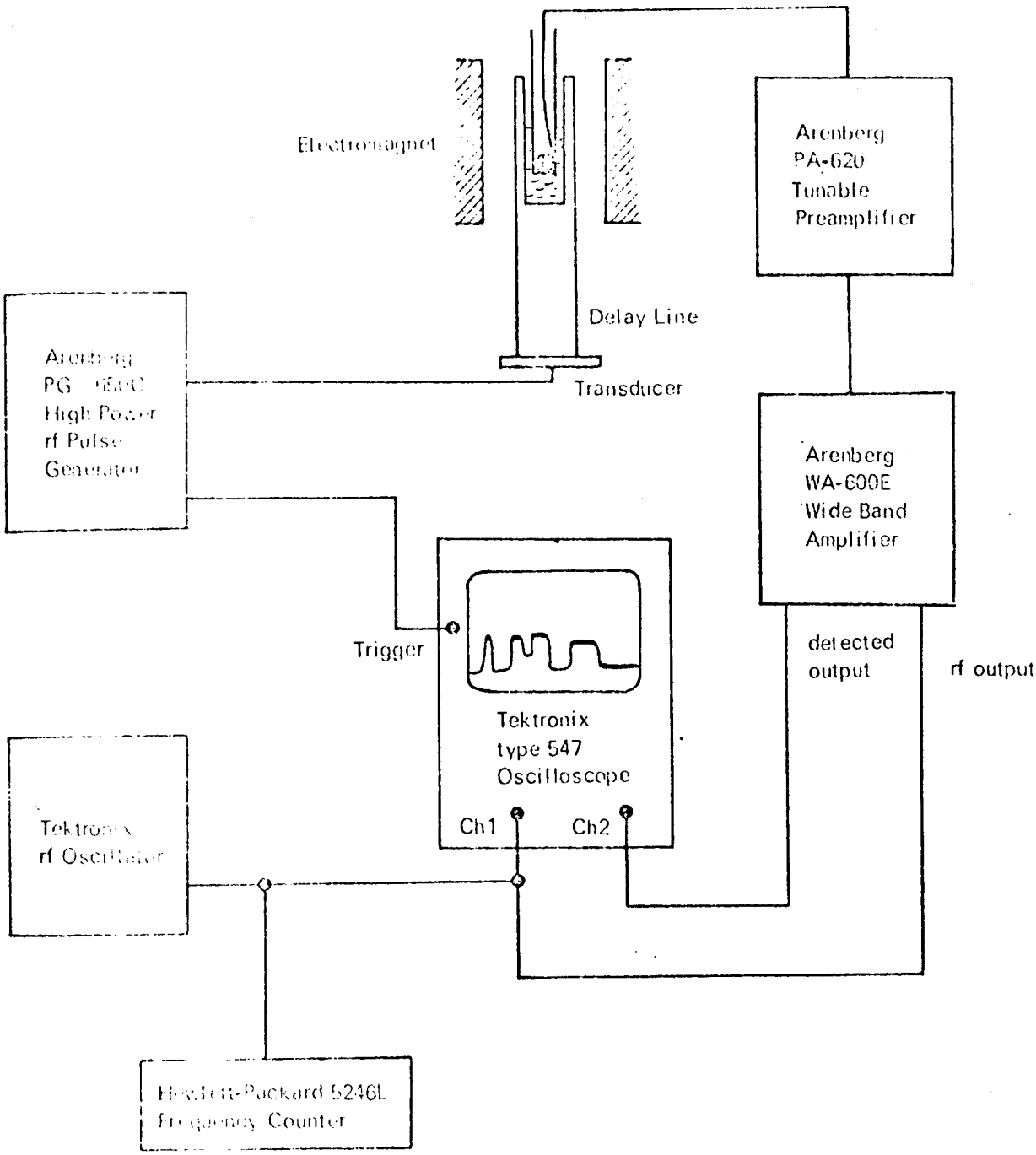

Fig. 3.4. Block diagram of electronics used in this experiment.

of the liquid became a problem. Ceramic transducers which had a higher fundamental frequency, being necessarily thinner, were found to give a smaller acoustic amplitude, possibly because they were being overdriven by a 2KV pulse, which would cause heating and perhaps depoling of the ceramic. In a thinner transducer the electric field is naturally higher for a given applied voltage.

3-4 Sample Preparation

The copper-tin alloys used in this experiment were chosen to be the pure materials Sn and Cu, and the intermediate compositions 10, 20, 30, 40, 50, 60, 70, 80 and 90 atomic percent Cu. The pure materials were Cominco 99.999% pure tin, in the form of wire, and 99.95% pure oxygen-free copper, in the form of 7/8" dia. rod. The pure materials were mass-spectrographically analysed, by Can-Test Incorporated, Vancouver, B.C., and the results are tabulated in Table 3.1. The copper, nominally 99.95% pure, was found to be considerably purer than that, somewhat to our surprise. An enquiry of the testing laboratory, however, revealed that the results were unequivocal. The alloys were prepared by a laboratory technician, in a vacuum induction furnace (10^{-5} torr), in the following manner. An appropriate mass of copper was sawed and filed to the shape shown in Fig. 3.5. It was then etched in dilute HNO_3 for several minutes to remove surface contamination, washed in water and propanol, dried, weighed on a Mettler* balance, and placed in the crucible in which the alloy would be formed (which had been previously washed with propanol and

*Mettler H-8 Balance, Mettler Instrumente AG, CH-8606 Greifenzee-Zürich, Switzerland.

TABLE 3.1. Mass Spectrometric Analysis of Cu and Sn Used in Alloys.

Accuracy for Trace Elements detected = 50%

Element Searched For	Percentage found, by weight	
	Cu sample	Sn sample
Al	<.0005	<.0005
Sb		
As		
Ba		
Be		
Bi		
B	<.0005	<.0005
Cd		
Ca		
Cr		
Co		
Cu	100	.0002
Ga		
Au		
Fe	.0002	
Pb	<.0002	
Mg		
Mn	.0005	
Mo		
Nb		
Ni		
Si	.0005	
Ag		
Sr		
Ta		
Sn		100
Ti		
W		
V		
Zn		

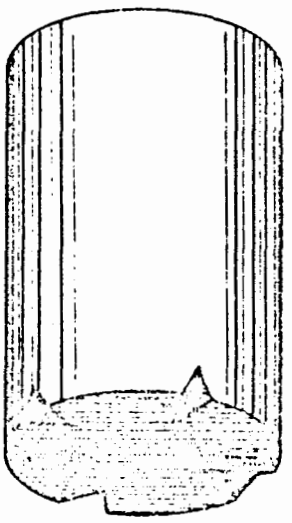

Fig. 3.5. Shape of copper ingots used in alloy formation. Grooves permit clean tin to run down onto generating surface of delay line, leaving oxide behind.

dried). A length of the tin wire was then cut, to roughly the correct weight demanded by the composition in question, washed in dilute HCl water and propanol, and dried. Enough wire was then cut off the end to bring the weight as close to the exact amount needed as possible. The weights and atomic compositions of the alloys can be found in Table 3.2; it is clear that this technique enables very specific compositions to be formed. For the low-tin alloys, the wire was then placed on top of the copper in the crucible, and the whole heated to about 1100°C, after thorough evacuation and outgassing at about 300°C. To avoid thermal shock to the fused quartz crucibles, the metals and crucible were heated with a graphite susceptor in the induction furnace, rather than heating the metals directly by induction. For the high-tin alloys, the tin wire, being bulky, could not all be stuffed into the crucible. A different procedure was therefore adopted. The wire was melted into an ingot of appropriate diameter in a graphite crucible beforehand (graphite is insoluble in tin; see Kirshenbaum and Cahill 1962) and then the ingot was placed in the quartz crucible above the copper.

The reason for forming the alloy in this way was to make sure that the bottom surface of the alloy did not get contaminated while the alloy was being formed, so that good wetting of the delay line could be ensured. When the tin melts, long before the copper, it runs down to the bottom of the crucible through the grooves in the copper block, leaving oxide and slag behind on top of the copper. Thus clean tin encounters a clean surface, and wetting is good. In subsequent melting of the copper, any slag (and very little was observed) remains on the top surface of the alloy.

TABLE 3.2. Alloy Compositions

Alloy (nominal) (At. % Cu)	Mass of Sn (gm)	Mass of Cu (gm)	c (Atomic fraction)
0	∿60	0.0000	0
10	72.1371	4.2921	.10002
20	45.7969	6.1300	.20000
30	48.1785	11.0553	.30001
40	41.5085	14.8174	.40003
50	38.4475	20.5834	.49999
60	31.2542	25.1030	.60003
70	25.3040	31.6152	.70003
80	19.9511	42.7132	.79995
90	9.2275	44.8500	.90078
100	0.0000	∿60	1.0000

After cooling, and upon reheating for an experimental run, one or two of the alloys cracked their quartz crucibles, due to the unequal thermal expansion coefficients of bronze and quartz (that of quartz is very small). This was the case for pure Sn and Sn 90 atomic % Cu. In these cases (and also for 70 at. % Cu and 100% Cu, for a different reason) the metals had to be first melted in the sound velocity measurement furnace itself; it was found in these cases that good wetting could only be achieved by heating the alloys to 1100-1200°C and stirring them vigorously with the probe. This was done by raising and lowering the probe rapidly by hand. The importance of a good vacuum during melting is clear; the vacuum in the sound velocity furnace was much poorer than that in the induction furnace in which most of the alloys wer formed. Another problem encountered with most of the samples was the presence of bubbles on their bottom surfaces. Often good stable signals could only be obtained by heating the alloy above 1000°C and stirring vigorously with the probe, to dislodge these bubbles. This will be discussed further in the next Section. After the alloys were thoroughly melted in the induction furnace, they were left for about half-an-hour to mix at a temperature a few hundred degrees above the melting point; however, for some alloys further heating and stirring in the sound velocity furnace were needed to ensure homogeneity of the liquid. After the alloys had been formed and cooled, pure argon gas was introduced into the induction furnace, at atmospheric pressure, and the crucibles were sealed with rubber bungs before the argon, which is heavier than air, could escape from the surface of the alloy. This prevented oxidation of the alloys in storage. The high-tin alloys all seemed to wet the quartz even after they had cooled down (the ingots could not be

moved in the crucibles); but the high-copper alloys had shrunk away from the sides of the crucible and could be removed easily, though this was not usually done, for obvious reasons. In the case of Sn 70 at. % Cu the crucible cracked on cooling, and the ingot was transferred into another crucible for the purposes of experimentation. For 100% Cu the delay line and crucible assembly used was too large to fit through the lower cooling chamber (because the rods from which the quartz delay lines were made varied somewhat in diameter), so the ingot of Cu was also transferred into another crucible.

Since the vapour pressures of both Cu and Sn are below 10^{-1} torr at 1400°C, and they are nearly equal, and furthermore, the mass of the samples was about 60 gm in each case, with an exposed surface area of $\sim$2 cm^2, the composition of the alloys was not expected to change due to differential evaporation. A rough calculation indicates a weight loss of $\sim$.1 gm/hour at 1300°C. Since the activity of Cu-Sn alloys is not far from ideal (Alcock et al. 1969) the proportions of Cu and Sn atoms lost in this way are close to their proportions in the alloy in question. Thus we might expect at most a percentage change in composition of $\sim 2\times10^{-2}$%. Our experience was that once the alloys had been thoroughly mixed the values of the sound velocity at a given temperature, measured after the alloy had been taken up to a high temperature were identical with those measured before, indicating no change in composition.

3-5 Method of Measurement of Sound Velocity

A typical run proceeded as follows. The crucible and delay line assembly containing the alloy to be investigated was placed in the furnace;

the rubber stopper was kept on until the last possible moment. The furnace was then evacuated, and allowed to pump down for several hours. It was found unnecessary to employ the cold-trap; the pressure of 30 microns normally obtained in the furnace was sufficient for our purposes, and the use of the cold-trap increased the turn-around time of the experiment. The transducer was attached to the lower end of the delay line, and the r.f. generator and amplifiers were switched on, to check that the acoustical system was in order. For some alloys it was possible at this stage to detect electromagnetically an acoustic signal at the surface of the alloy; these alloys were the high-tin alloys that wetted the crucible well even when solid. The water cooling was turned out (and the air cooling for the transducer, when it was used) and the furnace was heated up, usually to about 500°C to start with. The melting of the alloys was signalled usually by three indications: (a) the probe could be moved down through the liquid, (b) the acoustical echo signal from the end of the delay line observed using the transducer could be seen to become sensitive to vibration of the furnace, and (c) usually a large electromagnetically detected signal could be observed. To observe the latter signal the D.C. magnetic field had to be turned on, of course. Usually a field of about 6 kilogauss was used. For some of the alloys the acoustic signal could be electromagnetically detected at D.C. magnetic fields as small as 100 gauss, so that the signal to noise ratio at 10 kilogauss was $\sim$100:1 or more. The size of the signal is determined by (a) the quality of the acoustic bond between the transducer and the delay line; (b) the acoustic impedance mismatch between the quartz delay line and the alloy in question; (c) the wetting between the delay line and the

alloy in question (usually it was very good); (d) the size of the D.C. magnetic field used; (e) the presence or absence of bubbles at the bottom of the alloy or on the detection surface itself; (f) the resistance of the pickup coil, which varies with temperature and alters the Q of the detection circuit; (g) the alignment of the acoustical system. Under optimum conditions, as we have said, the signal:noise ratio was $\sim$100:1, which means an output signal from the coil of $\sim$100 μV at 10 kG. Since the coil area is $\sim$.5 cm^2, with 10 turns, this implies, using Equation (2.10), that the amplitude of the acoustic wave in the alloy was $\sim 10^{-7}$ cm, which is a very large amplitude for an acoustic wave, and must be close to the cavitation threshold (several atmospheres pressure judging from the results for liquid Hg (Webber and Stephens 1968), corresponding to $\sim 10^{-7}$ cm displacement for a wavelength of 3×10^{-2} cm). However, no indications of cavitation were observed.

In contrast with the signal observed using the transducer as an acoustic receiver, the acoustic signal observed using the coil was very clean and free from spurious echoes (see Fig. 3.6). If the coil was sufficiently far away from the generating surface so that no standing wave effects occurred, an input square pulse of $\sim$20 μs duration was faithfully reproduced by the electromagnetically detected acoustic signal; on the other hand, when the transducer was used as a detector even the echo pulse from the end of the delay line itself was broken up by acoustic waveguide effects. When the coil was brought close to the generating surface standing wave interference fringes could be seen, caused by overlap of the acoustic pulse with its reflection. This effect was greatest

for those alloys with some degree of acoustic mismatch with fused quartz (which would give a larger reflected wave). In the case of pure liquid Cu, with an acoustic impedance of $\sim 2.8 \times 10^6$ gm/cm^2 sec compared with that of quartz, 1.31×10^6 gm/cm^2 sec, an exponentially decaying train of several echoes could be seen, using a short generating pulse. Such echo trains are commonly used to measure acoustic attenuation in liquids and solids, but the attenuation observed was not observably dependent on the separation of probe and generating surface and thus could be attributed entirely to losses on reflection. It is well-known that at 10 MHz the attenuation lengths in liquid metals are of the order of 50 cm, much longer than the 2 cm path length available here. Higher frequency acoustic waves would be necessary to bring this length down to an experimentally useful size, since the attenuation length in a metal is proportional to $1/f^2$.

Bubbles in the liquid, particularly on the detection surface itself, caused some problems. The presence of a bubble on the detection surface could be recognised easily by observing the signal; it would become suddenly much smaller and also distorted, and very sensitive to the vibration of the furnace. Two remedies were found for this problem. The first is to agitate the liquid vigorously, by removing the yoke and micrometer from the probe, and raising and lowering it rapidly. The liquid could be felt slushing around in the crucible when this was done. If any bubbles remained (as they occasionally did) and found their way onto the detecting surface, they could be removed by lifting the probe

clear of the surface of the liquid, whereupon, on lowering the probe again, a large steady signal was immediately restored. Since it was possible to take a reading of the wavelength of sound even under conditions of "bubble trouble", and since such readings were neither in agreement with those made when the signal was large and steady, nor consistent with each other, a careful watch was made to detect signs of "bubble trouble" during a reading, and readings affected by such problems were discarded.

The method of making measurements of the wavelength of sound deserves some description. The Arenberg r.f. pulse generator can be made to produce two stably phase-coherent pulses of equal amplitude one after another, for each internally generated trigger pulse. The separation of these pulses can be manually varied from five to several hundred microseconds. The signal observed using the coil always includes (due to imperfect shielding) the direct electrical crosstalk of these pulses, which has a steady amplitude (of about 10μV) and phase (see Fig. 3.6a). When the D.C. magnetic field is applied, the electromagnetically-detected acoustic wave signals (EDA signal) also appear (Fig. 3.6b). By varying the delay of the second pulse of the pair, the EDA signal from the first pulse may be superposed on the crosstalk signal of the second pulse (Fig. 3.6c). Now if the probe is moved upwards through the liquid, the EDA signal of the first input pulse will move away from that input pulse, as viewed on the oscilloscope. Since the EDA signal is superposed on the crosstalk of the second pulse, it will alternately constructively and destructively interfere with that pulse. After the probe has been raised one wavelength through the liquid the EDA signal will have the same phase as when it

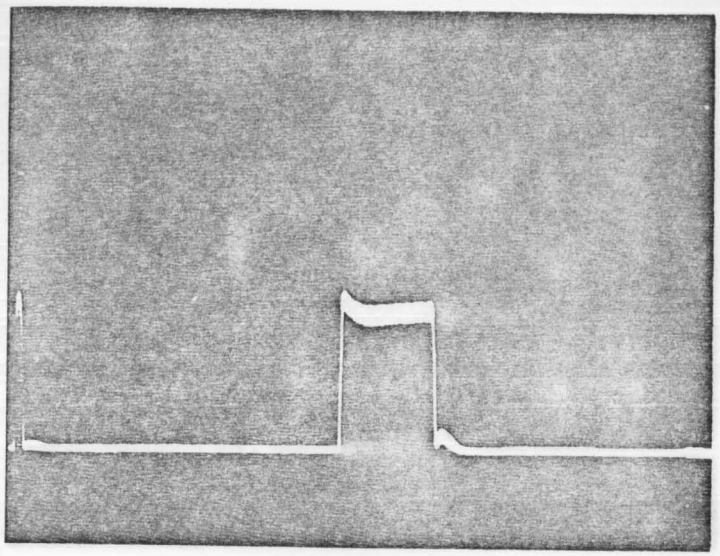

Fig. 3.6a

Crosstalk from pair of pulses generated by Arenberg rf pulse generator. B = 0

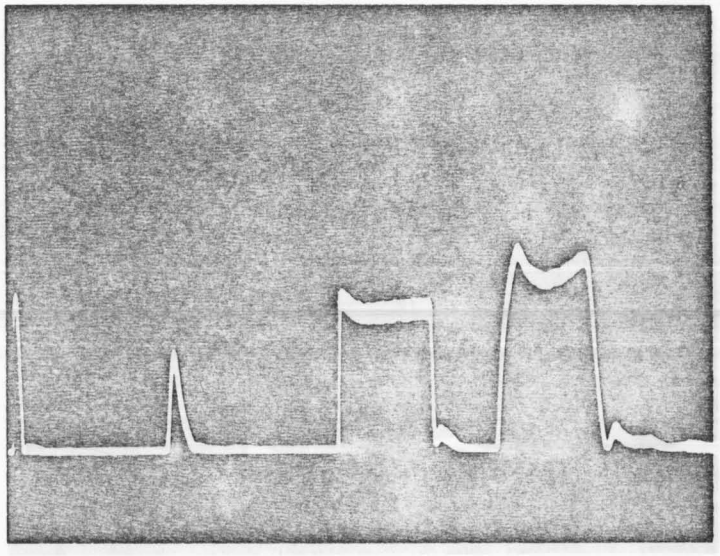

Fig. 3.6b

Appearance of EDA signals after static magnetic field switched on. B = 1 KG

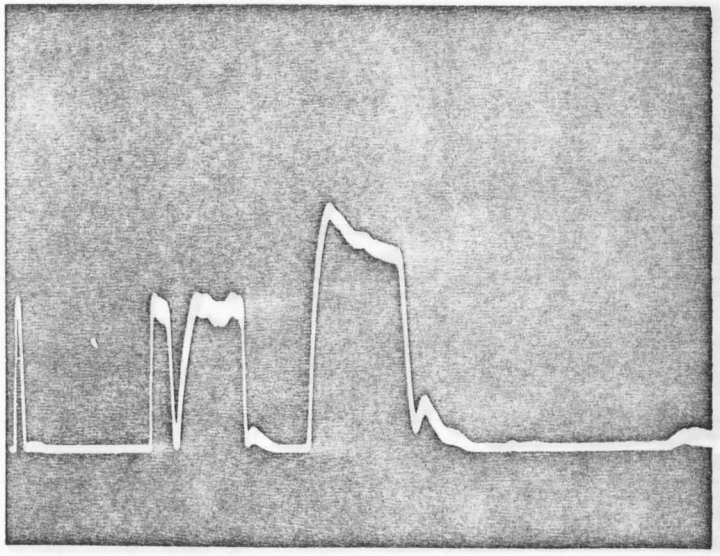

Fig. 3.6c

Appearance of signal at start of sound velocity measurement. EDA pulse superposed on cross-talk of second pulse.

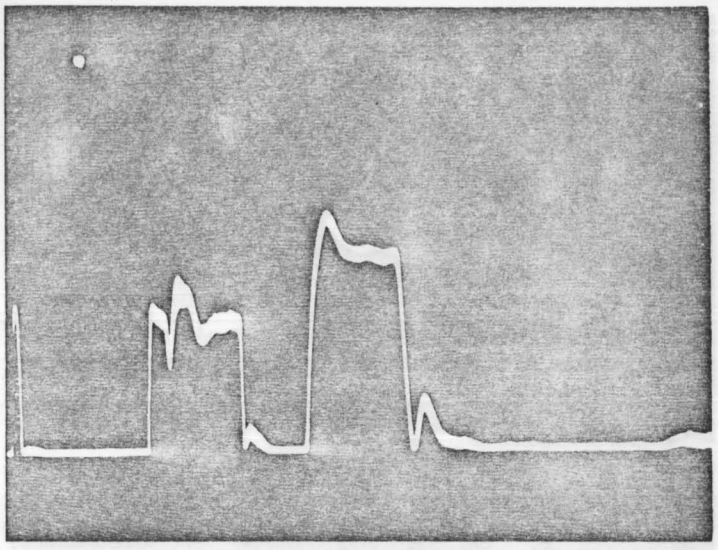

Fig. 3.6d
Probe raised by $\sim \frac{\lambda}{4}$

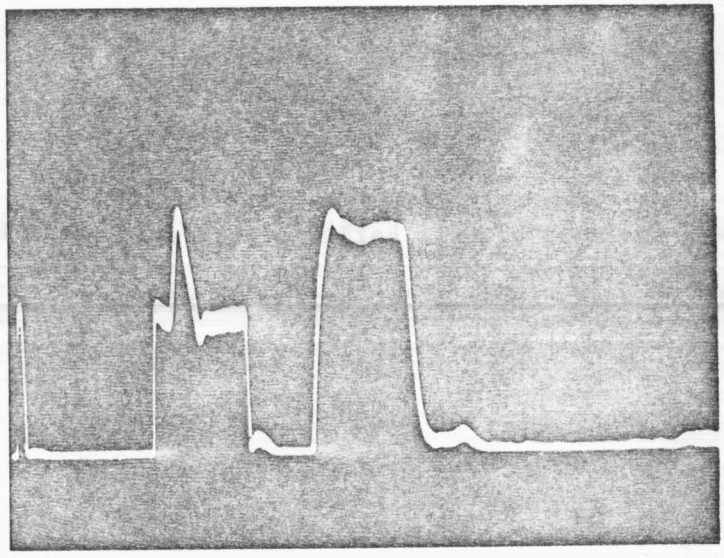

Fig. 3.6e
Probe raised by $\sim \frac{\lambda}{2}$

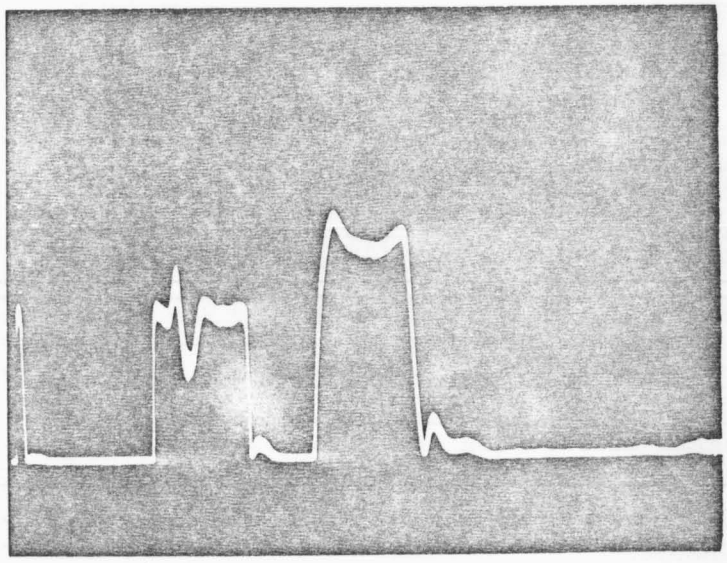

Fig. 3.6f
Probe raised by $\sim \frac{3\lambda}{4}$

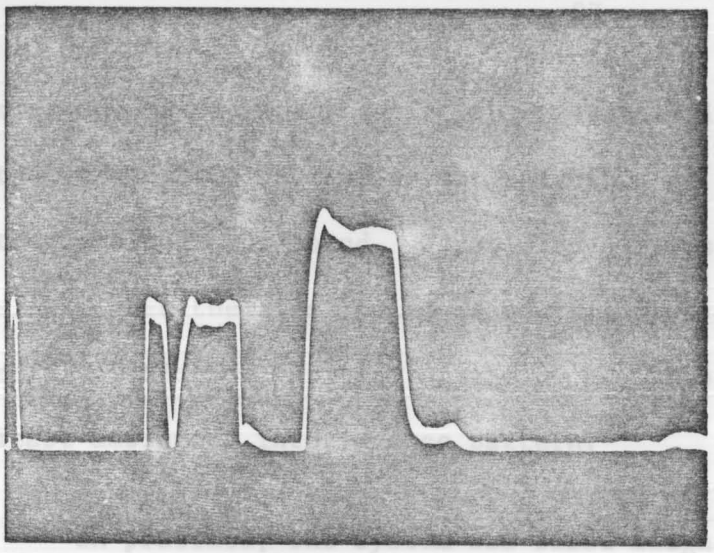

Fig. 3.6g

Probe raised by λ

Note: These are rectified signals from the WA-600E Amplifier displayed on the oscilloscope screen. The timebase is 20 μsec/cm.

started. Since the phase of the crosstalk is constant, we may conclude that the spatial period of the interference pattern observed is simply the wavelength of sound. Figs. 3.6d-g illustrate the appearance of the signal when the first pulse is short (∿3 μs) and the second long (∿25 μs) as a function of position of the probe. These pulse lengths provide the least ambiguous interference pattern.

In practice, the system was first aligned by systematically maximising the pickup signal. With the system aligned, the signal due to a short square input r.f. pulse (short enough to avoid reflection overlap) rises and falls as a whole when superposed on the crosstalk pulse. Misalignment causes a phase lag of the later parts of the EDA pulse, causing a characteristic "rocking" of the signal as the probe is moved through the liquid. Usually alignment had to be performed once for each run. After the acoustic system had been aligned, the furnace was allowed to come to equilibrium at some desired temperature. The probe was then adjusted so that there was room for the end of the probe to travel through at least 40 wavelengths without coming closer than 5 mm to either the generating surface or the free surface of the alloy. The micrometer was turned so as to eliminate backlash and set so that the (EDA + crosstalk) signal was at an interference minimum. The thermocouple voltage was then read, and the frequency of the longer crosstalk pulse was measured (the method will be described later). After its initial position had been noted, the micrometer was then turned slowly by hand until a predetermined number of fringes (40, 50 or 100 depending on the travel available) had been counted. The micrometer was adjusted to finish at a minimum, where its

position was again read off. The thermocouple voltage was noted again, after the thermocouple had come to equilibrium at its new position (which took a minute or so), and the frequency remeasured. After again eliminating backlash from the micrometer, the procedure was repeated for the opposite direction of micrometer travel. In all, about five minutes was necessary for each set of measurements at a given temperature. Twenty minutes, on average, were required for the system to come to thermal equilibrium at each new temperature.

Thus the measured variables were

(1) v_1 and v_2, the thermocouple voltage at each end of the travel.

(2) n, the number of fringes measured.

(3) ℓ_1 and ℓ_2, the initial and final micrometer readings.

(4) f_1 and f_2, the initial and final values of the frequency.

The temperature variation between the extreme micrometer positions was never more than 2% of the temperature of the metal, and usually much less than this. In all cases the average temperature was used. This can easily be shown to be the correct temperature (making the plausible assumption of a linear temperature gradient) which corresponds to the average wavelength, calculated from

$$\lambda = \frac{|\ell_1 - \ell_2|}{n}$$

Thus even in cases where there was an observable thermal gradient (25°C at 1200°C, for example) the errors introduced by it can be no greater than $\sim$.2% in the temperature, or an error of $\sim$.025% in the velocity of sound. We shall discuss sources of error in more detail in Section 4-2. To give an indication of the potential accuracy of this method, in several cases a given number of fringes was measured several times to give exactly the same value for $\ell_1-\ell_2$, to the readability limit of the micrometer (10^{-4} inches). In all cases, the value of $(\ell_1-\ell_2)$ for n fringes was measured at least four times at a given temperature, and a standard deviation computed from the scatter in those values.

The frequency was measured using a technique described in the Arenberg r.f. generator manual. A reference tunable cw signal was added to the pulsed signal and the cw oscillator (Tektronix) was tuned until the configuration in Fig. 3.7 was seen. If the cw oscillator had been in phase with the pulsed output of the Arenberg generator, one would have seen a beat of zero frequency at this point, but the pulses were phase coherent only with each other; thus several lines appeared across the pulse position. Note that this method essentially measures the <u>period</u> of the oscillations in the pulse; though the frequency has a bandwidth $\sim 1/\tau$, where τ is the length of the pulse, the <u>period</u> is very well defined and can be measured easily to the accuracy of .02% claimed below. Basically it is the period, t, that is of interest when the velocity of sound is measured in this way, because the interference pattern repeats when $\pi = \Delta\ell = st$. Thus the frequency bandwidth does not lead to errors in the computation of the sound velocity. The frequency of the cw oscillator is measured using a

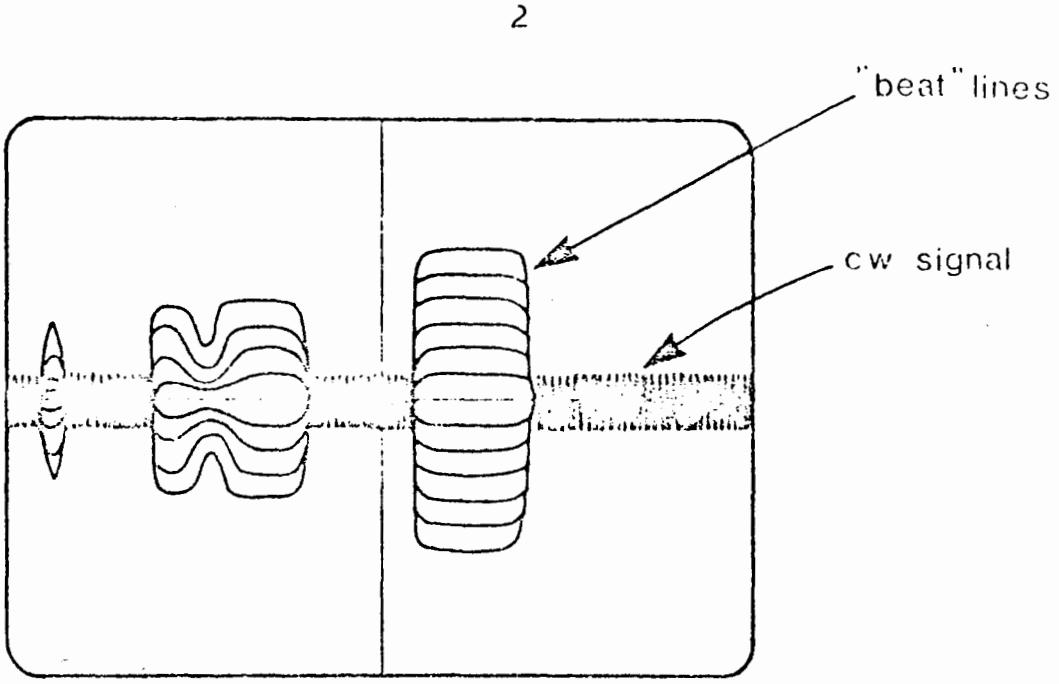

Fig. 3.7. Appearance of r.f. signal observed with pickup coil when added to a continuous r.f. signal at the same frequency.

frequency counter (Hewlett-Packard 5426L). This method is reproducible to .02%. Care must be taken, however, not to load the cw oscillator with the output from the wideband amplifier, and then to measure its frequency when unloaded. The frequency may shift by as much as 1%. Measurements on the Sn 10 at. % Cu alloy were incorrectly made in this way and had to be corrected afterwards using a correction factor which was very accurately determined (to .01%) by measuring the cw oscillator frequency when loaded and unloaded. Frequency drifts in the course of a measurement were never more than .1% and will be discussed in Section 4-2.

Measurements of the velocity of sound in each of the eleven alloys in Table 3.2 were made using the above technique, as a function of temperature over a temperature range at least 200°C. The results will be found in the next Chapter. Other possible measurement techniques include the cw version of the above. The Arenberg generator may be used as a continuous oscillator; thus a cw EDA signal can be observed. This signal can be added to a cw reference signal and the result rectified, giving rise to a d.c. signal which rises and falls as the probe is moved through the liquid. However, when the liquid is irradiated with continuous acoustic waves, there is a possibility of the formation of acoustic standing waves within the cavity formed by the generating surface and the free surface of the liquid. These standing waves would be detected by the probe, and would not necessarily have the desired periodicity of λ as the probe is raised, since their behaviour would depend on the height of the free liquid surface. In actual fact, when this technique was tried out for a Cu-Sn alloy, a very non-sinusoidal and erratic signal

was observed. In a liquid such as mercury, where the angle of contact of the surface with quartz is much greater, the surface is too convex to allow the formation of such standing waves and a clean sinusoidal signal was observed. A rough measurement of the sound velocity in mercury was made this way, at $22^{o}C$, and the value 1.46×10^{5} cm/sec was obtained, in fair agreement with the values reported in the literature (e.g. McAlister 1971).

Another suggested method is to display the r.f. pulse signal on the oscilloscope, instead of the detected pulse signal. One can then use the vertical axis on the oscilloscope screen as a fiducial mark, and count the actual oscillations comprising the EDA signal as they go by, as the probe is raised. This method has inherently the same accuracy as the method we employed, though it is perhaps more sensitive to misalignments of the system, which cause pulse distortion. Moreover, if the detection surface is close to the generation surface, standing waves may cause ambiguity in the phase of the observed oscillations.

3-6 Further Experimental Improvements

The accuracy of this experiment could be improved in several ways:

(a) The use of a higher frequency would mean that the acoustic wavelength λ would be shorter, and thus more interference fringes could be observed, giving a smaller percentage error.

(b) The length of the acoustic path could be lengthened (in conjunction with an increase in frequency, to nullify diffraction effects); again

more wavelengths could be measured and the effect of reading error in the micrometer would be diminished.

(c) The heating element and furnace could be redesigned to give much smaller thermal gradients; thus the temperature would be more accurately defined.

(d) The position of the probe could be measured with an optical interferometer, greatly increasing the accuracy of this measurement.

(e) The amplitude of the (EDA + crosstalk) signal could be plotted with an X-Y recorder, using a boxcar integrator to gate the total signal so that only the (EDA + crosstalk) signal was recorded. The gate could be made to move with the EDA signal as the probe was raised through the liquid. The X-coordinate of the X-Y recorder could be made accurately proportional to the height of the probe. Thus the wavelength could be measured on the graph, greatly increasing the potential accuracy.

(f) If the frequency were increased, measurements of the acoustic attenuation could be made accurately, providing that the applied static magnetic field was homogeneous. At 5 MHz the attenuation length is $\sim$50 cm, making the attenuation difficult to measure; while at 50 MHz the attenuation length is only $\sim$.5 cm, which is easily measurable. Measurement of attenuation using the electromagnetic detection technique is very easy, in principle; the amplitude of the EDA signal should decrease exponentially as the probe is raised, with a decay length equal to the attenuation length. No correction for losses at the liquid surfaces should be necessary. Note that a magnetic field of 10 KG increases the attenuation only by about one part in 10^3 (Alpher and Rubin 1954).

CHAPTER 4

EXPERIMENTAL RESULTS

4-1 Results for the Velocity of Sound

4-1-1 Analysis of Data

At each temperature, for a given composition, the acoustic wavelength was measured at least four times, with at least 40 wavelengths being counted each time. The arithmetic mean $\bar{\lambda}$ and root mean square deviation σ_λ were evaluated. If the frequency had shifted during the course of the measurements its mean $\bar{f}$ and root mean square deviation σ_f were also calculated. The mean of the thermocouple voltage reading was calculated using equal numbers of measurements from the top and bottom ends of the probe travel, and the temperature determined therefrom. The sound velocity $s = \bar{f}\bar{\lambda}$ was then evaluated, and the total root mean square deviation $\sigma_s = s\left(\frac{\sigma_f}{\bar{f}} + \frac{\sigma_\lambda}{\bar{\lambda}}\right)$ was calculated. The size of the error bars on the graphs of s versus T for the various alloys is given by σ_s.

Within experimental error every alloy composition gave a linear temperature dependence for the velocity of sound, and the temperature coefficient was always negative. To determine the best fit straight line a least mean squares fit to the data for each composition was performed using a computer. Intercepts and temperature coefficients reported here are the results of this calculation. The points were unweighted since the difficulties in making a measurement were not usually temperature dependent. The correlation coefficient (see Bevington 1969) calculated for each straight line fit was always between .992 and 1.0, indicating that the scatter in the experimental points was consistent with the size of the standard deviations

used. See Section 4-2 for a more detailed discussion of errors.

4-1-2 Pure Tin

The velocity of sound in pure tin was measured over a temperature range of 750°C, from 250°C to 1000°C. This metal has been measured many times; for comparison with our present work the results are tabulated in Table 4.1. With the exception of the work of Pronin and Filippov, which appears to be inaccurate, and that of Kleppa, who used a rather crude measurement technique with a fixed acoustic path length, the results are consistent with each other. Except for our work, all these measurements were made with a pulse technique using piezoelectric transducers to produce and detect the acoustic waves. Gitis and Mikhailov found a non-linear temperature dependence of the velocity of sound in pure tin; no trace of this was found in our results, nor in the careful measurements of Gordon, so we suspect that their result is erroneous.

4-1-2 Pure Copper

The only published data for the velocity of sound at the melting point of copper are the figures of Gitis and Mikhailov (1966b) and Pronin and Filippov (1963). They are given, with our result for comparison, in Table 4.2. It appears that as in the case of pure tin the work of Pronin and Filippov is unreliable. Again, work previous to ours was performed using a conventional pulse technique. In contact with pure copper at temperatures above 1100°C, quartz rapidly becomes very brittle, which restricted the maximum temperature for our measurements to 1300°C. The temperature dependence was linear, within the accuracy of the measurements.

TABLE 4.1. Velocity of Sound in Liquid Sn at the Melting Point

Reference	Sound Velocity ($\times 10^5$cm/sec) at 232°C	$-\frac{ds}{dT}$ ($\times 10^2$cm/sec)
Kleppa (1950)	2.27	.7
Polotskii and Khodov (1953)	2.458	
Gordon (1959)	2.464	.236
McSkimin (1959)	2.473	.247
Khodov (1960)	2.468	.2
Pronin and Filippov (1963a)	2.420	.211
Gitis and Mikhailov (1966b)	2.480	.30*
Litovitz and Jarzynski (1965)	2.47	
Coppens et al. (1967)	2.472	.26
Webber (1967)	2.474	.22
This work	2.473±.002	.255±.004

* At m.p.; $\frac{ds}{dT}$ changes with temperature.

TABLE 4.2. Velocity of Sound in Liquid Cu at the Melting Point

Reference	Sound Velocity ($\times 10^5$cm/sec) at 1083°C	$-\frac{ds}{dT}$ ($\times 10^2$cm/sec)
Pronin and Filippov (1963b)	3.270	.978
Gitis and Mikhailov (1966b)	3.459	.46
This work	3.440±.004	.42±.02

Judging from the scatter in the measurements of Gitis and Mikhailov, their standard error in s is ∿.3% and in $\frac{ds}{dT}$, ∿10%, bringing their results into good agreement with ours.

4-1-4 Copper-Tin Alloys

Results for the sound velocity as a function of temperature are presented as graphs in Figs. 4.1 and 4.2, the arrow on each line indicating the liquidus temperature (Hansen 1958) of that alloy. The best-fit straight line parameters are given in Table 4.3; note that the standard deviations for the T = 0°C intercept are much larger than the deviations would be for values of s derived from these straight lines in the temperature range in which measurements were made. Isotherms at 600°C, 800°C and 1100°C for the sound velocity as a function of composition are plotted in Fig. 4.3, and $-\frac{ds}{dT}$ is shown in Fig. 4.4. There are clearly no anomalies in the variation of sound velocity with composition. The peak in the -ds/dT at ∿80 At. % Cu is significant, however, and must be associated in some way with the structural changes taking place at this composition (see Chapter 5).

It might appear that the value of $\frac{ds}{dT}$ at 90 at. % Cu is anomalous and the result of an error in measurement. We therefore emphasize that the data obtained for this alloy were as good as those for the other alloys. The values used in Fig. 4.2 are those measured after the mixing of the alloy was observed to be complete (see next paragraph), and represent the results of several thermal cycles of the alloy. No special problems were encountered with this alloy. The rather rapid dependence of $\frac{ds}{dT}$ on composition at about

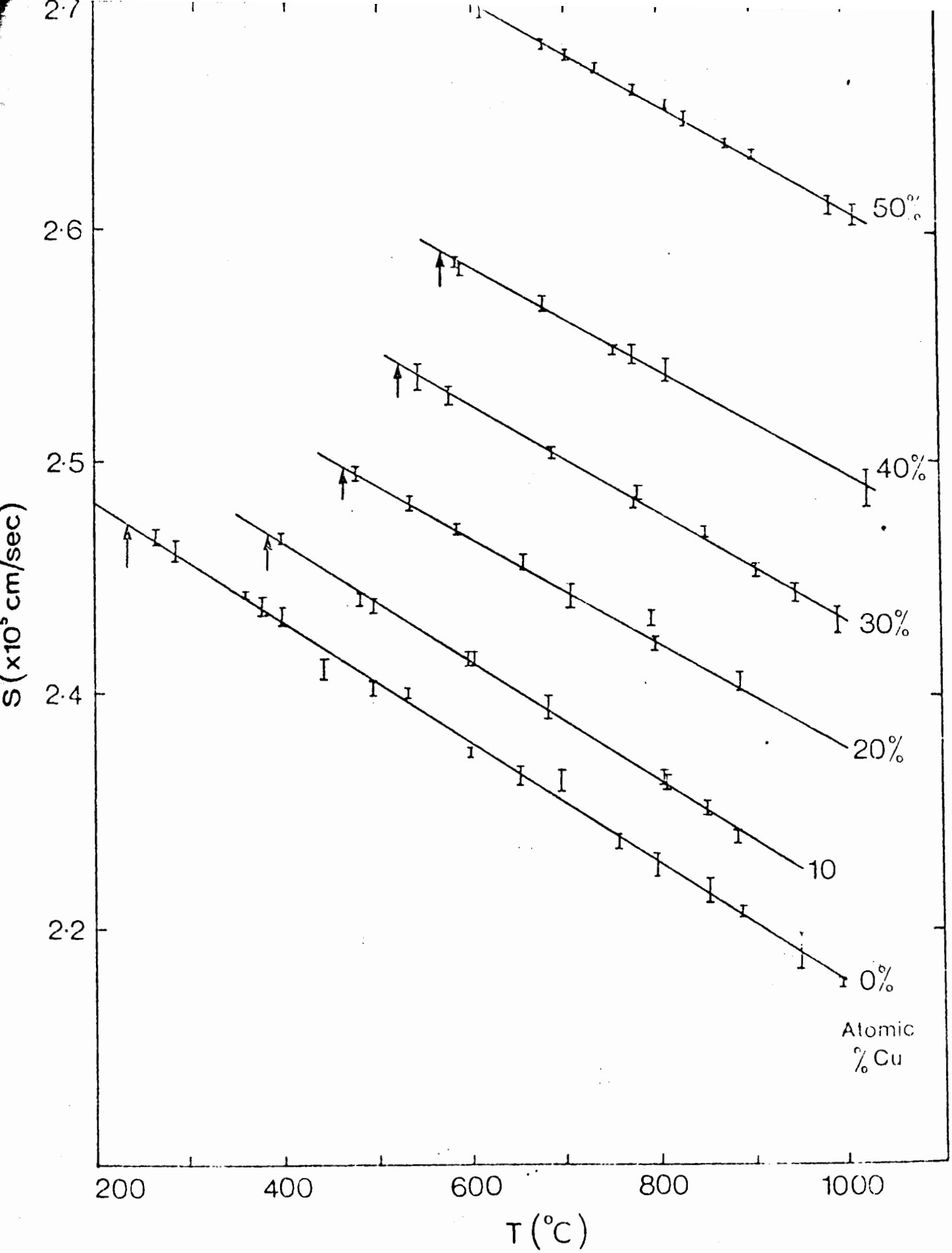

Fig. 4.1. Velocity of Sound in Cu-Sn Alloys as a Function of Temperature.

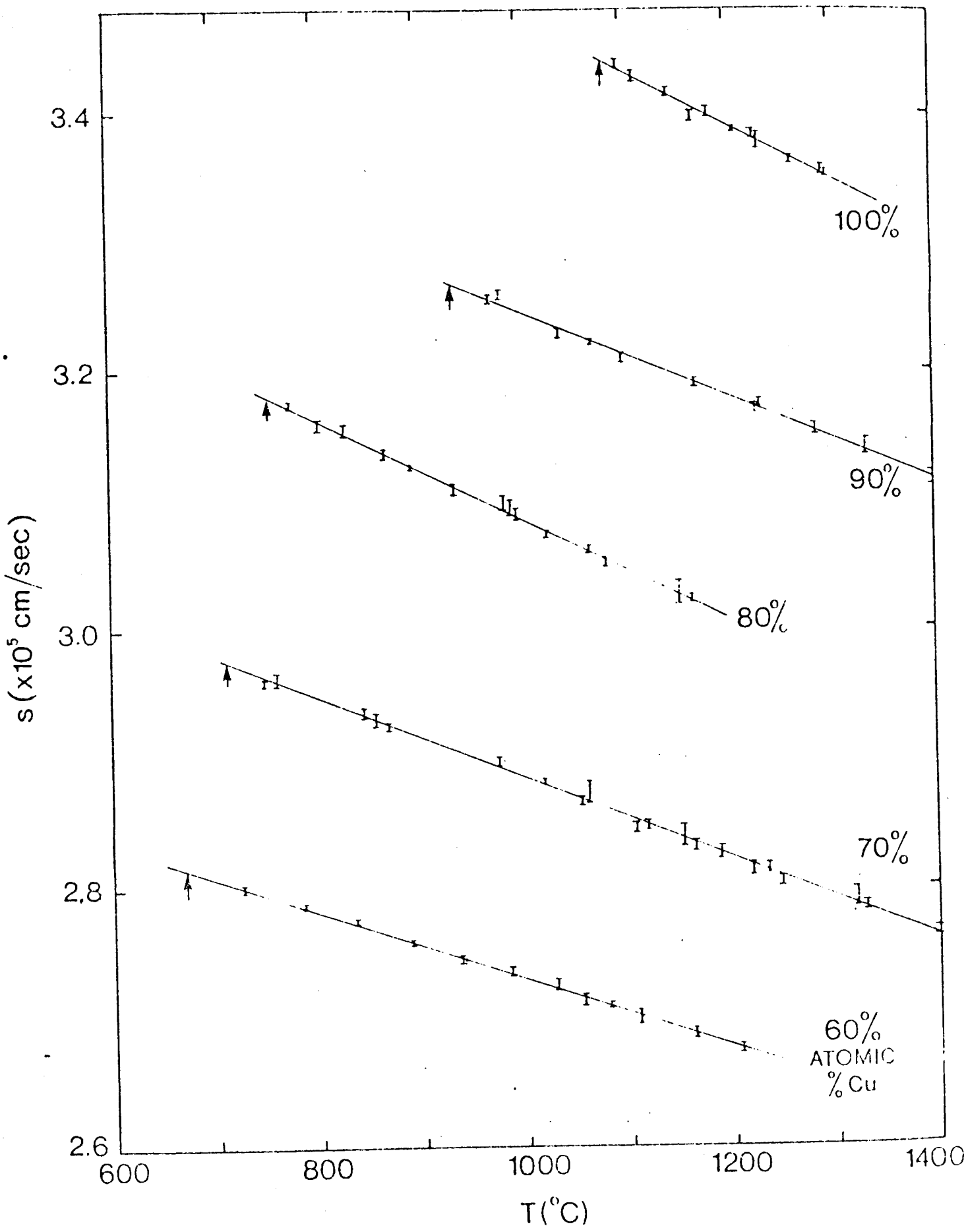
3.4
3.2
3.0
2.8
2.6
s (x10⁵ cm/sec)
600
800
1000
1200
1400
T(°C)
100%
90%
80%
70%
60%
ATOMIC
% Cu

TABLE 4.3. Velocity of Sound in Cu-Sn Alloys:Best-fit Parameters

Alloy (At. % Cu)	Intercept at T=0°C ($\times 10^5$cm/sec)	$-\frac{ds}{dT}$ ($\times 10^2$cm/sec)
0	2.5323±.0027	.2554±.0041
10	2.5643±.0032	.2515±.0047
20	2.6045±.0054	.2287±.0072
30	2.6620±.0036	.2306±.0045
40	2.7149±.0042	.2203±.0055
50	2.8358±.0028	.2260±.0035
60	2.9887±.0032	.2582±.0032
70	3.1953±.0054	.3091±.0049
80	3.4722±.0060	.3861±.0062
90	3.5695±.0091	.3236±.0077
100	3.8908±.0201	.4159±.0167

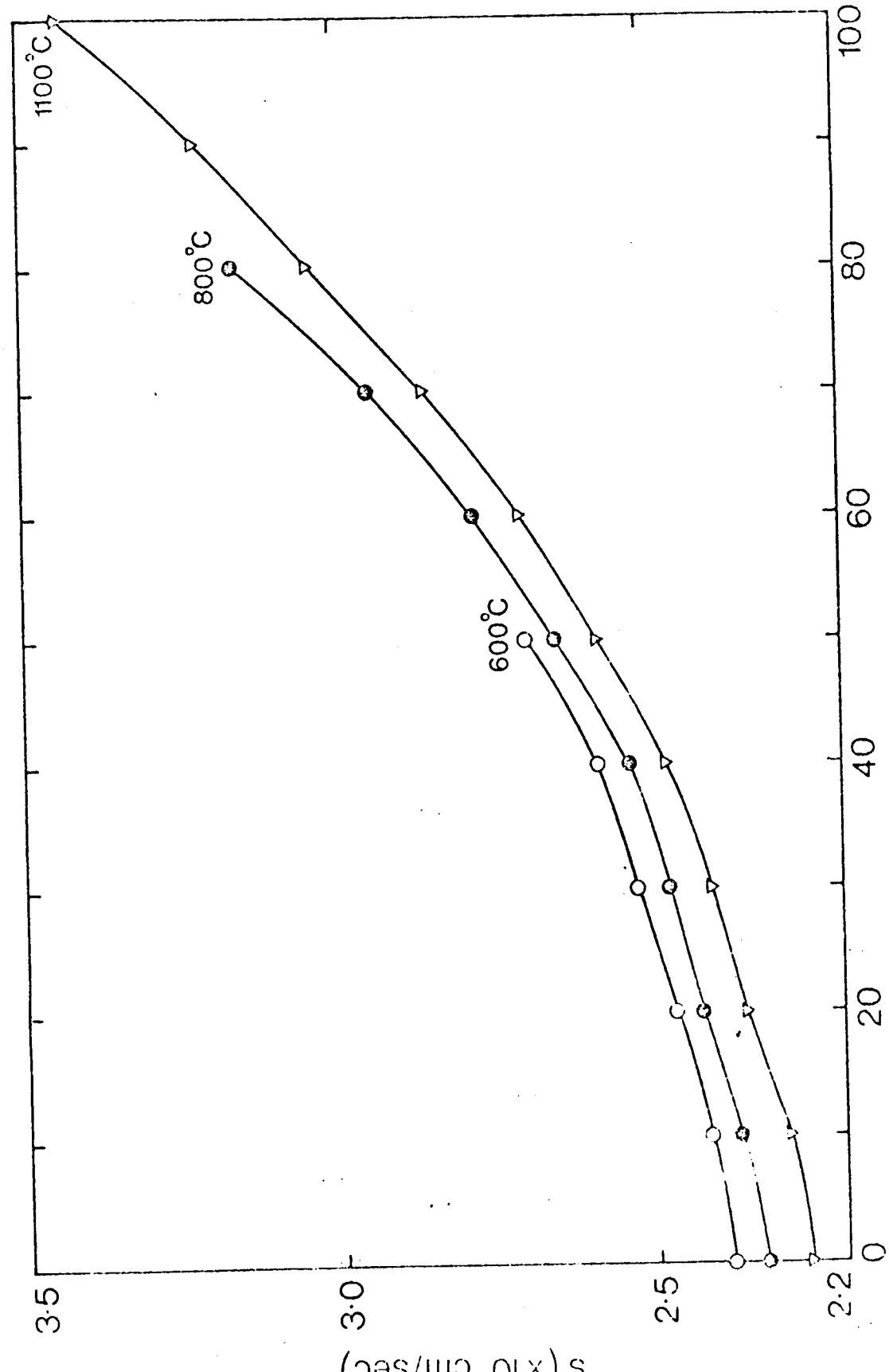

Fig. 4.3. Isotherms at T = 600°C, 800°C and 1100°C of the variation in the velocity of sound

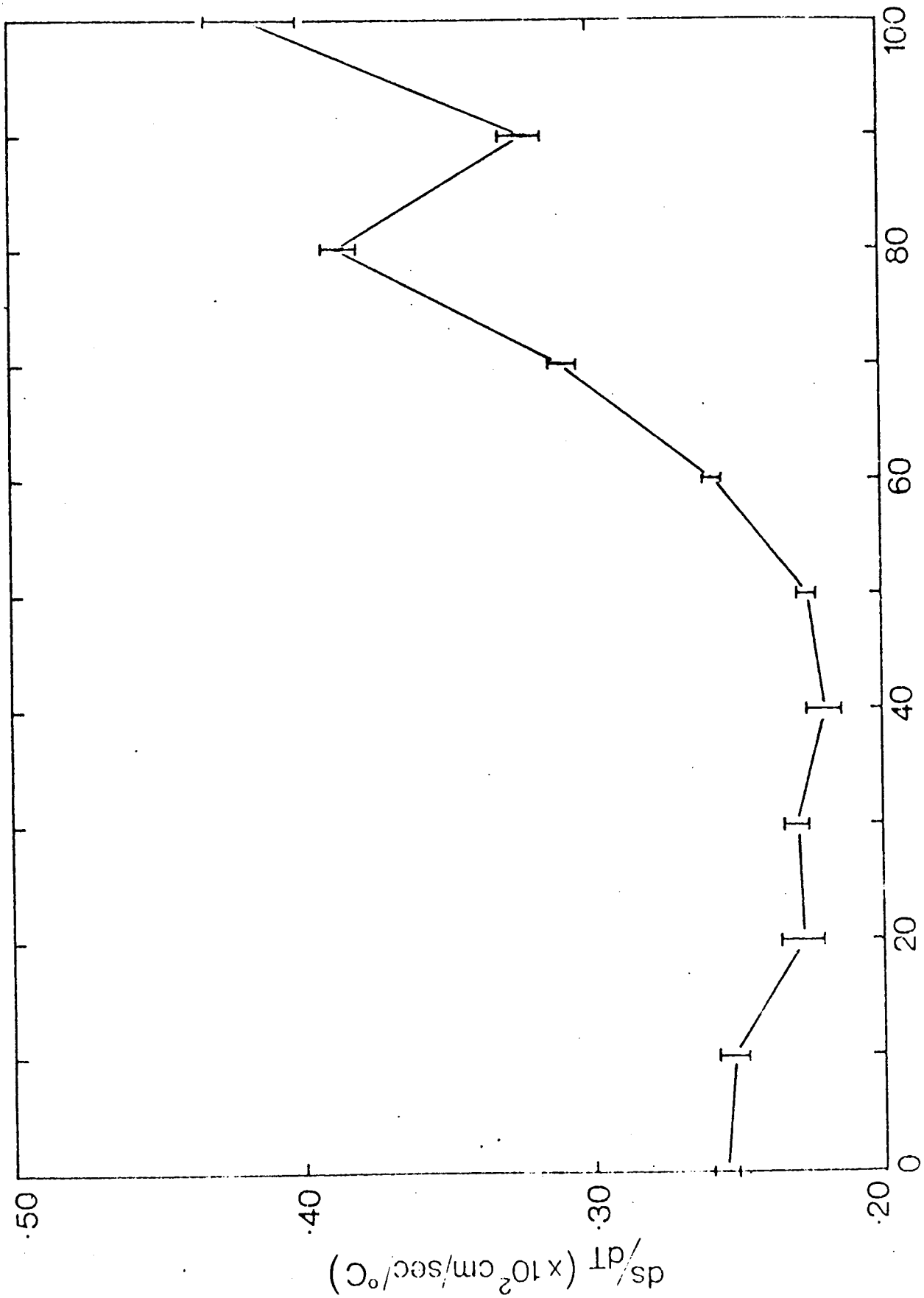

Fig. 4.4. Temperature Coefficient of Velocity of Sound in Cu-Sn Alloys as a Function of Composition.

80 at. % Cu can also be seen in the temperature dependence of the resistivity, as measured by Roll and Motz (1957). Their results for T = 1100°C are plotted in Fig. 5.5 for comparison with $\frac{1}{K_s}\frac{\partial K_s}{\partial T}$. The general features of the curve for $\frac{1}{K_s}\frac{\partial K_s}{\partial T}$ are clearly mirrored in the dependence of $\frac{\partial \rho}{\partial T}$ on composition. We shall not discuss the theoretical significance of this result.

For the alloys 50 at.%Cu, 60 at.%Cu, 70 at.%Cu and 90 at.%Cu it was found that the alloys, when first melted, were incompletely mixed. The clearest indication of this was a lack of reproducibility in the sound velocity measurements. A measurement would be made close to the melting point, on first heating, and then the temperature was raised to about 1200°C, where another measurement would be made. On cooling, making measurements every 100°C, it was found that the initial point did not lie on the same straight line as the subsequent points. For one alloy (70 at.%Cu) it took two heatings to 1100°C, at which temperature it was left for an hour while it was stirred vigorously from time to time, to obtain reproducible readings. Results obtained while cooling from a high temperature were compared with results obtained while heating, for all the alloys studied, in case this problem occurred. Only those readings were accepted which were made when the results defined a reproducible straight line. It was always found that the observed signal grew larger as the mixing improved; apparently inhomogeneity increases the acoustic attenuation considerably.

4-2 Discussion of Accuracy

In this experiment three quantities are measured; the acoustic wavelength, the frequency, and the temperature. There may be statistical or systematic errors associated with each of these.

4-2-1 Wavelength

Statistical error in measuring the wavelength is the major contribution to the scatter in the experimental values of the velocity of sound. In taking readings the main problem was to estimate when the interference signal (Fig. 3.6) was at a minimum. Since there is some backlash in the micrometer coupling one could approach the minimum only from one side, and thus one had to judge the minimum by comparison with the interference fringe before the one in question. Usually the position of the minimum could be judged reproducibly to $\sim$1/20th of the wavelength of sound, that is, to about 10^{-3} cm. More sophisticated electronics (see Section 3.6) could perhaps improve on this. One problem encountered in this estimation of the minimum was that in some alloys there was enough reflection of the acoustic pulse from the detection and then from the generation surfaces that subsidiary EDA echoes could be seen following the signal from the main EDA pulse superposed on the crosstalk (Fig. 4.5). These had the effect of confusing the observer, particularly when the probe was at the lower end of its travel, because they were then close (on the oscilloscope screen) to the signal of interest, distorting the shape of its trailing edge. Shortening the duration of the first generated pulse improved matters, by separating more clearly

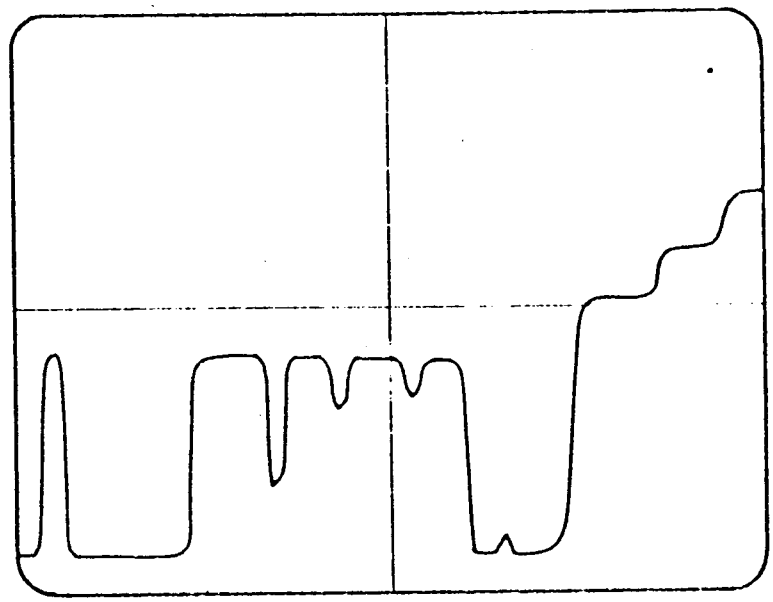

Fig. 4.5. Appearance of detected signal when echoes appear after first EDA signal.

the detected signal of interest from its subsequent echoes. Moreover, the lowest point of the probe travel was always at least .5 cm from the generating surface (the end of the delay line) giving at least 3 μ secs between the EDA pulse of interest and its first echo in the liquid metal. Since these pulses have a rise time of ∿.5 μs the first and second EDA pulses could easily be distinguished. In a liquid metal where these echo pulses are more pronounced than in the present series of alloys, they could also be used to determine the wavelength of sound, since the n'th echo will go through 2n interference fringes while the main EDA signal goes through one. This would enable more fringes to be counted, giving a higher accuracy for λ.

Expressed as a percentage, the root mean square statistical error in the wavelength λ was usually ∿.07%. The only sources of systematic error in the wavelength measurement are (a) the calibration of the micrometer, which was assumed to be correct to 10^{-4} inches (the accuracy to which it could be read); (b) diffraction of the acoustic waves in the liquid, and (c) the thermal expansion of the probe as it is lowered through the liquid metal. The diffraction associated with the detection surface is unimportant, since the waves are detected before they are diffracted; diffraction at the generation surface is the only problem. This surface is ∿1.5 cm in diameter, the acoustic path length d is ≤ 2 cm, and the acoustic wavelength is $\sim 3\times10^{-2}$ cm, so the detector is well within the near diffraction zone, defined by $\frac{d\lambda}{a^2} << 1$. Using the correction for the velocity given by Bass and Wiliams (1960)

$$\frac{\Delta s}{s} \approx \frac{\lambda^{3/2}}{4\pi^2 a d^{1/2}}$$

we deduce a maximum systematic error from this source in the wavelength of .02%.

Thermal expansion affects only a length of about 1 cm of the quartz probe sheath, whose temperature is increased by at most 200°C as it is lowered into the liquid metal. Since the thermal expansion coefficient of quartz is $\sim 10^{-6}{}^{\circ}C^{-1}$, the maximum change in length of the entire probe assembly is $\sim 2\times 10^{-4}$ cm, giving rise to a systematic error in the wavelength of at most .02%.

4-2-2 Frequency

Reproducibility in the measurement of frequency was about ~.02%. A larger error was introduced at high temperatures (above 900°C) in earlier runs, before the cooled transducer was developed, by frequency drifts during a measurement. These drifts were caused by heating of the transducer, which took perhaps an hour to reach thermal equilibrium when it was not cooled. Usually the measurements were begun before the transducer equilibrium temperature had been reached. The dielectric constant of the transducers used changes with temperature, thus changing the load on the r.f. generator and hence its frequency. The frequency drift at a given thermocouple temperature was at most .1%, however, and since the average frequency was used, the standard deviation in frequency was never more than .05%. This drift affected only a few measurements at high temperatures on the low-Cu alloys. When the cooled transducer mount was used, this

drift was not observed, though the frequency was observed to shift when the temperature of the furnace was changed. Clearly cooling enabled the transducer to reach thermal equilibrium much faster. Since the frequency counter is calibrated to one part in 10^8, there was no appreciable systematic error in the frequency measurement.

4-2-3 Temperature

Although there was a temperature gradient of at most 2%, this gave rise to an error of at most .2% in the temperature, since the average wavelength and the average temperature were used. The thermocouple calibration curve is linear enough so that the average temperature was given by the average thermocouple voltage reading. Temperature drifts in the course of a series of wavelength measurements were never more than .5%, and again using the average temperature for the series of measurements gives a standard error of $\sim\pm.2\%$ from this source. The accuracy to which the thermocouple voltage could be read was 10^{-5} V, equivalent to an accuracy of $\pm 1^{\circ}C$ in the temperature. A check of the calibration of the type of thermocouple used (see Section 3-2-5) showed that it was correct to $\pm 1^{\circ}C$ at $232^{\circ}C$ and $1083^{\circ}C$, and therefore it was most probably correct to this accuracy over the rest of the range over which it was used. Since the actual thermocouples used in the experiment were not checked in this way, an additional uncertainty is introduced, but this is not likely to exceed $5^{\circ}C$ since the thermocouples were identically made, from the same batch of wire.

Thus the statistical errors in temperature are not greater than .5%, and the systematic error involved in the calibration is about the same.

The total maximum estimated error in the temperature is then ∿1%, corresponding at 1000°C to a change in sound velocity of ∿.1%. Since the main effect of this would be an additional error of ∿.5% in the values of the temperature coefficient of the sound velocity, which already have a standard deviation of ∿2% owing to the statistical errors in the measurement of λ, this source of error is relatively small.

The maximum estimated error in the measured velocity of sound is thus .2%, and this error decreases as the temperature decreases. The maximum estimated error in $\frac{ds}{dT}$ is ∿2%.

CHAPTER 5

ANALYSIS OF RESULTS

5-1 The Compressibility of Cu-Sn Alloys

5-1-1 Density Data

In order to evaluate the adiabatic and isothermal compressibilities of the alloys studied, it is necessary to have accurate density data. Furthermore, a rough idea of the specific heat at constant pressure, Cp, is needed, though the value of γ is not very sensitive to this quantity. In any case, Cp is always fairly close to the ideal monatomic solid value of 3R calories/mole, where R is the universal gas constant. Equations (1.8), (1.10) and (1.11) can then be used. The major uncertainty in the evaluation of γ comes from uncertainty in α_p, the thermal expansion coefficient. This quantity appears squared in (1.11), and is hard to measure accurately because it is small ($\sim 10^{-4} {}^{o}C^{-1}$). Thus density measurements accurate to $\sim$.01% are needed to give $\sim$1% accuracy for α_p; and systematic errors in density measurements, which vary with temperature, appear to be common. For example, in the Archimedean method of density measurement, where the mass of liquid metal displaced by a sinker of known volume is observed, experimenters rely on previous data for the thermal expansion of the sinker. If these data are incorrect, the values of α_p deduced would also be wrong. Again, the effect of surface tension on the suspension of the sinker where it leaves the liquid metal surface must be accounted for, so the work of previous experimenters must be again

consulted; and it is well-known that surface tension measurements at high temperatures are not easy to make, and are not usually very accurate. The surface tension also depends critically on the condition of the liquid surface; an oxide surface layer in a density experiment could thus substantially alter the correction term needed.

A comprehensive literature search was therefore undertaken to obtain the most reliable values of the densities and thermal expansion coefficients of pure Sn, pure Cu, and the intermediate alloys. Results for the more recent investigations of pure Cu and pure Sn are presented in Table 5.1, together with the 1922 results of Bornemann and Sauerwald, who also measured several of the alloys. Only one other investigation has been made into the density of Cu-Sn alloys, by Watanabe and Saito (1971). Their values for the pure metals are in disagreement with most workers, by $\sim$2% for the density and $\sim$20% for the value of the thermal expansion coefficient. Otherwise, there is reasonable agreement between different workers. We consider the figures of Thresh et al. (1968) to be most reliable for pure Sn, and those of Cahill and Kirshenbaum (1962) for pure Cu, because their experiments appear to be the most carefully designed.

Unfortunately, the density data for the alloys given by Bornemann and Sauerwald give thermal expansion coefficients that seem to be unreasonably high; for pure Cu a value double that of more recent careful workers. This inaccuracy is highlighted by the value of γ calculated with their results, which exceeds 2 at one composition. Since a monatomic gas has a γ of only 1.66, this result is unphysical. As a result we were forced to use the density data of Watanabe and Saito to calculate γ and

TABLE 5.1. Density and Thermal Expansion Coefficient of Pure Liquid Copper and Tin at their Melting Points

Metal	Reference	Density (gm/cm^3)	α_p ($\times 10^{-4} °C^{-1}$)
Sn	Übelacker and Lucas (1962)	6.969	1.087
	Kirshenbaum and Cahill (1962)	7.000	0.875
	Wilson (1965)	6.969	0.88
	Schwaneke and Falko (1967)	7.014	0.90
	Thresh, Crawley and White (1968)	6.974	1.022
	Berthou and Tougas (1968)	6.980	0.79
	Watanabe and Saito (1971)	6.82	0.78
	Bornemann and Sauerwald (1922)	6.983	0.98
Cu	Widawski and Sauerwald (1930)	7.99	0.98
	Cahill and Kirshenbaum (1962)	7.992	1.002
	El-Mehairy and Ward (1963)	8.090	1.167
	Watanabe and Saito (1971)	7.86	0.84
	Bornemann and Sauerwald (1922)	7.99	1.99

the isothermal compressibilities for the alloys although their values for the thermal expansion coefficient α_p seem consistently about 15% low. This leads to an error in γ and thus K_T of $\sim$3%. The authors claim a statistical error of $\sim$2% in their data for the thermal expansion coefficient; a systematic error seems likely. They use the maximum bubble-pressure method to measure the density. Fig. 5.1 shows the molar volumes of the copper-tin alloys at 1100°C, calculated from the measurements of Bornemann and Sauerwald, and Watanabe and Saito. It is clear that the departure from ideal mixing is not great; we shall discuss this point in more detail later on in this Chapter. The average discrepancy between the two sets of measurements is $\sim$1%, which is much larger than the statistical errors claimed in each case. The curves have very similar shapes, however. For those alloys which we studied whose densities were not measured, we used a value for the density obtained from a smooth curve through the points of either Watanabe and Saito, or Bornemann and Sauerwald (plotted as in Fig. 5.1), depending on whose results were being used for the other alloys.

5-1-2 Compressibility Results

Table 5.2 gives the compressibilities and the ratio of the specific heats in pure tin and pure copper at their respective melting points, calculated from our sound velocity data and the density data of Thresh et al. (1968) for Sn and Cahill and Kirshenbaum (1962) for Cu. Data for the specific heat C_p were taken from Hultgren et al. (1963) for pure Sn and from Vollmer and Kohlhaas (1968) for pure Cu. Also given in Table 5.2 are the values of the compressibilities computed by Webber and

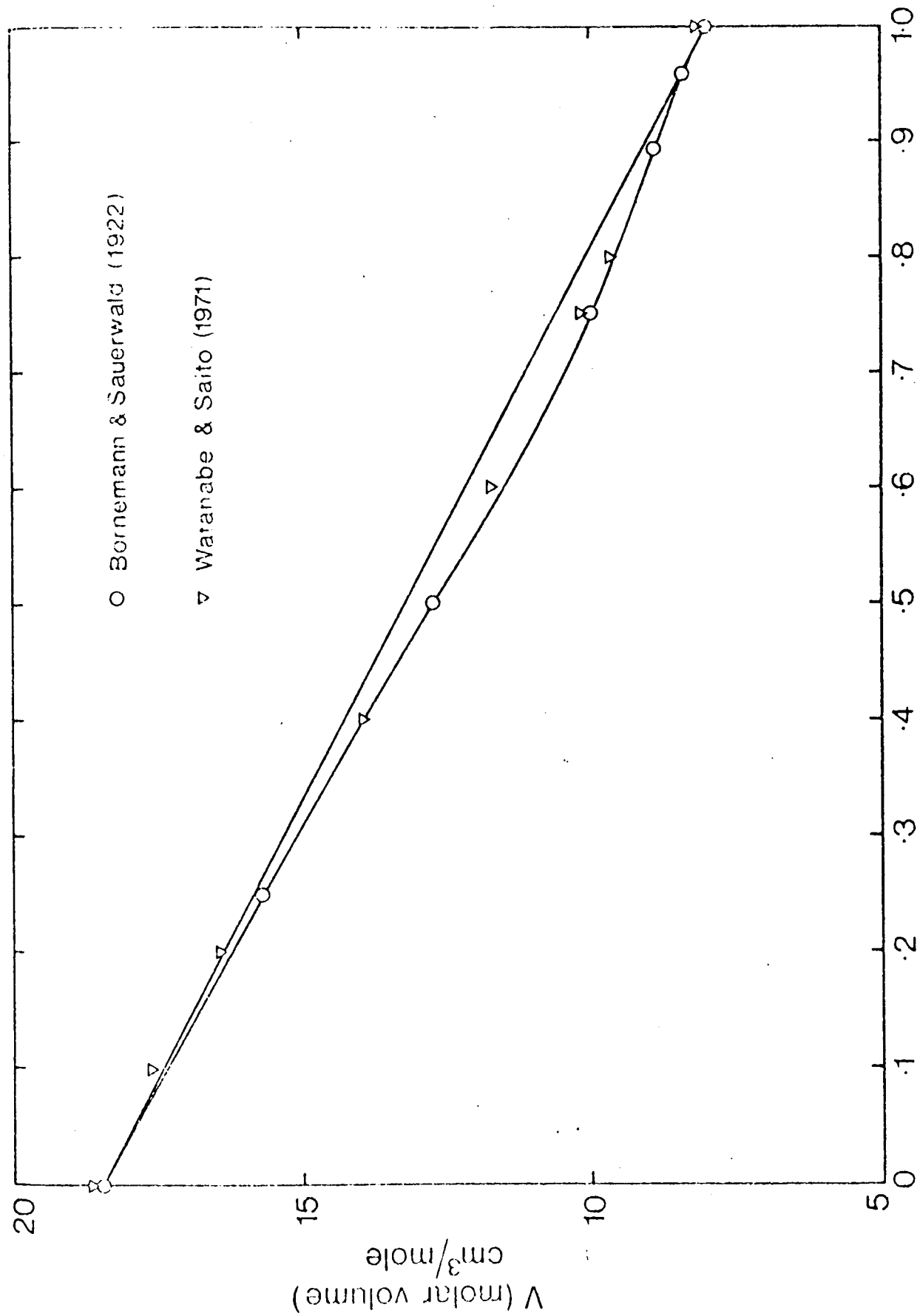

Fig. 5.1. The molar volume of Cu-Sn alloys at 1100°c.

TABLE 5.2. Values of the Adiabatic and Isothermal Compressibilities and Their Ratio, γ, of Pure Cu and Pure Sn at Their Respective Melting Points, and the Data used to obtain these Values

Metal	T(^{o}K)	Density (gm/cm^{3})	α_p ($^{o}C^{-1}$)	c_p (cals/gm^{o}C)	K_S^{exp} (cm^2/dyne)	K_T^{exp} (cm^2/dyne)	γ_{exp}
Cu	1356	7.992	1.002×10^{-4}	.121	$1.057\pm.003\times10^{-12}$ (1.03)	$1.40\pm.02\times10^{-12}$ (1.49)	1.33
Sn	505	6.974	1.022×10^{-4}	.0598	$2.344\pm.006\times10^{-12}$ (2.36)	$2.65\pm.05\times10^{-12}$ (2.71)	1.13

Sources of auxiliary data are given in the text.

Values in brackets are those of Webber and Stephens (1968).

Stephens from previous experimental data. It can be seen that agreement is good for Sn. The source of the slight disagreement for Cu is the use by Webber and Stephens of the density results of El-Mehairy and Ward (1963), which we consider suspect in view of their disagreement with the majority of published results, and also because of their method, which consists in measuring optically the dimensions of a levitated liquid drop of Cu whose mass is subsequently determined. Since our values of the velocity of sound in pure Cu and pure Sn appear to be the most accurate hitherto, the values of the compressibilities presented in Table 5.2 are probably the most reliable yet obtained.

In Table 5.3 we present the adiabatic and isothermal compressibilities of copper-tin alloys, using the density data of Watanabe and Saito throughout. The reason for using their data was that it appears to be comparatively accurate, even though it is systematically in error. Intermediate values of the specific heat C_p were needed to determine γ and hence K_T. To obtain these we appealed to the Neumann-Kopp Law, which states that the molar specific heat varies linearly as a function of composition. Kubaschewski et al. (1967) give a table of departures of real alloy systems from this Law, which are never more than 8% even for highly non-ideal alloys. Thus we can assume with some confidence that this linear interpolation will not give an error larger than 1% in the values for γ and K_T. The contribution to the total error by the sound velocity measurements is $\sim$.2%, while statistical errors in the density and α_p contribute $\sim$1% and $\sim$2% to the total error in the adiabatic and isothermal compressibilities respectively; the effect of error in the sound velocity measurements is

TABLE 5.3. Parameters Derived from Measurements of the Velocity of Sound in Cu-Sn Alloys Using the Density Measurements of Watanabe and Saito (1971) at 1100°C

(At. % Cu) Composition	Density (gm/cm^3)	Adiabatic Compressibility ($\times 10^{-12} cm^2/dyne$)	Isothermal Compressibility ($\times 10^{-12} cm^2/dyne$)	$\frac{N}{V} k_B T K_T$
0	6.36	3.103	3.74	.0229
10	6.44	2.966	3.54	.0230
20	6.58	2.745	3.31	.0231
30	6.75	2.555	3.07	.0232
40	6.93	2.359	2.83	.0232
50	7.09	2.107	2.56	.0227
60	7.30	1.872	2.30	.0224
70	7.51	1.634	2.03	.0217
80	7.75	1.390	1.75	.0208
90	7.87	1.230	1.54	.0200
100	7.84	1.082	1.33	.0187

negligible. The total probable error in K_S is 1.2%, and the probable error in K_T is 2%.

Fig. 5.2 shows the adiabatic compressibility as a function of composition at two different temperatures, 800°C and 1100°C. Since the 90 at. % and 100 at. % Cu alloys are not liquid at 800°C, points for them are not plotted on the former curves. Measurements of the sound velocity were not made for all of the alloys at 1100°C, but the quality of the straight lines obtained for the velocity as a function of temperature enables us to extrapolate by the 100°C needed in some cases to obtain the 1100°C values. A striking feature of the curves shown in Fig. 5.2 is that they are close to a linear dependence of compressibility on composition. Such a linear dependence is not predicted for ideal mixing (see Equation (1.50), and the next Section) and may be coincidental. Since the behaviour of the 800°C curve is very similar to the 1100°C curve, we shall henceforth discuss only the 1100°C case. The isothermal compressibility is plotted in Fig. 5.3; the variation with composition is even more nearly linear.

Table 5.3 also includes the quantity $\frac{N}{V} k_B T K_T$, which can also be calculated using the hard-sphere model (see Chapter 1). The experimental value stays remarkably constant up to a composition of 50 at. % Cu, and never becomes very much lower than the hard-sphere value (for a packing fraction of $\eta = .45$) of .0253. This behaviour will also be discussed in the next Section.

We note that the values of K_S and K_T for pure Cu and pure Sn given

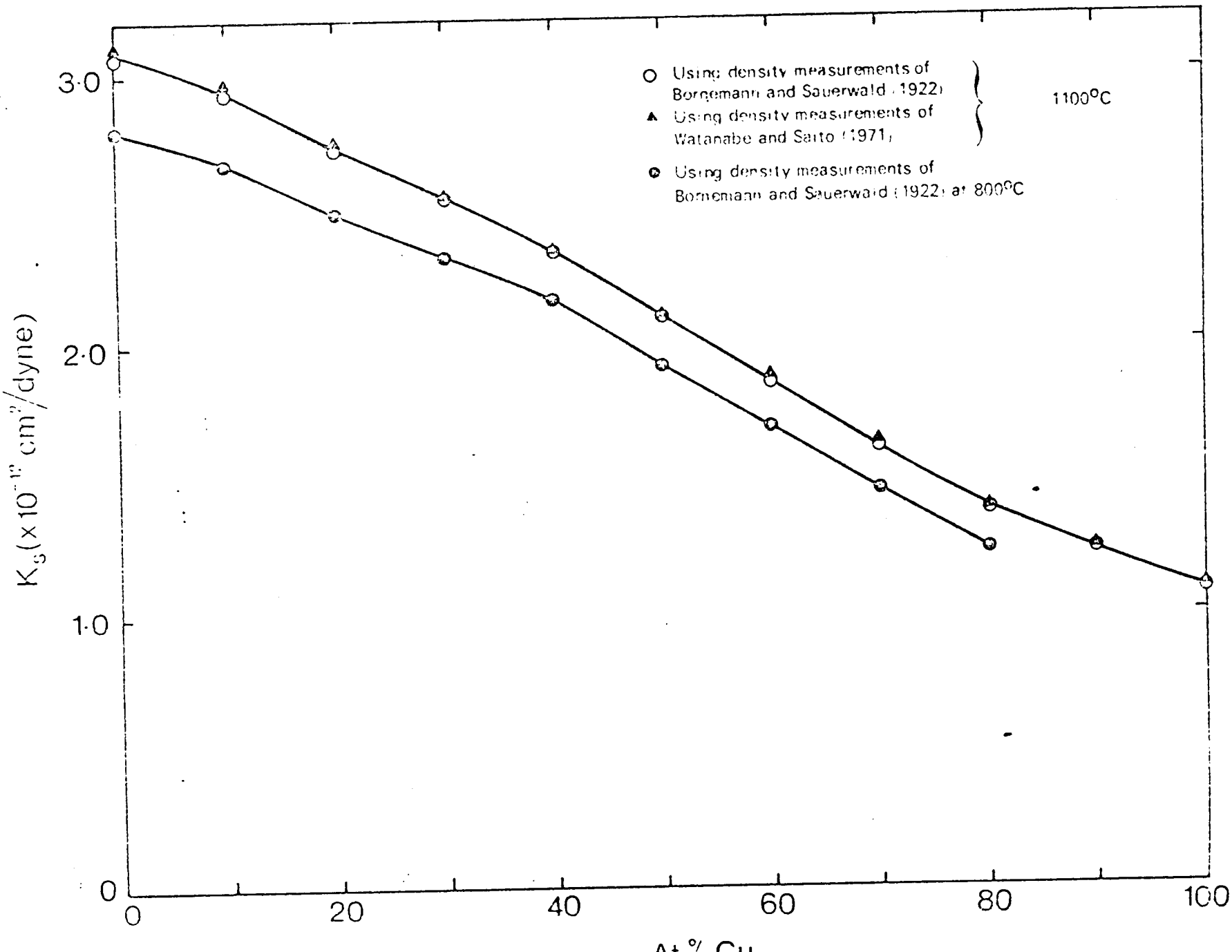

Fig. 5.2. The adiabatic compressibility of Cu-Sn Alloys at 1100°C and 800°C.

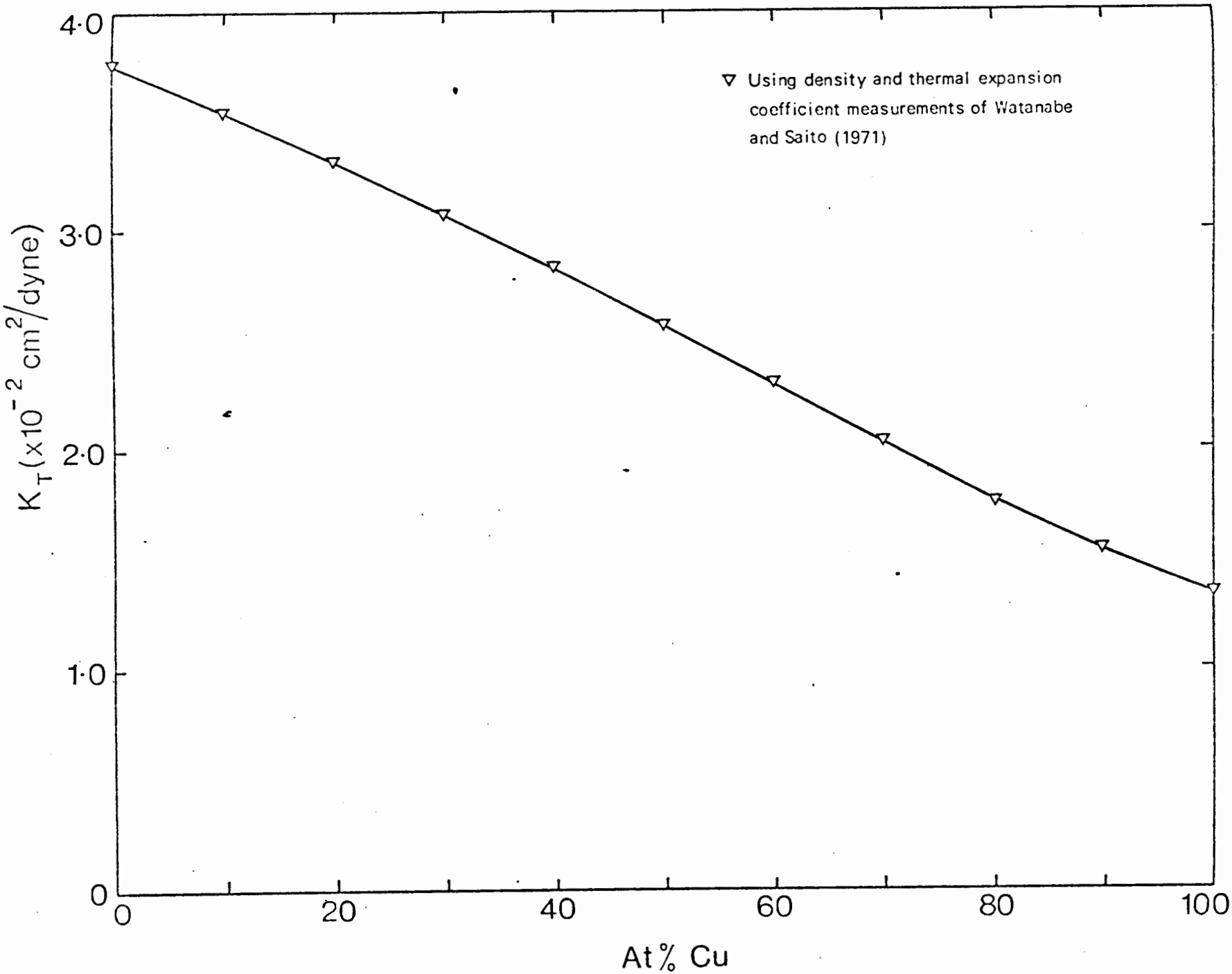

Fig. 5.3. Isothermal Compressibility of Cu-Sn alloys at 1100°C.

in Table 5.3 differ from those given in Table 5.2. For Sn this discrepancy is mainly due to the decrease in the velocity of sound and the density caused by the large temperature difference between the melting point and 1100°C. For Cu, however, it is caused by the fact that the values given by Watanabe and Saito for the density and coefficient of thermal expansion are lower than those used in Table 5.2. The values of K_S and K_T given in Table 5.3 will be used for comparative purposes only.

5-1-3 Comparison with Theories of Compressibility

Now we may attempt to use the theories of Section 1-4 to explain the observed composition dependence of the compressibility. It is obvious that the Bohm-Staver and Overhauser results will not give reasonable agreement with experiment, since they are quite inaccurate for the pure metals (see Table 1.1). The next theory to try is the Percus-Yevick binary mixture of hard spheres (Equation 1.69). Although the packing fraction η is not known for Cu-Sn alloys, we may consider two cases:

(a) Ashcroft and Langreth (1967b) give values of $\eta = .266$ and $\eta = .456$ for pure Sn and pure Cu respectively, at T = 1200°C. In the spirit of the Percus-Yevick approximation, we may linearly interpolate for the intermediate alloys, using the equation $\eta = \frac{N}{V} (cv_1\eta_1 + (1 - c)\, v_2\eta_2)$, and thereby evaluate Equation (1.69).

(b) We may adjust η so that agreement with experiment is obtained for K_T for the pure metals, and then interpolate linearly to obtain intermediate values of η, as before. The value $\eta_{Sn} = .461$ thus derived is wholly unrealistic, it must be pointed out; the packing fraction of Sn 900°C above the

melting point can be no greater than .3.

The results of the calculation for cases (a) and (b) are tabulated in Table 5.4, and plotted in Fig. 5.4. It can be seen immediately that the agreement with experiment for both estimates is extremely poor; even if the end points are corrected as in (b), the composition dependence is entirely wrong, there being a minimum instead of a maximum in $\frac{N}{V} k_B T K_T$.

The only other theory we have the parameters to evaluate is that of Ascarelli. He gives the expression

$$\frac{N}{V} k_B T K_T = \frac{1}{\frac{(1+2\eta)^2}{(1-\eta)^4} + \frac{2}{3}\frac{zE_f}{k_B T} - A\left(\frac{V_{m.p.}}{V}\right)^{1/3}\cdot\frac{4}{3}\frac{k_B T_m}{k_B T}} \qquad (5.1)$$

where

$$A = 10 + \frac{2}{5} zE_f(T_m)/k_B T_m$$

and $V_{m.p.}$ and T_m are the volume and temperature at the melting point, respectively. One would expect that this Equation needs to be slightly corrected for alloys; instead of the term $\frac{(1+2\eta)^2}{(1-\eta)^4}$ we write $\frac{(1+2\eta)^2-\Delta}{(1-\eta)^4}$ as in Equation (1.69). Using the fact that $\left(\frac{V_{m.p.}}{V}\right)^{1/3} \approx 1$ even for pure Sn, and thus $E_f(T) \approx E_f(T_m)$, we have finally

$$\frac{N}{V} k_B T K_T = \frac{1}{\frac{(1+2\eta)^2-\Delta}{(1-\eta)^4} + \frac{2}{15}\frac{zE_f}{k_B T} - \frac{40}{3}\frac{T_m}{T}} \qquad (5.2)$$

We have taken T_m as the liquidus temperature of the alloy concerned, though, as pointed out in Section 1-4, this choice is somewhat arbitrary. Once again we have two choices of values for the packing fraction. We may again use Ashcroft and Langreth's figures of $\eta_{Sn} = .266$ and

TABLE 5.4. Comparison of Observed $\frac{N}{V} k_B T K_T$ with Various Theoretical Results

C	$\frac{N}{V} k_B T K_T$ exp	$\frac{N}{V} k_B T K_T$ (P-Y*) Hard Sphere (a) η_{Sn}=.266 η_{Cu}=.456	(b) η_{Sn}=.461 η_{Cu}=.482	$\frac{N}{V} k_B T K_T$ (Ascarelli) η_{Sn}=.266 η_{Cu}=.456	η_{Sn}=.234 η_{Cu}=.492
0	.0229	.121	.0228	.0220	.0229
.1	.0230	.115	.0225	.0244	.0255
.2	.0231	.104	.0214	.0266	.0281
.3	.0232	.092	.0201	.0288	.0308
.4	.0232	.080	.0188	.0309	.0335
.5	.0227	.069	.0179	.0326	.0360
.6	.0224	.058	.0168	.0339	.0376
.7	.0217	.047	.0158	.0336	.0377
.8	.0208	.036	.0151	.0315	.0347
.9	.0200	.029	.0158	.0299	.0289
1.0	.0187	.024	.0187	.0278	.0188

*Percus-Yevick

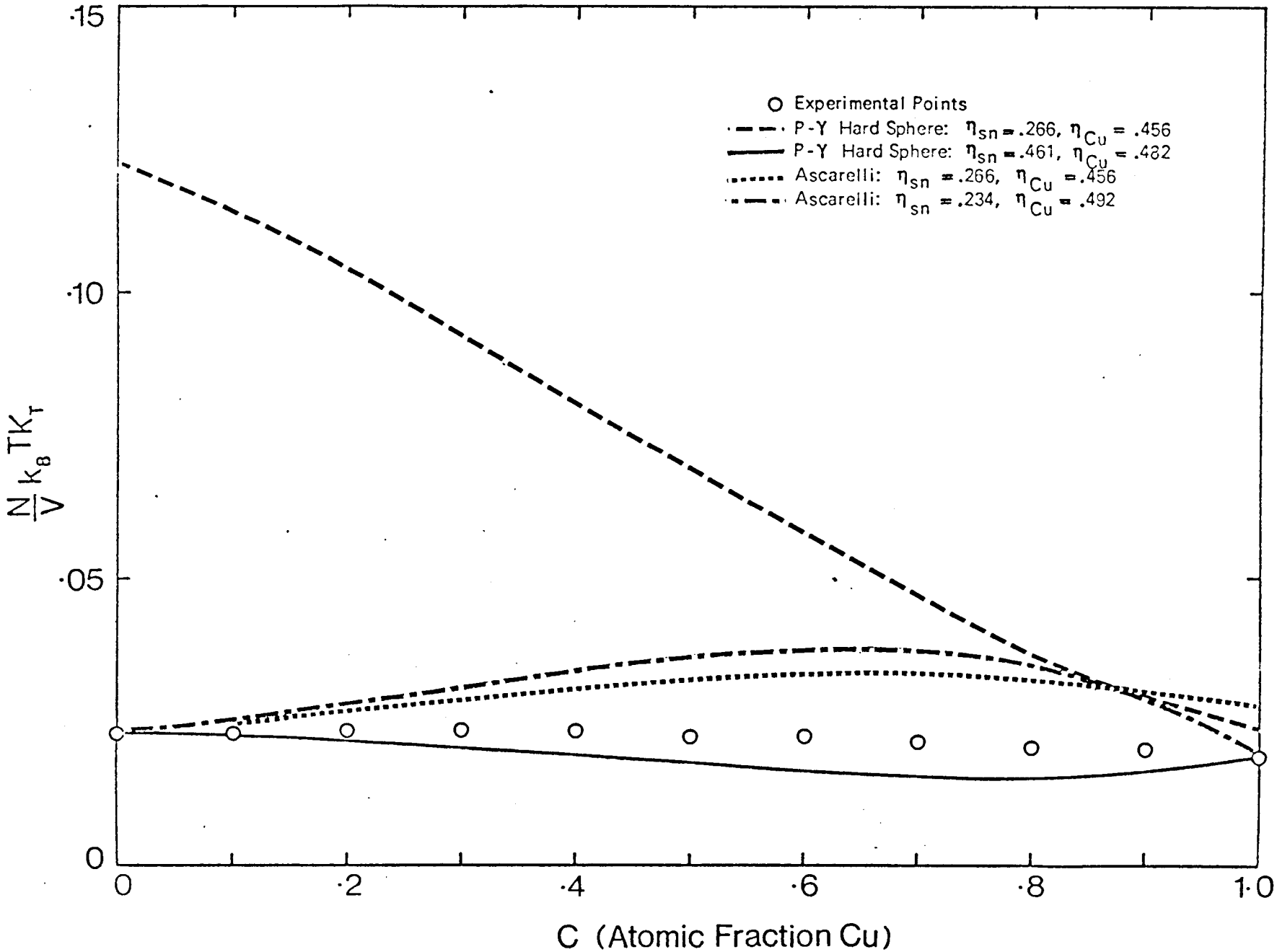

Fig. 5.4. Comparison of Observed $\frac{N}{V} k_B T K_T$ with Theoretical Results for Cu-Sn Alloys at 1100°C.

η_{Cu} = .456, or we may adjust these figures to get good agreement for pure Sn and pure Cu, giving η_{Sn} = .234 and η_{Cu} = .492. In both cases we interpolate as before for the intermediate alloys. The results for both cases are presented in Table 5.4 and plotted in Fig. 5.4. The values of Z and E_f to be substituted into (5.2) were found by assuming that the number of free electrons per atom in the alloy varies linearly with composition from one to four, a hypothesis supported by the Hall effect data of Busch and Güntherodt (1967), and the optical work of Comins (1972).

Note that when we use Ashcroft and Langreth's packing fractions there are no adjustable parameters in the theory. Thus, although the compressibility is overestimated, we regard the overall agreement as good. Note that indeed $\frac{N}{V} k_B T K_T$ has a maximum, though it is displaced somewhat. When η_{Sn} and η_{Cu} are adjusted to correct the end points, the overall agreement is poorer; this is caused mainly by the adjustment of η_{Sn}.

Ashcroft and Langreth obtain their packing fractions from an analysis of the pair potential functions they derive during a calculation of the resistivities of binary alloys. Their derived resistivities are in fairly good agreement with experiment.

The partial success of Ascarelli's approach suggests that it is worth pursuing further, using better estimates for the packing fractions. It is interesting to note that for pure Sn, the important term in the Ascarelli formula (5.2) is that involving E_f, the hard-sphere contribution being relatively unimportant; while the reverse is true for pure Cu. The reason for this is that the packing fraction in Sn at 1100°C, far above the melting point, is small, so the hard spheres do not interact as much

as in Cu, which at 1100°C has a high packing fraction, because it is just above its melting point. As a liquid metal is heated, it appears, in general, that the hard-sphere contribution to the compressibility diminishes, while the contribution due to the electron gas becomes relatively more important. At temperatures far enough above the melting point it would appear that Overhauser's result (1.58) should give agreement with experiment.

We can also compare the observed compressibilities with those of an ideal alloy system with the same atomic volumes for the pure metals. We shall make an explicit comparison for K_s, because our data for this quantity are more reliable. We have

$$K_{s_{ideal}} = \frac{N}{V_{ideal}} \left(c_1 v_1 K_{s_1} + c_2 v_2 K_{s_2} \right) \tag{5.3}$$

where $V_{ideal} = N(c_1 v_1 + c_2 v_2)$, the molar volume for an ideal system. Thus, if the system were ideal, VK_s would have a linear dependence on concentration. In the present alloy system VK_s is always smaller than K_s ideal, except of course at the end points. Fig. 5.5 shows the fractional deviation of VK_s from ideal mixing at 1100°C. The data points at 75, 85 and 95 at. % Cu are taken from a smooth curve of VK_s versus composition. Roughly half of the 28% maximum deviation from the ideal can be explained by the departure by ∿6% of the molar volume from ideal mixing (Fig. 5.1); the remainder of the deviation comes from the sound velocity itself.

Fig. 5.6 shows the variation in $\frac{1}{K_s} \frac{\partial K_s}{\partial T}$ with composition. It shows the same anomaly as $\frac{\partial s}{\partial T}$, at a composition ∿80 at. % Cu. Also plotted in

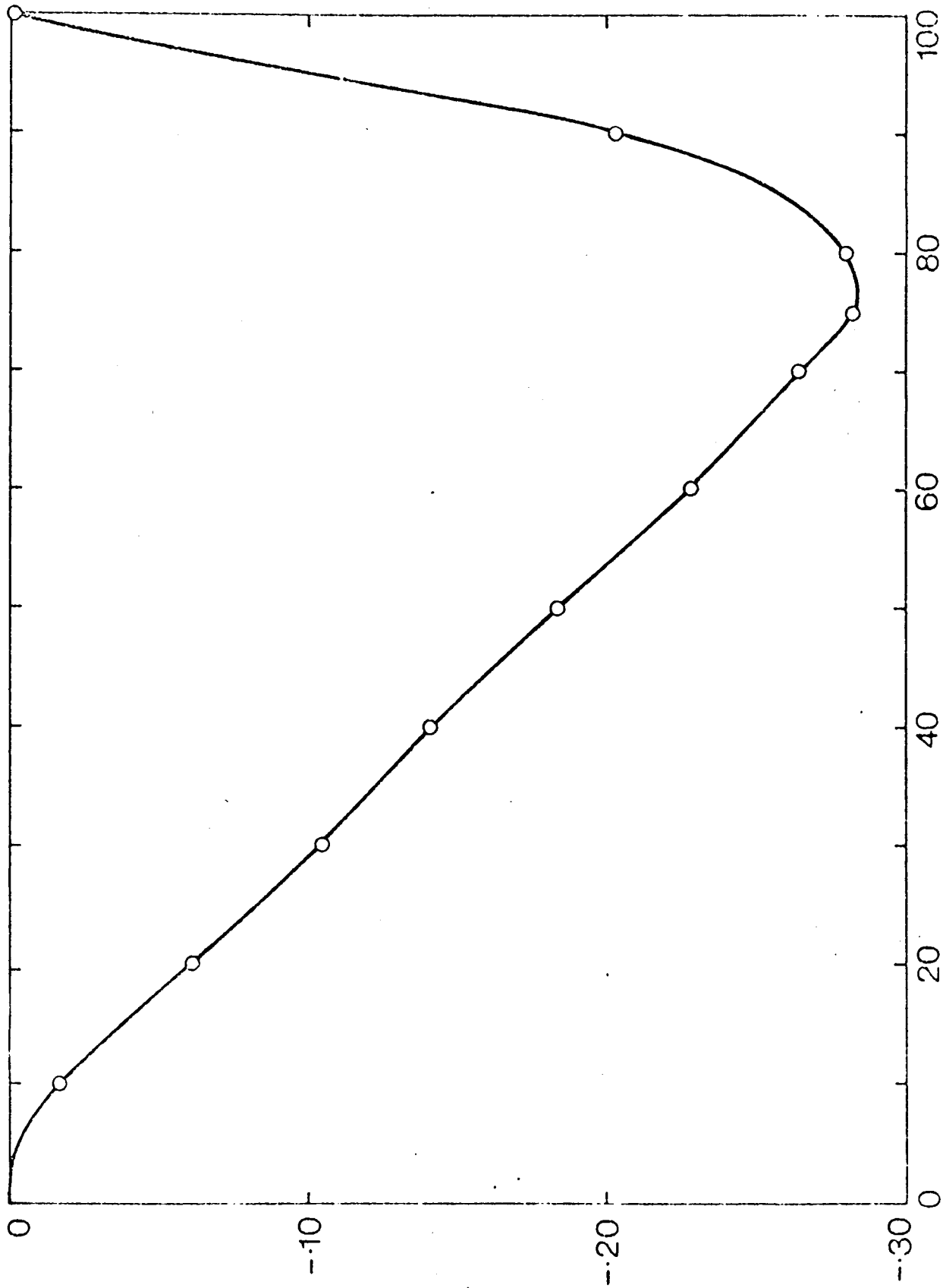

Fig. 5.5. Fractional Deviation of $V_m K_s$ from Ideal Mixing at 1100°C

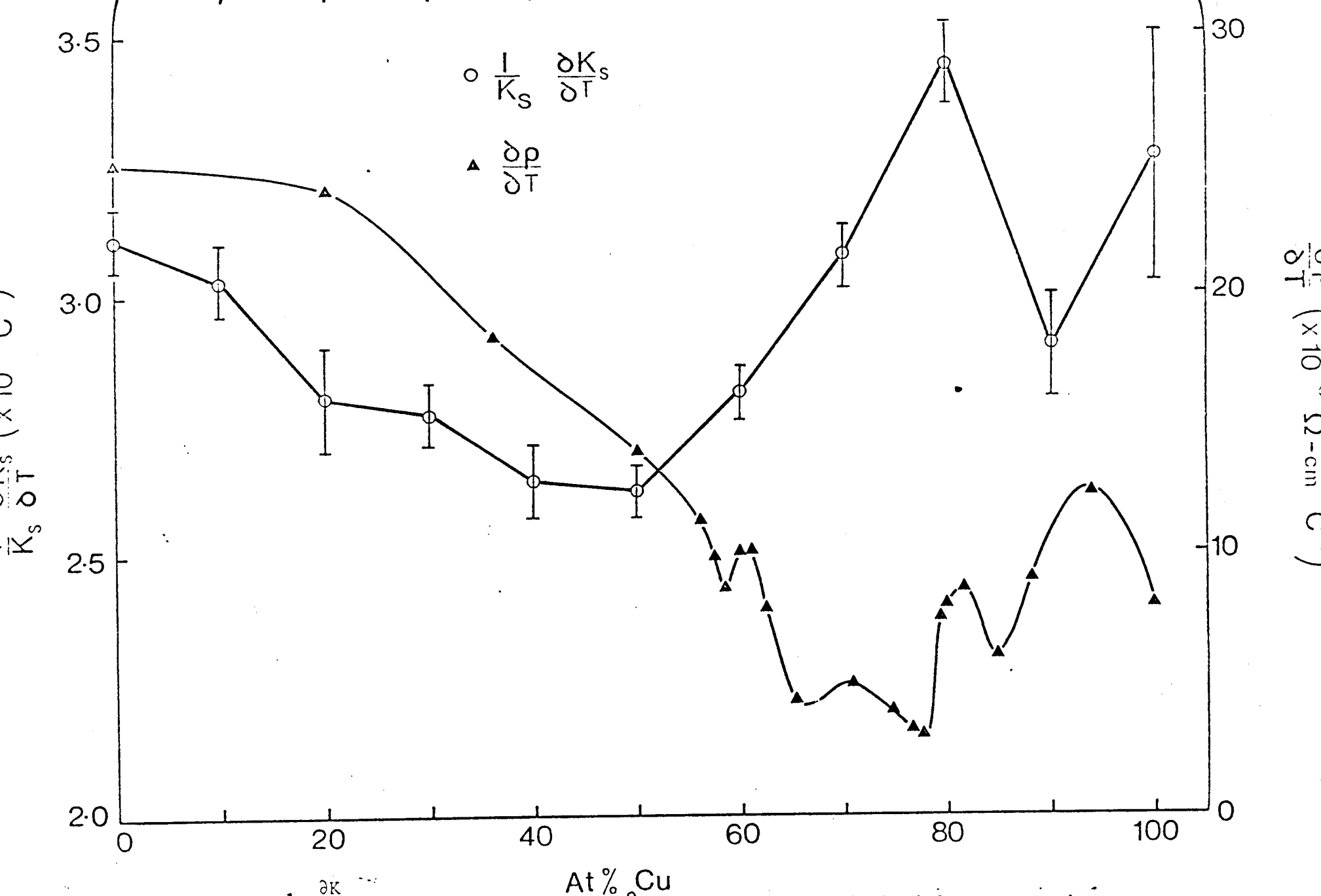

Fig. 5.6. Variation of $\frac{1}{K_s}\frac{\partial K_s}{\partial T}$ with composition at 1100°C. Error bars are derived from errors in $\frac{ds}{dT}$. The temperature coefficient of the resistivity, $\frac{d\rho}{dT}$, at the same temperature, is also shown

Fig. 5.6 are the results of Busch and Güntherodt (1967) for the temperature coefficient of the resistivity, $\left(\frac{d\rho}{dT}\right)_p$, for these alloys at 1100°C. There is some controversy about the detailed structure in these results, but the similarity of the overall shape of their curve (which is not a matter of controversy) to our results for $\frac{1}{K_s}\frac{\partial K_s}{\partial T}$ is obvious, though the departures from a smooth curve are in the opposite direction.

5-2 Other Properties of Cu-Sn Alloys

In an effort to understand more clearly the behaviour of the compressibility as a function of composition, we may compare it with other physical properties of these alloys which may be more amenable to theoretical explanation. We shall find that by doing so we will be in a position to sketch the outlines of a theory of the structure of Cu-Sn alloys, from which we could, in principle, derive the behaviour of the compressibility as a function of composition. While the details of such a theory are beyond the scope of this thesis, we shall indicate the general lines of the argument, which can also be used to explain the calculated composition dependence of the partial structure factors at zero-wavevector.

5-2-1 Correlation of the Compressibility with Other Properties of Cu-Sn Alloys

Surveying the other properties of Cu-Sn alloys that have been measured, one notices, in general, that if there is unusual behaviour as a function of concentration, it is centred on the composition 78 at. % Cu, in exactly the same way as the departure of VK_s from the ideal. We shall

consider the enthalpy of mixing and the electrical resistivity.

A plot (Fig. 5.7) of the molar enthalpy of mixing ΔH_m (Hultgren 1963) shows a striking similarity to the plot of the departure of VK_s from the ideal (Fig. 5.6). The position of the minimum is identical, and the overall shape of the curve is also very similar to that of Fig. 5.6. Note that for an ideal mixture $\Delta H_m = 0$, so it is reasonable to make this comparison. Now

$$K_s = -\frac{1}{V}\left(\frac{\partial^2 H}{\partial p^2}\right)_{S,N,c} \tag{5.4}$$

where H is the molar enthalpy (note that $V = \left(\frac{\partial H}{\partial p}\right)_{S,N,c}$, a familiar thermodynamic identity). We may write

$$H = cH_1 + (1-c)H_2 + \Delta H_m \tag{5.5}$$

where H_1 and H_2 are the molar enthalpies of the pure species. This Equation is in fact the definition of ΔH_m. Taking the second derivative of Equation (5.5), we get

$$VK_s = V_{ideal} K_{s_{ideal}} - \left(\frac{\partial^2 (\Delta H_m)}{\partial p^2}\right)_{S,N,c} \tag{5.6}$$

Thus the similarity of Figs. 5.6 and 5.7 suggests that $\frac{\partial^2}{\partial p^2}(\Delta H_m) \sim \Delta H_m$, as a function of composition. Indeed, it is very reasonable that the departure of H from the ideal should be reflected in the departure of its second derivative with respect to pressure from the ideal. A good general

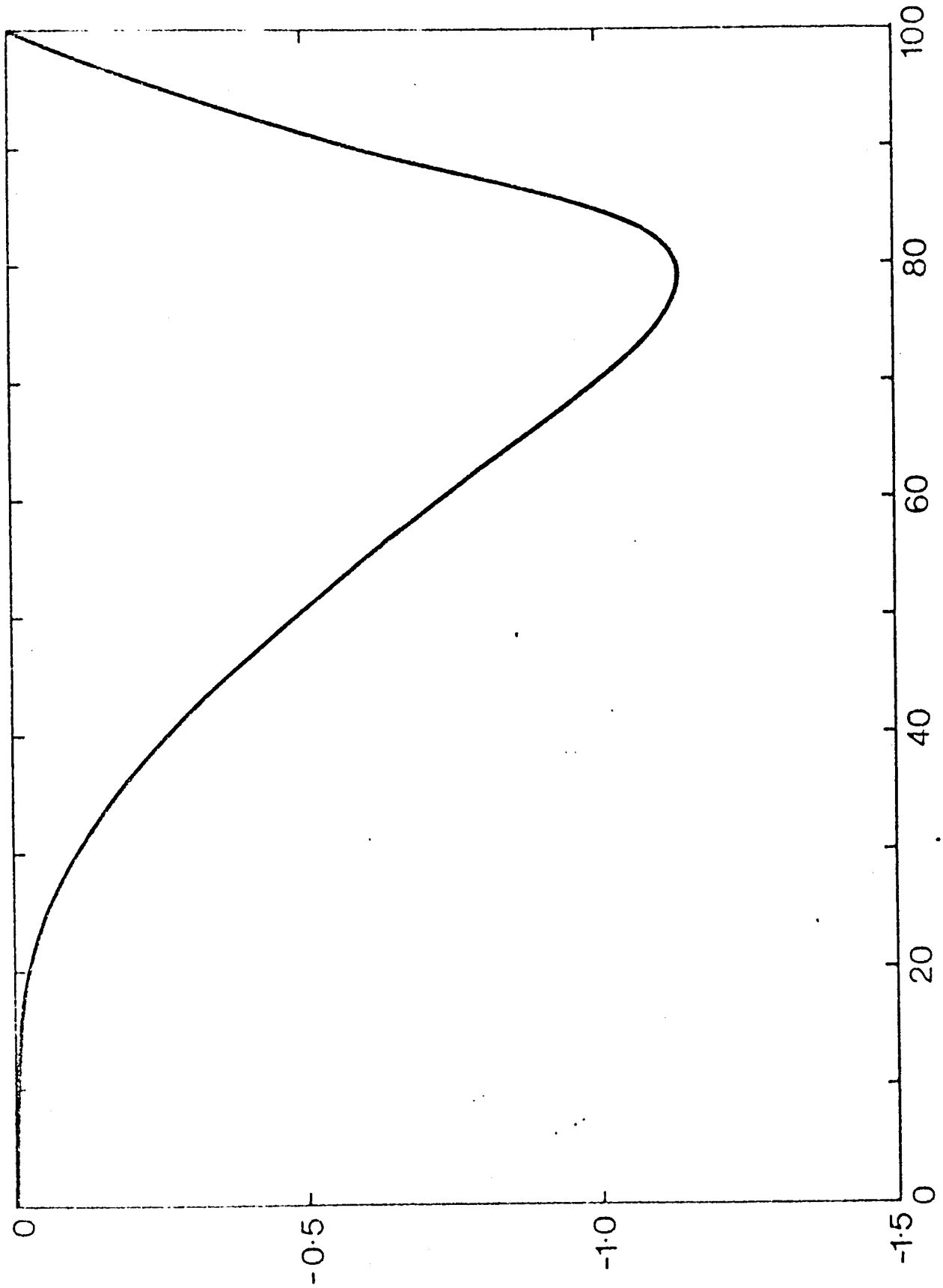

Fig. 5.7. Heat of Mixing of Cu-Sn Alloys (Hultgren et al.).

rule-of-thumb for metals is that the compressibility decreases as the cohesive energy increases, and the negative enthalpy of mixing of these alloys indicates an increase in cohesive energy greater than one would expect from ideal mixing; hence we see a decrease in compressibility below that of an ideal mixture.

Now consider the composition dependence of the resistivity of Cu-Sn alloys (Fig. 5.8, taken from Roll and Motz 1957). The resistivity has a maximum at ~76 at. % Cu, which correlates well with the position of the minima in Figs. 5.6 and 5.7. Busch and Güntherodt (1967) discuss the behaviour of the resistivity in this and several similar alloy systems. They are able to make the general statement that a resistance maximum, accompanied by a minimum in the temperature coefficient of resistivity, occurs at a concentration such that the position k_f of the Fermi surface of the free electrons is halfway out to the first peak in the effective structure factor, located at $q = k_p$. In a solid metal, this is where the Fermi surface would fill the first Brillouin zone. In pure liquid metals this condition ($2k_f = k_p$) is used (Chapter 1) to explain the high resistivities and negative temperature coefficients of resistivity of the divalent metals. Busch and Güntherodt use a constant value for k_p for Cu-Sn alloys, taken from Enderby et al. (1966); it corresponds to the position of the first peak in $a_{CuSn}(q)$ at 55 at. % Cu. In actual fact this peak position may shift somewhat with composition. Throop and Bearman (1964), for example, show that the main periodicity of $g_{ij}(r)$, which corresponds to the position of the main peak in $a_{ij}(q)$, changes slowly with composition in binary mixtures of hard spheres, according to

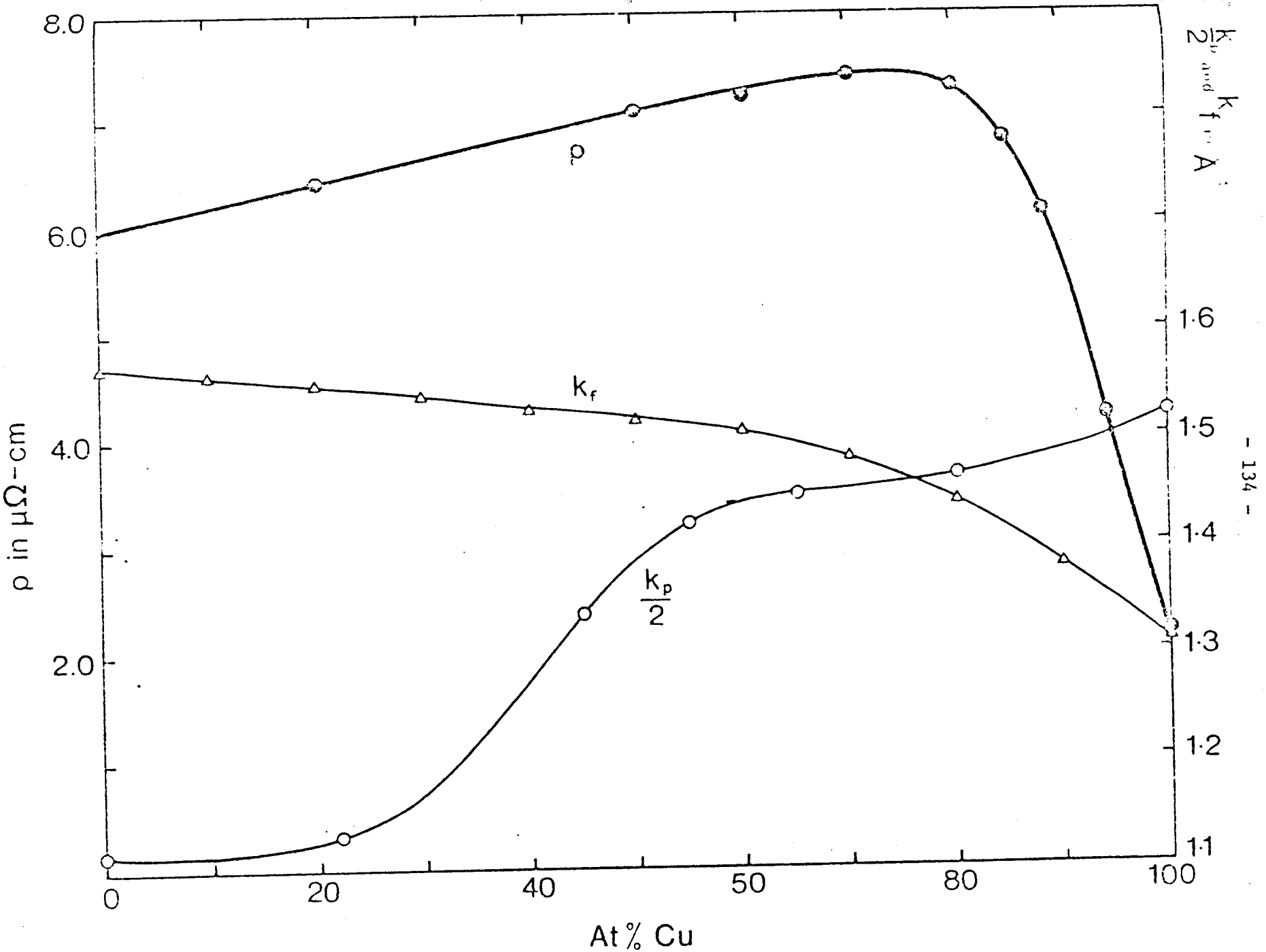

Fig. 5.8. Resistivity of Cu-Sn Alloys at 1100°C (Roll & Motz 1957). $k_p/2$ and k_f are also shown.

their Percus-Yevick calculation. However, as a first approximation, the assumption that the first peak in $a_{ij}(q)$ is stationary will suffice.

Using Faber and Ziman's theory (Chapter 1), Ashcroft and Langreth (1967b) were able roughly to fit the experimental resistivity data for Cu-Sn alloys. They started with appropriate pseudopotentials for the ions (which, however, neglect the d-electrons of the Cu ions), from which they derived ion-ion interaction potentials and hence effective hard-sphere radii and packing fractions. They used these parameters to evaluate the Percus-Yevick hard-sphere structure factors, which they then employed, together with their pseudopotentials, in the Faber-Ziman formula (Equations (1.13) and (1.23)). Examination of these Equations reveals that in fact the resistivity will most probably be a maximum the composition at which $|U(2k_f)|^2$ is largest, because of the weighting factor proportional to q^2 in the integrand of Equation (1.13). Now $|U(q)|^2$ is a weighted sum of the partial structure factors (Equation (1.23)), and thus when $2k_f$ is equal to the position of the main peak in one or other of these partial structure factors, we expect an increase in the resistivity. The experimental evidence, such as it is (Enderby et al. 1966; North and Wagner 1970), suggests very strongly that the major peaks in $a_{CuCu}(q)$ and $a_{CuSn}(q)$ are close to each other and of larger amplitude than that in $a_{SnSn}(q)$; thus we may expect a resistivity maximum for $2k_f = k_p$ where k_p is the position of the main maximum in $a_{CuCu}(q)$ and $a_{CuSn}(q)$, in agreement with the findings of Busch and Güntherodt.

Measurements of the three partial structure factors over the entire composition range do not yet exist, unfortunately. However, the total X-ray intensity function I(q) has been measured for several different compositions, by North and Wagner (1970). This quantity (see Equation (1.20)) is very similar to $|U(q)|^2$, but the partial structure factors are weighted differently. However, we may suppose that the position of the main peak of $I(q)/I_o$ is the same as the peak in $|U(q)|^2$, so that its position relative to $2k_f$ should correlate with the resistivity. In Fig. 5.8 we show the values of $k_p/2$ taken from North and Wagner's work, and the value of k_f as a function of composition. In order to calculate k_f we assumed that (a) the free-electron model is valid, and (b) the number of free electrons that each atom of Cu or Sn brings with it into the alloy is equal to its normal value, one for Cu and four for Sn; thus the average number of free electrons per atom varies linearly with composition from one to four. The latter assumption is supported by the Hall effect measurements of Busch and Güntherodt (1967), and by the optical measurements of Comins (1972), who fitted the Drude expression for the optical conductivity to his observed results and thereby derived an effective electron per atom ratio.

The fruit of these labours is the striking agreement between the compositions at which the resistivity is a maximum for Cu-Sn alloys and at which $k_p/2 = k_f$ (Fig. 5.8). Recalling that this composition is also that at which the deviations in the compressibility and the heat of mixing from the ideal are maximal, it appears reasonable to suggest that these deviations may be explained in terms of the relationship of the

position of the Fermi surface to the first peak in the structure factors. Before we make more comments on this idea, we shall present further new experimental data on the structure of Cu-Sn alloys.

5-2-2 The Partial Structure Factors at Zero-Wavevector For Cu-Sn Alloys

Using our measured values of the sound velocity, the density data of Bornemann and Sauerwald, and the activity data of Alcock et al. (1969) we have calculated the partial structure factors at zero-wavevector, with the aid of Equations (1.39). These are plotted in Fig. 5.9. The dashed curves indicate the composition dependence of the partial structure factors for an ideal alloy which has the partial molar volumes of pure Sn and pure Cu (which volumes, of course, do not change with composition in an ideal system). The estimated error in the curves for the real alloys is ∿10%; thus the deviation from the ideal curve of a_{CuCu} for $c \leq .2$ is not significant. It can be seen at once that the Cu-Sn alloy system behaves in a nearly ideal way up to 40 at. % Cu. This is surprising in view of the fact that the range of ideal behaviour for such a simple system as Na-K is much smaller (McAlister and Turner 1972).

Since the partial structure factors are related to the partial radial distribution functions, we are now able to say something about the atomic arrangements in the alloy. Departures from ideal behaviour in $a_{ij}(o)$ represent the effects of preferential grouping of the two species. To show this explicitly, we rewrite $a_{ij}(o)$:

$$a_{ij}(0) = 1 + \frac{N}{V} \int_0^\infty (g_{ij}(r) - 1) 4\pi r^2 dr \qquad (5.7)$$

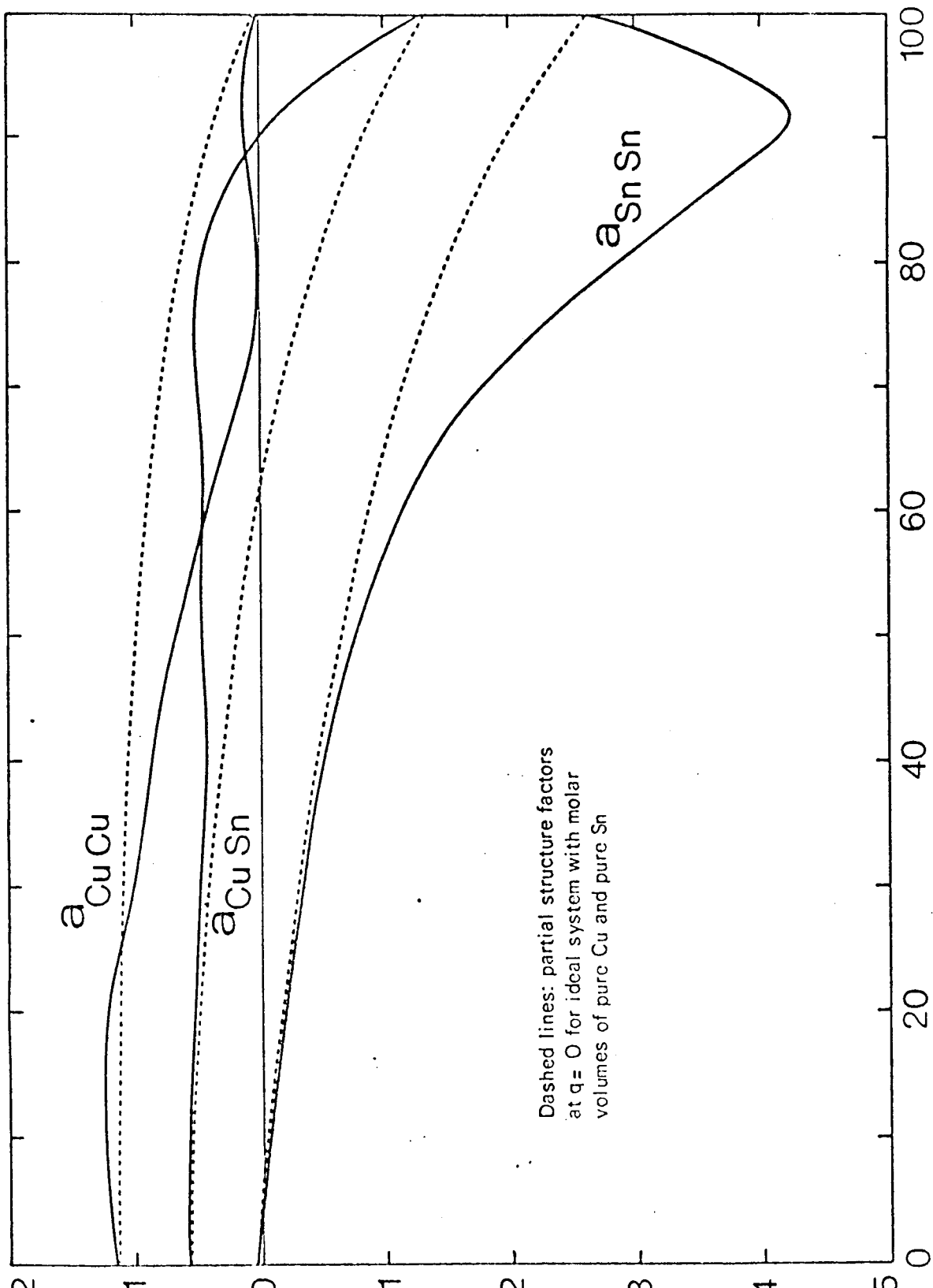

Fig. 5.9. Partial structure factors at q = 0 for Cu-Sn alloys.

$g_{ij}(r)$ is defined in such a way that the number $n_{ij}(r)$ of atoms of species j at a distance r from an atom of species i at the origin is given by

$$n_{ij}(r) = c_j \frac{N}{V} g_{ij}(r) \cdot 4\pi r^2 \qquad (5.8)$$

Now consider the quantity

$$\Delta N_j \equiv N_{ij} - N_{jj} \equiv \int_0^\infty (n_{ij}(r) - n_{jj}(r))\, dr \qquad (5.9)$$

ΔN_j can clearly be seen to be equal to the difference between the total number of j atoms surrounding an i atom and the total number of j atoms surrounding a j atom. We could call N_{ij} the <u>total co-ordination number</u> for species j around an atom of species i; then ΔN_j represents the difference in total coordination numbers, that is, the extent to which j atoms prefer to group round an i atom rather than a j atom. Even in an ideal alloy $\Delta N_j \neq 0$, unless the atomic volumes of the constituents are equal, because there is an excluded volume effect, which means that, if the i atoms are bigger than the j atoms, fewer j atoms can be grouped round an i atom than about a j atom, for a given sample volume V. It can be easily shown using this reasoning that in an ideal alloy, $\Delta N_j = \frac{c_j N}{V}(v_1 - v_2)$, where v_1 and v_2 are the atomic volumes of the individual species. This result is in agreement with that obtained from Equation (1.53). Note that $\Delta N_j = c_j(a_{ij}(o) - a_{jj}(o))$.

Now the question arises: where are the additional atoms (represented by ΔN_j) located? The experimental results for any alloy system indicate

that $g_{ij}(r) \to 1$ within about 10 atomic diameters, and thus for larger radii than this there can be no contribution to the value of the integral in Equation (5.9). Hence the difference in the $g_{ij}(r)$'s for small r (that is, the difference in the short range order surrounding the atoms of the different species) provides the entire effect.

In the case of a real alloy system there may be additional grouping beyond that caused by the excluded volume effect. To separate these effects we have calculated

$$\Delta N_j' \equiv \Delta N_j - c_j \delta, \tag{5.10}$$

(where $\delta \equiv \frac{1}{V}\left(\frac{\partial V}{\partial c}\right)_N = \frac{N}{V}(v_{10} - v_{20})$ for an ideal system) for Cu-Sn alloys, using the definition of $\Delta N_j'$,

$$\Delta N_j = c_j \left(a_{ij}(0) - a_{jj}(0)\right), \tag{5.11}$$

and our previous results for the $a_{ij}(o)$'s. For an ideal system $\Delta N_j' = 0$. The results for $\Delta N_{Cu}'$ and $\Delta N_{Sn}'$ are shown in Fig. 5.10. It is immediately obvious that the Cu atoms prefer to group around Sn atoms than about each other, and Sn atoms prefer to group around Cu atoms than about each other, particularly at certain compositions. We shall discuss the significance of these results in the next Section, in an attempt to formulate a model to describe the Cu-Sn alloy system.

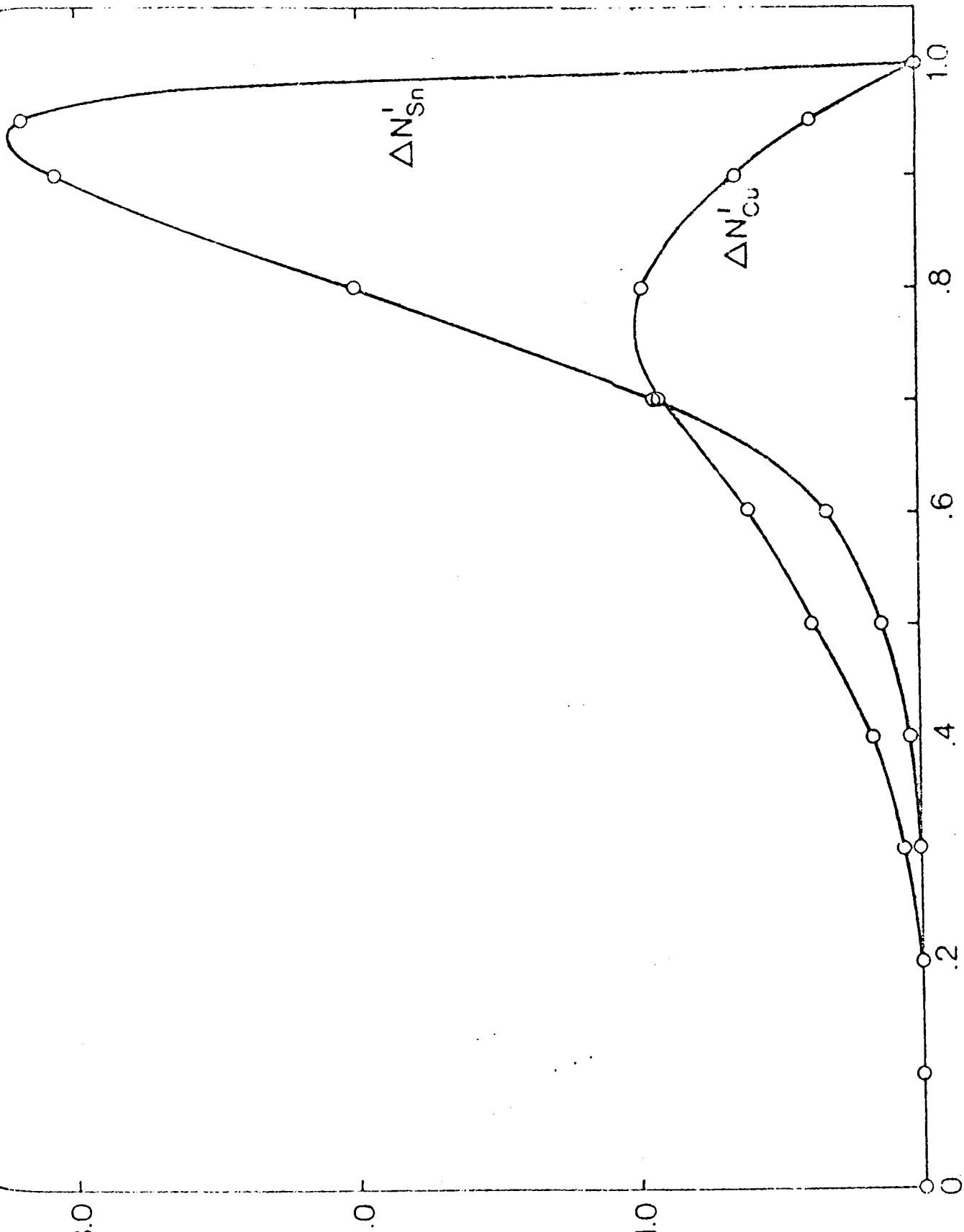

Fig. 5.10. $\Delta N'_{Cu} = c(a_{SnCu}(o) - a_{CuCu}(o) - \delta)$ and $\Delta N'_{Sn} = (1-c)(a_{CuSn}(o) - a_{SnSn}(o) + \delta)$

5-2-3 The Structure of Cu-Sn Alloys: Speculative Remarks

We shall construct our model from two basic experimental facts. (i) There is an intermetallic compound in the solid alloy system at 75 at. % Cu, with h.c.p. crystal structure and chemical composition Cu_3Sn (see the phase diagram, Fig. 5.11, taken from Hansen 1958). (ii) The Fermi wavevector, k_f, is equal to $k_p/2$, where k_p is the position of the main peak in the effective structure factor, at 76 at. % Cu (Fig. 5.8). The experimental evidence we might hope to explain, at least qualitatively, is the behaviour, as a function of composition, of: (a) the resistivity (already explained qualitatively using fact (ii) by Busch and Güntherodt (1967)), (b) the enthalpy of mixing, (c) the molar volume, (d) the compressibility, and (e) the differential co-ordination numbers ΔN_j.

The assumptions constituting this model are:

(1) The total energy of the alloy can be written as

$$E = E_e + E_I + E_{I-e} \qquad (5.12)$$

where E_e is the purely electronic energy, E_I the ionic energy and E_{I-e} the ion-electron interaction energy.

(2) The electronic energy E_e varies smoothly with composition from pure Cu to pure Sn.

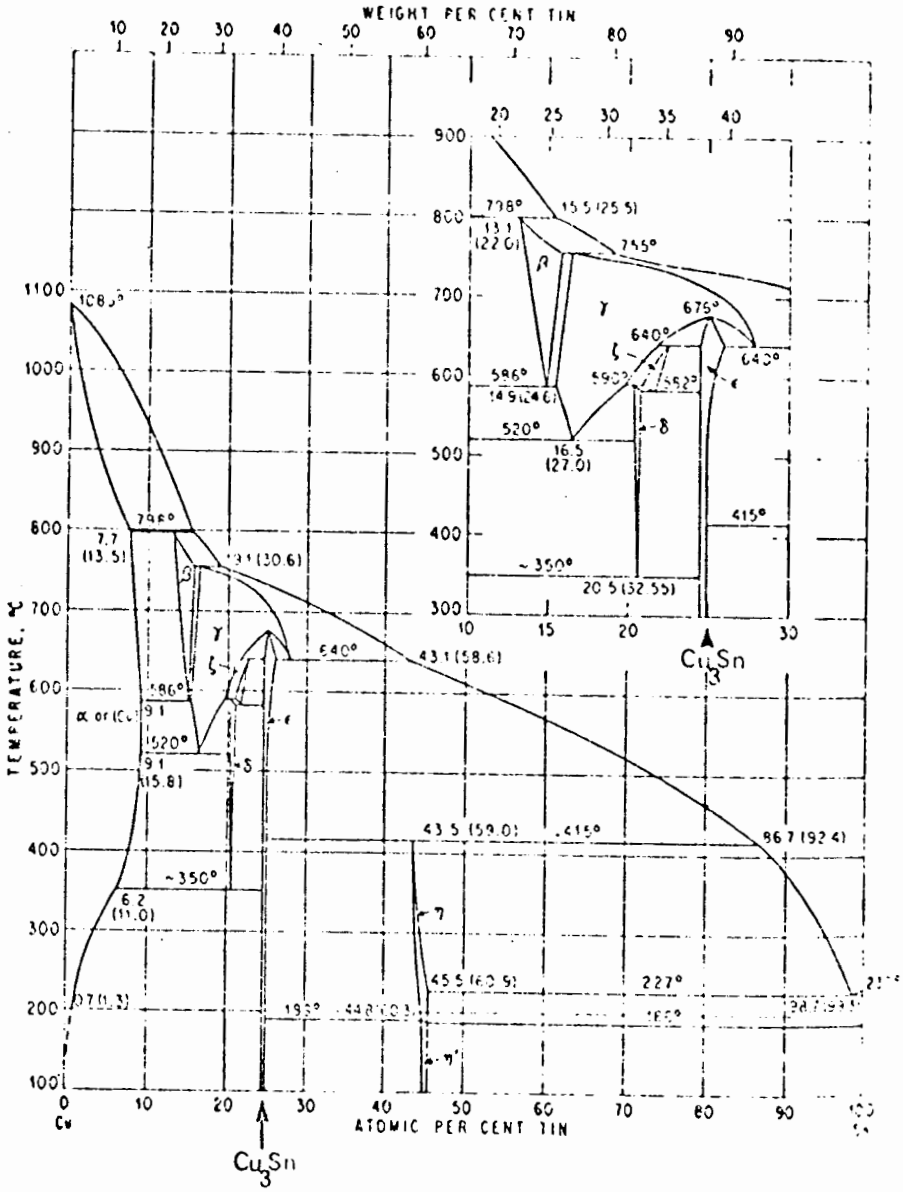

Fig. 5.11. Phase Diagram for Cu-Sn Alloys (Hansen 1958)

(3) The ionic energy E_I is primarily responsible for structural changes in the alloy as a function of composition.

(4) The ionic energy may be written in terms of pairwise additive ion-ion interaction potentials $\phi_{ij}(r)$.

Then we have

$$E_I = \frac{2\pi N}{V}\left\{ c_1 \int_0^\infty \phi_{11}(r)\, g_{11}(r)\, r^2 dr + c_2 \int_0^\infty \phi_{22}(r)\, g_{22}(r)\, r^2 dr + c_2 \int_0^\infty \phi_{12}(r)\, g_{12}(r)\, r^2 dr \right\} \qquad (5.13)$$

where 1 refers to Cu and 2 refers to Sn. Consider now (for example), the first integral in Equation (5.13). The general forms of $\phi(r)$ and $g(r)$ are sketched in Fig. 5.12. The essential points to notice are these:

(a) $g_{11}(r)$ has a periodicity (after the initial peak) of $\frac{2\pi}{k_p}$, where k_p is the position of the first peak in $a_{11}(q)$. This result is mathematically implied by the fact that this peak in a(q) is always narrow and of much larger magnitude than the rest of the curve, so that it dominates the periodicity of the Fourier transform of a(q), that is, g(r). The experimentally measured a(q) and g(r) for pure Al (Fessler et al. 1966) confirm this conclusion.

(b) $\phi_{11}(r)$ has an oscillatory tail, of period $\frac{2\pi}{2k_f}$ for large r. This oscillatory behaviour is associated with the sharpness of the Fermi surface (March 1968) which persists even in a liquid metal, the atomic disorder blurring the Fermi surface only by a few percent (Chan 1971). The oscillations are directly related to the well-known Friedel oscillations in the electron density around a positive charge in a metal. At what

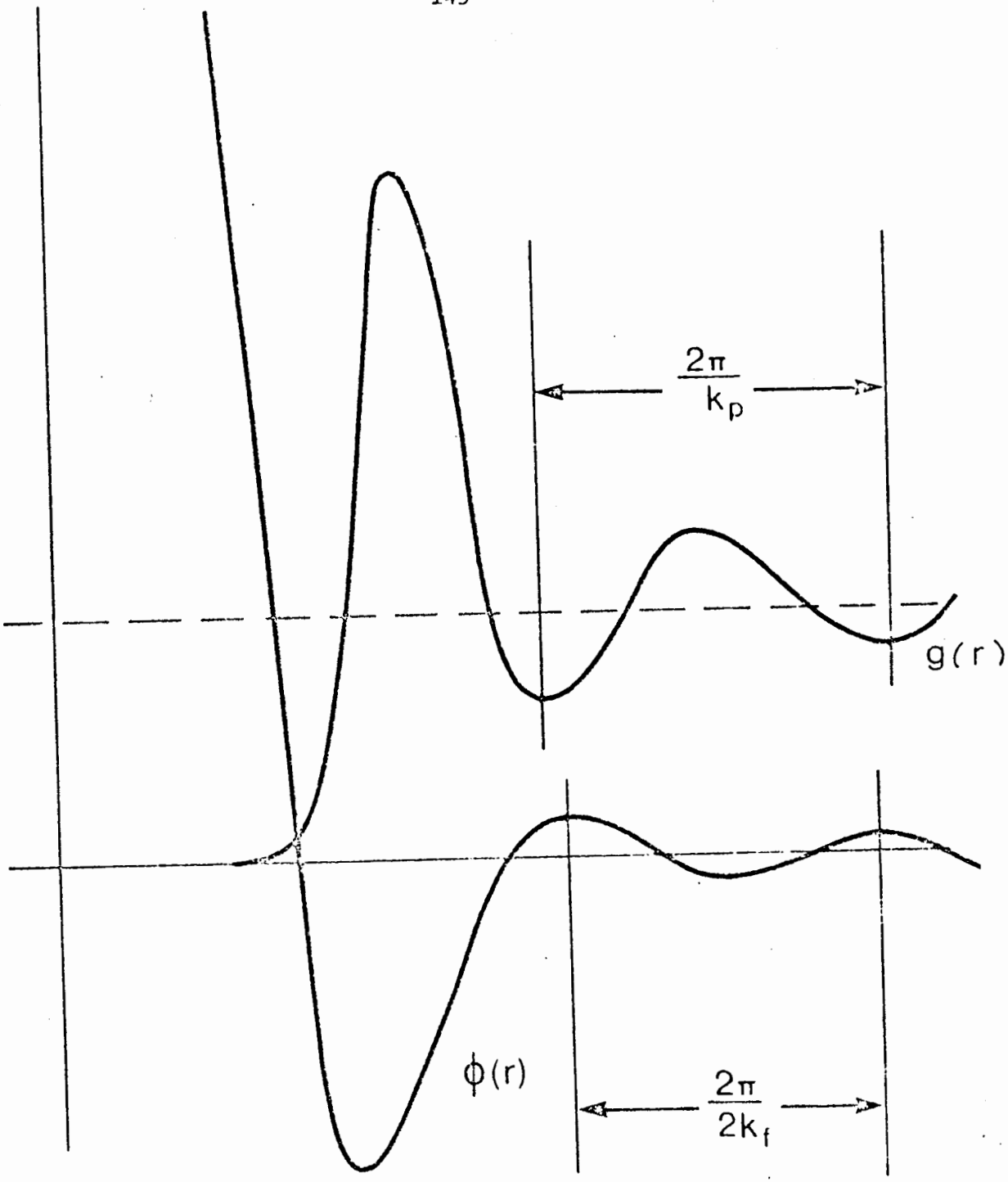

Fig. 5.12. Typical forms for g(r) and $\phi(r)$ in liquid metals.

values of r the oscillations develop exactly the period $\frac{2\pi}{2k_f}$ is uncertain; but calculations by Gupta (private communication) using realistic ionic pseudopotentials indicate that the periodicity is close to $\frac{2\pi}{2k_f}$ even in the first oscillation of $\phi(r)$, as indicated in Fig. 5.12.

As a result of these considerations, the integrands in Equation (5.13) are products of two oscillatory functions of different periods, in general (multiplied by a term dependent on r which ensures convergence of the integrals). Thus the values of the integrals will be rapidly varying around compositions which equalise these periodicities. Phase matching is provided by the fact that the first peak in g(r) must coincide with the main minimum in $\phi(r)$. The value of these integrals will be a minimum, and hence E_I will be a minimum, when $\frac{2\pi}{2k_f} = \frac{2\pi}{k_p}$, i.e. $k_f = k_p/2$, the same condition that we noted before in connection with the resistivity. The alloy is most tightly bound when the electrons at the Fermi surface interact most strongly with the ions; and this also maximises the resistivity. An analogous result in solid alloys is provided by the Hume-Rothery rules (Hume-Rothery et al. 1969). These imply that in a solid alloy it is energetically favourable to put as many gaps (in the electron dispersion curves) at the Fermi surface as possible. Thus alloys take up crystal structures, sometimes by the formation of long period superlattices (Sato and Toth 1963, brought to our attention by Professor A. Arrott) such that this effect is achieved. Again, strong interaction of Fermi surface electrons with the ions lowers the energy of the metal.

Now we can see why there is a minimum in the heat of mixing of Cu-Sn alloys at the composition where $k_f = k_p/2$. The ionic energy, and hence the total energy, is minimised here. Assumption (3) justifies this

explanation. Furthermore, we can also explain the change in volume on mixing. At compositions near where $k_f = k_p/2$, the alloy can lose energy by changing its density in such a way as to approach the $k_f = k_p/2$ condition; thus there will be a volume contraction in the alloy, centred on this composition. This contraction is additional to the small contraction normally expected (Wood 1968) for mixtures of hard spheres of unequal diameters.

The result of tighter binding is to make the liquid stiffer; thus the compressibility is decreased. The maximum decrease in compressibility (below the ideal case) will naturally occur when the binding is tightest, that is, where the heat of mixing is a minimum, and where $k_f = k_p/2$. Thus, using only experimental fact (ii) (see the beginning of this Section) we have qualitatively explained the data (a), (b), (c) and (d). We must still find an explanation for (e), the behaviour of $\Delta N_j'$ as a function of composition.

Using the work of North and Wagner (1970) we may estimate where in the liquid the additional atoms, implied by the departure of $\Delta N_{Cu}'$ and $\Delta N_{Sn}'$ from the ideal, are located. North and Wagner assume composition-independence of the partial structure factors in order to calculate the partial radial distribution functions $g_{ij}(r)$ from their X-ray measurements. They give a co-ordination number p_{ij}, defined by $p_{ij} = \int_0^{r_2} 4\pi r^2 g_{ij}(r)dr$, where r_2 is the position of the first minimum in $g_{ij}(r)$. The value for p_{SnSn} is 9, while $p_{CuCu} = p_{CuSn} = 13$. Thus in the nearest neighbour shell of a Cu atom there are roughly four more Sn atoms than in that of an Sn atom. This is in fair agreement with the maximum value of three for

$\Delta N'_{Sn}$ we obtain for c = .95. Furthermore, in pure liquid Cu, $p_{CuCu} = 12$, so that the difference between p_{CuSn} and p_{CuCu} (pure Cu) is 1, in agreement with our maximum value of $\Delta N'_{Cu}$ for c = .78. Thus it is reasonable to assume that most of the extra atoms $\Delta N'_j$ are located in the nearest neighbour shell of the atom to which we are referring.

Making this assumption, we may explain the values of $\Delta N'_{Cu}$ and $\Delta N'_{Sn}$ by the use of fact (i), that the solid alloy has an h.c.p. intermetallic compound Cu_3Sn. An h.c.p. structure has the co-ordination number 12. Each Sn atom is surrounded by 12 Cu nearest neighbours. We explain the changes in $\Delta N'_{Cu}$ and $\Delta N'_{Sn}$ by asserting that the liquid alloy takes advantage of this favourable packing at the Cu_3Sn composition, and changes its structure. It becomes favourable for Cu ions to be surrounded by Sn ions, and vice versa. The liquid takes up an arrangement similar to the h.c.p. lattice in the solid; though this structure cannot extend more than about two atomic diameters. The force requiring close packing is provided by the tighter binding at this composition, as discussed previously.

By combining these structural considerations with the energy considerations mentioned earlier, we believe that a full quantitative theory of Cu-Sn alloys can be developed, which could be used to improve the Ascarelli-type calculation presented in Section 5-1-3.

5-3 The Hall Effect Controversy

There is a controversy about the behaviour of Sn atoms in solution in Cu. Enderby et al. (1967) claim, from their Hall effect measurements, that Sn behaves like a divalent metal when dissolved in Cu. We cannot

entirely rule out this possibility. However, an Ascarelli-type calculation using this effective electron density would give even poorer agreement with experiment for $\frac{N}{V} k_B T K_T$, since the term $\frac{2}{15} \frac{ZE_f}{k_B T}$ in the denominator of Equation (5.2) would be reduced, increasing the deduced value of $\frac{N}{V} k_B T K_T$.

The measurements of Busch and Güntherodt (1967) and Comins (1972), both of which are in agreement with the theory that each Sn atom contributes four free electrons to the alloy, disagree with the conclusions of Enderby et al., in any case.

CHAPTER 6

SUMMARY

To summarise this experiment and the subsequent analysis:

(i) The phenomenon of the generation of electromagnetic waves at a metal surface by acoustic waves in the presence of a static magnetic field was observed up to temperatures of 1400°C in Cu-Sn alloys. This supports the theory of Turner et al. (1969), which contains no temperature-dependent parameters.

(ii) This phenomenon has been used as the basis of very accurate measurements of the velocity of sound in liquid metals.

(iii) The velocity of sound was measured in nine liquid alloys of copper and tin, and in the pure metals, at temperatures ranging from 250°C to 1400°C.

(iv) The compressibilities of these alloys were evaluated using the experimental sound velocity data, and the data of previous workers for the density and specific heat. The observed compressibilities of the alloys were then compared with values derived from various theories. A theory patterned after that of Ascarelli (1968) gave best agreement.

(v) The partial structure factors at zero wavevector of Cu-Sn alloys were calculated using the theory of Bhatia and Thornton (1970), together with our compressibility data and the activity and density data of previous workers. These structure factors show a considerable departure from ideal behaviour, for alloys with a high concentration of copper.

(vi) A qualitative explanation of the bulk properties of Cu-Sn alloys was advanced. The anomalous behaviour at high Cu concentrations is caused by the proximity of $2k_f$ to k_p at these concentrations, where k_f is the Fermi wavevector and k_p is the position of the major peak in the effective structure factor.

APPENDIX A

THE CONNECTION BETWEEN BHATIA AND THORNTON'S CORRELATION FUNCTIONS AT ZERO-WAVEVECTOR AND THE THERMODYNAMICS OF ALLOY MIXING

To demonstrate this connection, we must use the properties of the grand canonical ensemble. In a fixed volume V with variable numbers N_1 and N_2 of particles of species 1 and 2 respectively, connected to a thermal and particle reservoir, we may write the grand canonical probability function as (Tolman 1962, for example)

$$P(N_1, N_2, M) = \exp\left\{\frac{1}{k_B T}\left(-\Omega + \mu_1 N_1 + \mu_2 N_2 - E_M\right)\right\} \qquad (A.1)$$

where E_M is an eigenvalue of the energy of the system, μ_1 and μ_2 are the chemical potentials of species 1 and 2, and Ω is the grand potential. $P(N_1,N_2,M)$ is the probability of finding N_1 particles of species 1 and N_2 particles of species 2 at an energy E_M. Normalization demands

$$\sum_{N_1, N_2, M} P(N_1, N_2, M) = 1 \qquad (A.2)$$

where the sum extends over all possible values of N_1, N_2 and M. To obtain the fluctuations in N_1 and N_2, caused by fluctuations in μ_1 and μ_2 the following trick is employed. Taking the partial derivative with respect to μ_1, holding V, T and μ_2 constant, of both sides of (A.2), gives

$$0 = \sum_{N_1, N_2, M} \frac{1}{k_B T}\left(\left(\frac{\partial \Omega}{\partial \mu_1}\right)_{T,V,\mu_2} + N_1\right) \exp\left\{\frac{1}{k_B T}\left(-\Omega + \mu_1 N_1 + \mu_2 N_2 - E_M\right)\right\} \qquad (A.3)$$

Now a most important property of $P(N_1,N_2,M)$ is that if X is any thermodynamic quantity, its average, $\bar{X}$, is given by

$$\bar{X} = \sum_{N_1,N_2,M} X\, P(N_1,N_2,M) \tag{A.4}$$

(A.3) and (A.4) give

$$\frac{1}{k_B T}\left(\left(\frac{\partial\Omega}{\partial\mu_1}\right)_{T,V,\mu_2} + \bar{N}_1\right) = 0 \tag{A.5}$$

that is, $$\bar{N}_1 = -\left(\frac{\partial\Omega}{\partial\mu_1}\right)_{T,V,\mu_2}$$

Now we take the partial derivative of both sides of (A.3) with respect to μ_2, holding V, T and μ_1 constant:

$$\sum_{N_1,N_2,M}\left[\left(\frac{1}{k_B T}\right)^2\left(\left(\frac{\partial\Omega}{\partial\mu_1}\right)_{T,V,\mu_2}+N_1\right)\left(\left(\frac{\partial\Omega}{\partial\mu_2}\right)_{T,V,\mu_1}+N_2\right)+\frac{1}{k_B T}\left(\frac{\partial^2\Omega}{\partial\mu_1\partial\mu_2}\right)_{T,V}\right] \tag{A.6}$$
$$\times \exp\left\{\frac{1}{k_B T}\left(\Omega+\mu_1 N_1+\mu_2 N_2-E_M\right)\right\} = 0$$

Using (A.4) and (A.5) in (A.6),

$$\overline{\Delta N_1\,\Delta N_2} \equiv \overline{(N_1-\bar{N}_1)(N_2-\bar{N}_2)} = k_B T\left(\frac{\partial\bar{N}_1}{\partial\mu_2}\right)_{T,V,\mu_1} \tag{A.7a}$$

Similarly,

$$\overline{(\Delta N_1)^2} \equiv \overline{(N_1-\bar{N}_1)^2} = k_B T\left(\frac{\partial\bar{N}_1}{\partial\mu_1}\right)_{T,V,\mu_2} \tag{A.7b}$$

$$\overline{(\Delta N_2)^2} \equiv (N_2 - \bar{N}_2)^2 = k_B T \left(\frac{\partial \bar{N}_2}{\partial \mu_2}\right)_{T,V,\mu_1} \tag{A.7c}$$

Note that

$$\left(\frac{\partial \bar{N}_1}{\partial \mu_2}\right)_{T,V,\mu_1} = \left(\frac{\partial^2 \Omega}{\partial \mu_2 \partial \mu_1}\right)_{T,V} = \left(\frac{\partial \bar{N}_2}{\partial \mu_1}\right)_{T,V,\mu_2} \tag{A.8}$$

Equations (1.35) may be rewritten, for q = 0

$$\begin{aligned} S_{NN}(0) &= \frac{1}{N} \overline{(\Delta N_1 + \Delta N_2)^2} \\ S_{Nc}(0) &= \frac{1}{N^2} \overline{(\Delta N_1 + \Delta N_2)((1-c)\Delta N_1 - c\Delta N_2)} \\ S_{cc}(0) &= \frac{1}{N^2} \overline{((1-c)\Delta N_1 - c\Delta N_2)^2} \end{aligned} \tag{A.9}$$

To express the right-hand sides of (A.9) in measurable quantities, we need to convert $\left(\frac{\partial N_i}{\partial \mu_j}\right)_{T,V,\mu'}$ where μ' is the chemical potential of the other species to a quantity dependent on T, P, c and $N = N_1 + N_2$, since these are the quantities usually held fixed in an experiment. First of all,

$$\left(\frac{\partial N_i}{\partial \mu_j}\right)_{T,V,\mu'} = \frac{1}{\left(\frac{\partial \mu_j}{\partial N_i}\right)_{T,V,\mu'}} \tag{A.10}$$

Using the chain rule for $\left(\frac{\partial \mu_1}{\partial N_1}\right)_{T,V,\mu_2}$, for example, changing variables from (T,V,N_1,μ_2) to (T,V,N_1,N_2)

$$\left(\frac{\partial \mu_1}{\partial N_1}\right)_{T,V,\mu_2} = \left(\frac{\partial \mu_1}{\partial N_1}\right)_{T,V,N_2}\left(\frac{\partial N_1}{\partial N_1}\right)_{T,V,\mu_2} + \left(\frac{\partial \mu_1}{\partial N_2}\right)_{T,V,N_1}\left(\frac{\partial N_2}{\partial N_1}\right)_{T,V,\mu_2} \quad \text{(A.11)}$$

$$= \left(\frac{\partial \mu_1}{\partial N_1}\right)_{T,V,N_2} - \left(\frac{\partial \mu_1}{\partial N_2}\right)_{T,V,N_1} \frac{\left(\frac{\partial \mu_2}{\partial N_1}\right)_{T,V,N_2}}{\left(\frac{\partial \mu_2}{\partial N_2}\right)_{T,V,N_1}}$$

Defining

$$\beta_{ij} \equiv \left(\frac{\partial \mu_i}{\partial N_j}\right)_{T,V,N'} \quad \text{(A.12)}$$

it is easy to show that similarly

$$\left(\frac{\partial \mu_1}{\partial N_2}\right)_{T,V,\mu_2} = \left(\frac{\partial \mu_2}{\partial N_1}\right)_{T,V,\mu_1} = \beta_{12} - \frac{\beta_{22}\beta_{11}}{\beta_{12}} \quad \text{(A.13)}$$

and

$$\left(\frac{\partial \mu_2}{\partial N_2}\right)_{T,V,\mu_1} = \beta_{22} - \frac{\beta_{12}^2}{\beta_{11}}$$

Now using the chain rule again on β_{11} changing variables from (T,V,N_1,N_2) to (T,P,N_1,N_2), say, gives

$$\left(\frac{\partial \mu_1}{\partial N_1}\right)_{T,V,N_2} = \left(\frac{\partial \mu_1}{\partial N_1}\right)_{T,P,N_2}\left(\frac{\partial N_1}{\partial N_1}\right)_{T,V,N_2} + \left(\frac{\partial \mu_1}{\partial P}\right)_{T,N_1,N_2}\left(\frac{\partial P}{\partial N_1}\right)_{T,V,N_2} \quad \text{(A.14)}$$

$$= \left(\frac{\partial \mu_1}{\partial N_1}\right)_{T,P,N_2} - v_1 \left(\frac{\partial V}{\partial N_1}\right)_{T,P,N_2} \Big/ \left(\frac{\partial V}{\partial P}\right)_{T,N_1,N_2}$$

where we have used the fact that

$$dG = Vdp - SdT + \mu_1 dN_1 + \mu_2 dN_2 \qquad \text{(A.15)}$$

and equated the second partial derivatives of G with respect to p and N_1, and vice-versa, to get

$$\left(\frac{\partial \mu_1}{\partial p}\right)_{T,N_1,N_2} = \left(\frac{\partial^2 G}{\partial p \partial N_1}\right)_{T,N_1,N_2} = \left(\frac{\partial^2 G}{\partial N_1 \partial p}\right)_{p,T,N_2} = \left(\frac{\partial V}{\partial N_1}\right)_{T,p,N_2} \qquad \text{(A.16)}$$
$$= v_1$$

v_i is the partial atomic volume of species i in the mixture; in a mole of mixture Nv_i is the partial molar volume. Except where stated explicitly, from now on in this Section we use molar quantities only, which greatly simplifies matters. Now note in (A.14) that

$$\left(\frac{\partial V}{\partial p}\right)_{T,N_1,N_2} = -V K_T \qquad \text{(A.17)}$$

where K_T is the isothermal compressibility. Hence, from (A.14)

$$\left(\frac{\partial \mu_1}{\partial N_1}\right)_{T,V,N_2} = \left(\frac{\partial \mu_1}{\partial N_1}\right)_{T,p,N_2} + \frac{v_1^2}{V K_T}$$

Similarly

$$\beta_{ij} = \alpha_{ij} + \frac{v_i v_j}{V K_T} \qquad \text{(A.18)}$$

where

$$\alpha_{ij} = \left(\frac{\partial \mu_i}{\partial N_j}\right)_{T,p,N'}$$

Now for constant T and P the Gibbs-Duhem relation gives

$$N_1 \left(\frac{\partial \mu_1}{\partial N_1}\right)_{T,P,N_2} + N_2 \left(\frac{\partial \mu_2}{\partial N_1}\right)_{T,P,N_2} = 0 \qquad \text{(A.19)}$$

and $$N_1 \left(\frac{\partial \mu_1}{\partial N_2}\right)_{T,P,N_1} + N_2 \left(\frac{\partial \mu_2}{\partial N_2}\right)_{T,P,N_1} = 0$$

Since $c = \frac{N_1}{N_1+N_2}$, we have

$$\alpha_{22} = \left(\frac{c}{1-c}\right)^2 \alpha_{11} \qquad \text{(A.20)}$$

$$\alpha_{12} = \frac{-c}{1-c} \alpha_{11}$$

and hence, after some manipulation, using (A.10), (A.13), (A.18) and (A.20)

$$\left(\frac{\partial N_1}{\partial \mu_1}\right)_{T,V,\mu_2} = \frac{\beta_{22}}{\alpha_{11}} \frac{K_T (1-c)^2}{V} \qquad \text{(A.21)}$$

$$\left(\frac{\partial N_1}{\partial \mu_2}\right)_{T,V,\mu_1} = -\frac{\beta_{12}}{\alpha_{11}} \frac{K_T (1-c)^2}{V}$$

$$\left(\frac{\partial N_2}{\partial \mu_2}\right)_{T,V,\mu_1} = \frac{\beta_{11}}{\alpha_{11}} \frac{K_T (1-c)^2}{V}$$

Now α_{11} must be transformed from the variables (T,P,N_1,N_2) to variables (T,P,N,c). The most convenient way of doing this is to use a relationship between the activity a_i and the chemical potential μ_1. a_i is defined by

$$\mu_i(c_i) = k_B T \ln a_i + \mu_i(0) \qquad \text{(A.22)}$$

Here $\mu_i(o)$ is the chemical potential of pure species i at the same temperature and pressure (see Hatsopoulos and Keenan 1965). To complete the definition we require

$$\lim_{c_i \to 0} \frac{a_i}{p_i(c_i)/p_i(0)} = 1 \qquad \text{(A.23)}$$

where $p_i(c_i)$ is the partial vapour pressure of the species i at a concentration, c, and $p_i(o)$ is the vapour pressure of pure species i. At low pressures, when the vapours can be treated as ideal gases, we may write

$$a_i = \frac{p_i(c_i)}{p_i(0)} \qquad \text{(A.24)}$$

Thus

$$\alpha_{11} = \left(\frac{\partial \mu_1}{\partial N_1}\right)_{T,P,N_2} = \left(\frac{\partial \mu_1}{\partial c}\right)_{T,P,N} \left(\frac{\partial c}{\partial N_1}\right)_{T,P,N_2} \qquad \text{(A.25)}$$

$$= \frac{k_B T}{N} \frac{(1-c)}{a_1} \left(\frac{\partial a_1}{\partial c}\right)_{T,P,N}$$

Combining (A.18), (A.21) and (A.25) with Equations (A.9), we obtain finally

$$S_{cc}(0) = \frac{1-c}{\frac{1}{a_1}\left(\frac{\partial a_1}{\partial c}\right)_{T,P,N}} \qquad \text{(A.26)}$$

$$S_{Nc}(0) = -\frac{1}{V}\left(\frac{\partial V}{\partial c}\right)_N \frac{(1-c)}{\frac{1}{a_1}\left(\frac{\partial a_1}{\partial c}\right)_{T,P,N}}$$

$$S_{NN}(0) = \frac{N k_B T}{V} K_T + \left(\frac{1}{V}\left(\frac{\partial V}{\partial c}\right)_N\right)^2 \frac{(1-c)}{\frac{1}{a_1}\left(\frac{\partial a_1}{\partial c}\right)_{T,P,N}}$$

Here we have written $$\nu_1 - \nu_2 = \frac{1}{N}\left(\frac{\partial V}{\partial c}\right)_N \equiv \frac{V}{N}\,\delta$$

These results, in a slightly different form, were first derived by Bhatia and Thornton. They are exact.

BIBLIOGRAPHY

Alcock, C.B., Sridhar, R. and Svedberg, R.C. (1969), Act. Met. 17, 839.

Alpher, R.A. and Rubin, R.J. (1954), J. Acoust. Soc. Am. 26, 452.

Animalu, A.O.E. and Heine, V. (1965), Phil. Mag. 12, 1249.

Ascarelli, P. (1968), Phys. Rev. 173, 271.

Ashcroft, N.W. and Lekner, J. (1966), Phys. Rev. 145, 83.

Ashcroft, N.W. and Langreth, D.C. (1967a), Phys. Rev. 156, 685.

Ashcroft, N.W. and Langreth, D.C. (1967b), Phys. Rev. 155, 682.

Ballentine, L.E. (1966), Can. J. Phys. 44, 2533.

Bass, R. and Williams, A.O. (1960), private communication in McSkimin (1964).

Berthou, P.E. and Tougas, R. (1968), J. Less-Comm. Met. 16, 465.

Bevington, P.R. (1969), "Data Reduction and Error Analysis for the Physical Sciences" (McGraw-Hill, New York).

Bhatia, A.B. and Thornton, D.E. (1970), Phys. Rev. B 2, 3004.

Bornemann, K. and Sauerwald, F. (1922), Z. Metallknde 14, 145.

Busch, G. and Güntherodt, H.J. (1967), Phys. Kondens. Mat. 6, 325.

Cahill, J.A. and Kirshenbaum, A.D. (1962), J. Phys. Chem. 66, 1080.

Chan T. (1971), Ph.D. Thesis (Simon Fraser University).

Christman, J.R. and Huntington, H.B. (1965), Phys. Rev. 139, A83.

Comins, N.R. (1972), Phil. Mag. (to be published).

Coppens, A.B., Beyer, R.T. and Ballou, J. (1967), J. Acoust. Soc. Am. 41, 1443.

Del Grosso, V.A., Smura, E.J. and Fougere, P.F. (1954), Naval Research Lab. Rept. NRL-4439.

Egelstaff, P.A. (1967), "An Introduction to the Liquid State" (Academic Press, New York).

El-Mehairy, A.E. and Ward, R.G. (1963), Trans Metall. Soc. A.I.M.E. 227, 1226.

Enderby, J.E., North, D.M. and Egelstaff, P.A. (1966), Phil. Mag. 14, 961.

Enderby, J.E. and March, N.H. (1966), Proc. Phys. Soc. 88, 717.

Enderby, J.E., Hasan, S.B. and Simmons, C.J. (1967), Adv. Phys. 16, 673.

Enderby, J.E. and Howe, R.A. (1968), Phil. Mag. 18, 923.

Enderby, J.E. and North, D.M. (1968), Phys. Chem. Liquids 1, 1.

Faber, T.E. and Ziman, J.M. (1965), Phil. Mag. 11, 153.

Faber, T.E. (1972), "An Introduction to the Theory of Liquid Metals", to be published (University Press, Cambridge).

Fessler, R.R., Kaplow, R. and Averbach, B.L. (1966), Phys. Rev. 150, 34.

Fisher, I.Z. (1964), "Statistical Theory of Liquids" (University Press, Chicago).

Gaerttner, M.R. and Maxfield, B.W. (1971), Phys. Rev. Letters 26, 119.

Gitis, M.B. and Mikhailov, I.G. (1966a), Soviet Physics-Acoustics 12, 131.

Gitis, M.B. and Mikhailov, I.G. (1966b), Soviet Physics-Acoustics 11, 372.

Gordon, R.B. (1959), Acta. Met. 7, 1.

Greenfield, A.J. and Wiser, N. (1971), Phys. Letters 34A, 123.

Halder, N.C. and Wagner, C.N.J. (1967), Phys. Letters 24A, 345.

Halder, N.C., North, D.M. and Wagner, C.N.J. (1969), Phys. Rev. 177, 47.

Hansen, M. (1958), "Constitution of Binary Alloys" (McGraw-Hill, New York).

Harrison, W.A. (1966), "Pseudopotentials in the Theory of Metals" (W.A. Benjamin, New York).

Hatsopoulos, G.N. and Keenan, J.H. (1965), "Principles of General Thermodynamics" (John Wiley & Sons, New York).

Hill, J.E. and Ruoff, A.L. (1965), Rev. Sci. Instr. 36, 1465.

Houck, J.R., Bohm, H.V., Maxfield, B.W. and Wilkins, J.W. (1967), Phys. Rev. Letters 19, 224.

Huang, K. (1967), "Statistical Mechanics" (John Wiley & Sons, New York).

Hultgren, R.R., Orr, R.L., Anderson, P.D. and Kelley, K.K. (1963), "Selected Values of Thermodynamic Properties of Metals and Alloys" (John Wiley & Sons, New York).

Hume-Rothery, W., Smallman, R.E. and Haworth, C.W. (1969), "The Structure of Metals and Alloys" (Institute of Metals, London).

Jarzynski, J., Smirnow, J.R. and Davis, C.M. (1969), Phys. Rev. 178, 288.

Khodov, Z.L. (1960), Phys. Met. Metall. (U.S.S.R.) 10, 129.

Kirkwood, J.G. and Buff, F.P. (1951), J. Chem. Phys. 19, 774.

Kirshenbaum, A.D. and Cahill, J.A. (1962), Trans. Am. Soc. Metals 55, 844.

Kleppa, O. (1950), J. Chem. Phys. 18, 1331.

Kravchenko, V.Ya. (1969), Soviet Phys.-J.E.T.P. 27, 801.

Kubaschewski, O., Evans, E.Ll. and Alcock, C.B. (1967), "Metallurgical Thermochemistry" (Pergamon, Oxford).

Kurtz, W. and Lux, B. (1969), High Temp.-High Press. 1, 387.

Lebowitz, J.L. (1964), Phys. Rev. 133, A895.

Lloyd, P. (1968), In "Theory of Condensed Matter" (International Atomic Energy Agency, Vienna).

Lyall, K.R. (1970), Ph.D. Thesis (Simon Fraser University).

McAlister, S.P. (1971), Ph.D. Thesis (Cambridge University).

McAlister, S.P. and Turner, R. (1972) J. of Phys. (to be published).

McSkimin, H.J. (1959), J. Acoust. Soc. Am. 31, 287.

McSkimin, H.J. and Fisher, E.S. (1960), J. Appl. Phys. 31, 1627.

McSkimin, H.J. (1964) in "Physical Acoustics, IA", 271 (ed. W.P. Mason, Academic Press, New York).

North, D.M. and Wagner, C.N.J. (1970), Phys. Chem. Liquids 2, 87.

Overhauser, A.W. (1971), Phys. Rev. B 3, 1888

Pierce, G.W. (1925), Proc. Am. Acad. Sci. 60, 271.

Pines, D. (1964), "Elementary Excitations in Solids" (W.A. Benjamin, New York).

Polotskii, I.G. and Khodov, E.L. (1953), Soviet Physics-Acoustics 4, 185.

Price, D.L. (1971), Phys. Rev. A 4, 359.

Pronin, L.A. and Filippov, S.I. (1963a), Izv. Vuzov. ChM. 5, 10.

Pronin, L.A. and Filippov, S.I. (1963b), Izv. Vuzov. ChM. 11, 11.

Quinn, J.J. (1967), Phys. Letters 25A, 522.

Randall, R.H., Rose, F.C. and Zener, C. (1939), Phys. Rev. 56, 343.

Roll, A. and Motz, H. (1957), Z. Metallknde 48, 435.

Schwaneke, A.E. and Falko (1967), U.S. Bureau of Mines Report BM-RI-7372.

Shyu, W.M. and Gaspari, G.D. (1969), Phys. Rev. 177, 1041.

Thiele, E. (1963), J. Chem. Phys. 38, 1959.

Thresh, H.R., Crawley, A.F. and White, P.W.G. (1968), Trans. Metall. Soc. A.I.M.E. 242, 819.

Throop, G.J. and Bearman, R.J. (1965), J. Chem. Phys. 42, 2838.

Tolman, R.C. (1962), "The Principles of Statistical Mechanics" (University Press, Oxford).

Turner, R., Lyall, K.R. and Cochran, J.F. (1969), Can. J. Phys. 47, 2293.

Übelacker, E. and Lucas, L.D. (1962), Compt. Rendu. Acad. Sci. 254, 1622.

Vollmer, O. and Kohlhaas, R. (1968), Z. Metallknde. 59, 273.

Watanabe, S. and Saito, T. (1971), J. Jap. Inst. Metals 36, 554.

Webber, G.M.B. and Stephens, R.W.B. (1968) in "Physical Acoustics IV B", 53 (ed. W.P. Mason, Academic Press, New York).

Webber, G.M.B. (1967), unpublished (quoted in Webber and Stephens 1968).

Wertheim, M. (1963), Phys. Rev. Letters 8, 32.

Widawski, E. and Sauerwald, F. (1930), Z. Anorg. u. Allgem. Chem. 192, 145.

Wilson (1965), Metallurgical Reviews 10.

Wood, W.W. (1968), in "Physics of Simple Liquids" (ed. H.N. Temperley et al., North-Holland, Amsterdam).

Ziman, J.M. (1961), Phil. Mag. 6, 1013.